Assessment of satellite based soil moisture products at various spatial scales for dry-down cycles analysis

PAULINE WANJIKU NYAMU
February, 2019

Assessment of satellite based soil moisture products at various spatial scales for dry-down cycles analysis

PAULINE WANJIKU NYAMU
Enschede, The Netherlands, February, 2019

Thesis submitted to the Faculty of Geo-Information Science and Earth Observation of the University of Twente in partial fulfillment of the requirements for the degree of Master of Science in Geo-information Science and Earth Observation.
Specialization: Water Resources and Environmental Management

SUPERVISORS:
Dr. Ir. Rogier van der Velde
Dr. Ir. Suhyb Salama

ADVISOR:
Ir. H.F. Benninga

THESIS ASSESSMENT BOARD:
Prof. Dr. Z. Bob Su (Chair)
Dr. D.C.M. Augustijn (External Examiner, ET-WEM University of Twente)

ABSTRACT

Soil moisture (SM) influences the hydrological response of an area by governing the partitioning of rainfall into surface runoff, infiltration and evapotranspiration. Investigating soil moisture dynamics may, therefore, improve understanding of fluxes which contribute to soil moisture dry-down (SMDD) dynamics. The SMDD can be modeled from soil moisture from either *in-situ* based measurements or satellite-based estimates. Hence, in-depth knowledge of the quality of satellite-based soil moisture products with respect to the 'ground truth' can contribute to their application and possible improvements of the respective retrieval algorithms. In this regard, characterizing satellite retrievals becomes a major venture to explore for purposes of acquiring data with high accuracy. Therefore, the objective of this study was three-fold; *(i)* to assess the performance of three soil moisture satellite products with varying spatial scales against *in-situ* measurements, *(ii)* analyse the dry-down cycles embedded within Level two Soil Moisture Active Passive (L2-SMAP) 36 km and SMAP Enhanced (L2-SMAP-E) 9 km products and the *in-situ* SM measurements and, *(iii)* relate the accuracy to the underlying physical characteristics.

First, the L2-SMAP and L2-SMAP-E at respective resolutions of 36 km and 9 km and Sentinel-1 SAR SM products were validated with respect to *in-situ* measurements at an observation depth of *5* cm for three monitoring networks including Twente, Raam and Flevoland regions in the Netherlands for the period April 2016 – April 2018. Since Sentinel-1 SAR is not a fully dedicated soil moisture product, a procedure for deriving soil moisture estimates was implemented in the Google Earth Engine using change detection algorithm. Microwave remote sensing has been widely used in various fields of applications in the recent past because of its capacity to provide land surface imagery irrespective of the atmospheric conditions. It employs L-band operating at a wavelength of 21.4 cm and frequency of 1.4 GHz which is considered as the most optimal band for soil moisture remote sensing. This is because water has the largest sensitivity on the dielectric permittivity at this band and therefore the choice for NASA's SMAP products in this study was calculated. On the other hand, the Sentinel-1 mission which is part of the European Copernicus Program operating at C-band (5.405 GHz and 5.6 cm wavelength) offers soil moisture estimates at a high spatiotemporal resolution even though the signal is usually confounded by effects of surface roughness and vegetation. Second, relating identified differences between the satellite and the *in-situ* measurements to physical characteristics of the study area to demystify the probable error sources. Finally, soil moisture dry-down cycles embedded within the SMAP products and the *in-situ* measurements were modeled as an exponential decay function using the least square fitting method for Twente, Raam and the Netherlands to derive the e-folding dry-down time-scale (τ), the duration (*t*) and magnitude (*A*) of soil moisture drying.

Results show that Sentinel-1 SAR on average had the largest unbiased root mean square difference (UbRMSD) followed by SMAP-E and SMAP of 0.07, 0.052 and 0.05 $m^3\ m^{-3}$, respectively. Considering the effects of surface roughness and vegetation cover on the validation process, the obtained retrieval accuracy of the products is deemed good. For the three SM networks, each product performed differently depending on the underlying physical characteristics. The soil drying process is also different for each satellite product with the SMAP products exhibiting a faster drying than their *in-situ* counterparts. SMAP and SMAP-E have a slight difference in observing the dry-down. Dry-downs also vary spatially and temporally. Slower drying process was observed during winter than summer seasons while based on the regions, there are variations within short distances, but faster drying was observed in areas dominated by sandy soils.

Keywords: Soil moisture dry-down*, In-situ* soil moisture, SMAP, SMAP-E, Sentinel-1, Validation, Google Earth Engine

ACKNOWLEDGMENTS

TABLE OF CONTENTS

LIST OF FIGURES

LIST OF TABLES

LIST OF ABBREVIATIONS

asc	Ascending
BOFEK	BOdemFysische EenhendenKaart
CD	Change Detection
des	Descending
ESA	European Space Agency
ET	Evapotranspiration
FP	Flevoland
G.E. E	Google Earth Engine
GRD	Ground Range Detected
ITCSM	ITC soil moisture (Twente network)
IW	Interferometric Wide
L2	Level-2
L2_SM_P	Level 2 SMAP Passive Soil Moisture
L2_SM_P_E	Level 2 SMAP Enhanced Passive Soil Moisture
MD	Mean difference
NASA	National Aeronautics and Space Administration
NSIDC	National Snow and Ice Data Centre
PTF	Pedotransfer function
PYSMM	PYthon Sentinel-1 soil Moisture MappingToolbox
R^2	Coefficient of Determination
Rm	Raam
RMSD	Root Mean Square Difference
SAR	Synthetic Aperture Radar
SCA-V	Single Channel Algorithm for V polarized
SDI	Standardized Drought Index
SM	Soil moisture
SMAP	Soil Moisture Active Passive
SMDD	Soil moisture dry down
SMDD	Soil moisture dry down
SMOS	Soil Moisture Ocean Salinity
SVR	Support Vector Regression
UbRMSD	Unbiased Root Mean Square Difference
US	United States
USDM	United States Drought Monitor
VH	Vertical transmit and Horizontal receive
VV	Vertical transmit and Vertical receive
WUR	Wageningen University and Research

1. INTRODUCTION

1.1. Background information

Soil moisture influences the hydrological response of an area by governing the partitioning of rainfall into surface runoff, infiltration and evapotranspiration (ET) (Corradini, 2014). The infiltration, that is part of rainfall reaching the soil column, is a key component of the soil water balance inflows while ET and surface runoff are losses from the soil water balance (Laio et al., 2001). A rise or a fall in the soil moisture content contains information about various hydrological fluxes and processes in the land-water budget (Salvia et al., 2018). Investigating soil moisture dynamics may, therefore, improve an in-depth understanding of involved fluxes (Akbar et al., 2018). Information on these various hydrological parameters including infiltration, soil hydraulic properties, and evapotranspiration contribute to soil-moisture dry-down (SMDD) dynamics (Dirmeyer et al., 2009). According to McColl et al. (2017), SMDD is defined as periods after rain where the soil moisture is decreasing due to evapotranspiration and drainage. Under normal circumstances, the losses within the soil are attributed to evaporation and drainage while the inflows are associated with precipitation and irrigation processes (Laio et al., 2001).

Depending on the most dominant characteristics, the soil moisture (hereafter SM) losses are categorized based on three regimes: wet, medium wet and dry soils (McColl et al., 2017). The dominant loss in wet soils is attributable to drainage and run-off. For the medium wet soils, evapotranspiration is the main loss term when drainage and runoff reduce (stage I evapotranspiration). The evapotranspiration level in the dry soils is limited due to less water availability. This is referred to as stage II evapotranspiration (Laio et al., 2001; McColl et al., 2017). The SMDD time series is usually subject to stage II evapotranspiration and characterized by the e-folding time scale (τ) because drainage, runoff, and phase I evapotranspiration usually take place over a relatively short time period in the dry-down cycle.

As argued in Akbar et al. (2018), based on estimated SMDD (whether from *in-situ* or satellite estimates), they can be categorized to their characteristic hydrological regimes. The SMDD are usually affected by annual shifts in the hydrological regimes and/or area-based incongruities that result from either abnormal water scarcity or downpours. Carranza et al. (2018) reported that surface soil moisture (SSM) has a good connection with the root zone soil moisture (RZSM) which has a more robust connection with the hydrological changes; thus one can be used as a reference to the other. As observed in Ford et al. (2015) research, where flash drought events were monitored in the United States and result compared with the U.S Drought Monitor (USDM), observations of SMDD at the surface can inform on critical and continuous anomalies that define the onset of epidemics such as drought. They used weekly percentiles of volumetric soil moisture (VSM) relative to the cumulative distribution function.

Droughts (lasting for shorter to longer periods) are major world natural disasters causing widespread negative impacts that include but not limited to ecosystem damage, water scarcity, heat waves, and crop water inadequacy (Chen et al., 2014). So, they require constant monitoring as highlighted by Hayes et al. (2011) based on different tools and indices (e.g., standardized drought index (SDI) proposed by Mckee et al. (1993)). Previous studies (e.g., Sun et al., 2015) have shown that soil moisture dynamics can be utilized to define drought onsets and cessations. Most drought monitoring tools like the USDM generally capture drought incidences that are slowly evolving but lack the capability to define the onset of flash droughts related to precipitation deficits. Based on Ford et al. (2015) provision, flash droughts are relatively short

periods of abnormal low and rapid SM decrease. In their study, Ford et al. (2015) successfully used *in-situ* SM from a dense network to monitor flash droughts using SM measurement anomalies captured as dry-downs, a confirmation that drought episodes can be defined in near real-time. *In-situ* SM measurements can be used to monitor dry-downs and provide timely information on SM anomalies that can be integrated with drought early warning systems. However, most regions have limited or no *in-situ* SM measurements available to facilitate drought monitoring. In addition, SM measured in the field is typically point-based and is, thus, not spatially representative (Ebrahimi et al., 2018).

New advancements such as the smart sensor webs measurements that are areal representative are additional sources of SM data. Such avenues are, however, not cost effective and therefore less utilized (Moghaddam et al., 2010). In the recent past, global efforts to provide readily available and accessible SM network data have been initiated. And as a promising alternative, satellite-based SM products have emerged to provide continuous SM data at high spatial-temporal resolutions via microwave instruments (Hornacek et al., 2012). Examples of SM satellite-based products that may be applicable for monitoring of dry downs are the Soil Moisture Active Passive (SMAP). and Soil Moisture Ocean Salinity missions (SMOS) (McColl et al., 2017; Rondinelli et al., 2014). Like the other SM sources, these satellite products are also limited since they have a coarse spatial resolution and only periodically pass over a particular location (Njoku and Entekhabi, 1996).

Several techniques for SM remote sensing have been explored using observations from optical, thermal and microwave remote sensing (Lievens et al., 2017). As of today, great progress has been made in the remote sensing of soil moisture according to Petropoulos et al. (2015), by using the microwave domain of the electromagnetic spectrum within the low-frequency range of 1-5 GHz where fine changes of dielectric permittivity of the soils are detected (Hallikainen and Ulaby, 1985). Microwave remote sensing makes use of active (e.g., radars) and passive sensors (e.g., radiometers). Examples include SMAP and SMOS satellites designed to globally monitor soil moisture, and the Sentinel-1 satellites.

SMAP is designed to make use of both active (SAR) and passive (radiometers) sensors. Radiometers measure microwave emission from the earth's surface as brightness temperature (T_B) (Das and Dunbar, 2017), while SAR provides the backscatter coefficient (σ^o) which is the ratio between the transmitted and the received radiation (Kim et al., 2018). The SMAP and SMOS radiometers use L-band which provide low spatial resolution SM data at a relatively high temporal resolution (SMOS, 2005; SMAP, 2015). L-band operating at the wavelength of 21.4 cm and frequency of 1.4 GHz is considered as the most optimal band for soil moisture remote sensing because water has the largest sensitivity on the dielectric permittivity at this band (Li et al., 2018). In contrast to radiometers, SAR observations provide SM data at high spatial resolutions (Chan et al., 2018).

The SMAP mission provides global observations on SM and its freeze/thawed state at resolutions of 36 km, 9 km, and 3 km (Das and Dunbar, 2017). Unfortunately, on July 7, 2015, SMAP radar malfunctioned due to a power supply problem. For this reason, only 2.5 months data is available for SMAP products based on both active and passive observations through the NASA DAAC at National Snow and Ice Data Centre (NSIDC) (Das et al., 2016). To continue providing the combined radar and radiometer high-resolution data, replacing the missing SMAP L-band radar data has been explored in many ways leading to the creation of two enhanced data products (Das et al., 2017). These are *i)* the SMAP Enhanced Passive Soil Moisture Product (L2-SMAP-E)-9 km and *ii)* the SMAP/Sentinel-1 Active-Passive Soil Moisture Product (L2-SMAS-P)-3km that were released on December 2016 and April 2017, respectively (Colliander et al., 2018).

The Sentinel-1 mission which is part of the European Copernicus Program operates at C-band (5.405 GHz and 5.6 cm wavelength). It consists of the identical Sentinel-1A and Sentinel-1B satellites, which together offer a high spatiotemporal resolution (e.g. 10 m by 10 m grid size every 2 days for the Sentinel-1 satellites) (Alexakis et al., 2017). The main challenge for the retrieval of soil moisture content (SMC) from Sentinel-1 is that the signal is confounded by the effects of surface roughness and vegetation (van der Velde et al., 2012) and therefore appropriate retrieval techniques must be applied. Examples of such retrieval algorithms are change detection (CD) (Wien and Zürich, 2018), Neural Network (NN) (Rodriguez-Fernandez et al., 2015) and Support Vector Regression (SVR) (Dileep et al., 2015).

In-depth knowledge of the quality of satellite-based SM products can contribute to their application and possible improvements of the respective retrieval algorithms. Therefore, characterizing satellite retrievals becomes a major venture to explore for purposes of acquiring data with high accuracy. In this research, the L2-SMAP, L2-SMAP-E at 36 km and 9 km resolutions respectively and Sentinel-1 SAR SM products were validated with respect to *in-situ* measurements at an observation depth of *5 cm* from three monitoring networks including Twente, Raam and Flevoland regions in the Netherlands. Estimation of SM from Sentinel-1 was done based on the CD approach, implemented in the Google Earth Engine (GEE) platform. Pixel matchup approaches through spatial averaging method were applied. Possible error sources for each satellite product were also investigated. The error sources considered for this research were both spatial and temporal related. Examples include land cover and soil texture. After the validation exercise, the SMAP satellite products and the *in-situ* SM measurements were used to identify SMDD events, their duration, and magnitude for the Netherlands.

1.2. Research problem

Many biophysical processes (e.g., growing of crops) depend on water content in the upper few centimeters of the soil profile. How wet or dry the topsoil is or the rate at which it dries/wets can determine the hydrological response of an area, e.g., the occurrence of floods or drought. Soil moisture content can also inform water resources managers about the effectiveness of the wetting measures already taken or ought to be taken by defining the areas drying faster than others. Monitoring surface soil moisture, therefore, forms a basis to characterize hydrological systems. Rondinelli et al. (2014) reported that *in-situ* SM can be used to identify the onset of droughts by monitoring dry-downs after rainfall events. Therefore, with reference to the prevailing *in-situ* soil moisture measurements available for the Netherlands at the Twente and Raam regions and SMAP SM estimates, soil moisture dry-down analysis forms the basis of this study. The study is also motivated by an interest to understand drying process with respect to soil moisture measurements considering the 2018 rainfall deficiency in the Netherlands, where consistently hot weather was experienced during spring and summer seasons.

The *in-situ* SM measurements are, however, limited in terms of coverage and are typically only representative for a small area. Nonetheless, space agencies have launched several satellites dedicated to global soil moisture monitoring and their sensing depth is between the surface and a moisture-dependent depth, usually not exceeding 5 centimeters. Also, out of the SM products available over the Netherlands (i.e., Level 2 SMAP, level 2 SMAP-E, and Sentinel-1 SM based product), only the SMAP products have been validated for the Twente network but of different levels from the afore-mentioned SMAP products. Validation in other available networks i.e., Raam and Flevoland have also not been previously explored. Also, validation of these products under varying soil textures and land cover has not yet been explored, hence their accuracy at such levels is not fully known.

From the previous studies in other regions, characterization of dry-downs can be used to define wet and dry areas and this contributes to the hydrological categorization of different regimes. The study will contribute to the hydrological characterization of the Netherlands into faster and slower drying areas. Again, the comparison between satellite estimates and the *in-situ* measurements during dry-down periods can contribute to the validation process.

1.3. Research objectives and questions

1.3.1. Objectives
The main objective of this research is to assess the performance of three soil moisture satellite products with varying spatial scales of 36 km, 9 km, and 10 m against *in-situ* measurements and analyze the dry-down cycles embedded within the 36 km and 9 km SMAP products and the *in-situ* SM measurements.

The specific objectives are to: -
i. Validate the performance of L2-SMAP 36 km, L2-SMAP-E 9 km, and 10m by 10m grid size for sentinel-1 SM estimates against the *in-situ* measurements,
ii. Derive soil moisture content from Sentinel-1 satellites,
iii. Quantify the intensity and timescale of the soil moisture dry down episodes captured by SMAP satellite products and *in-situ* measurements, and
iv. Analyze the accuracy between the SM satellite estimates and the *in-situ* measurements spatially and temporally with respect to physical characteristics.

1.3.2. Questions
i. How do satellite-based soil moisture products at different spatial resolutions compare with *in-situ* measurements?
ii. Is it possible to relate the differences in the matchups identified in *(i)* to the physical characteristics of the study area?
iii. How does the spatial resolution of the satellite SM products affect the intensity and timescale of the observed dry down episodes?
iv. How do land cover and soil texture affect the intensity and timescale of the observed dry-down episodes?

1.4. Research method
In this study, *in-situ* soil moisture observations and satellite-based products were used. The *in-situ* soil moisture measurements were obtained from ITC Water department while the SMAP satellite products were retrieved from the National Snow and Ice Data Centre (NSIDC) site accessible at https://nsidc.org/data as discussed in chapter 3. An IDL code was used to retrieve VSM from the SMAP imageries for the period 2016 – 2018 for the regions of interest. SM was retrieved from Sentinel-1 SAR backscatter coefficient observations using the CD algorithm, implemented in the Google earth engine. Wilting point and saturation point SM maps, adopted from BOFEK2012 (Wösten and De, 2016) were used as the dry and wet references between which the saturation index from the CD approach was scaled.

The focus of the first part of the study was to assess the accuracy of the satellite-based SM estimates with respect to the *in-situ* soil moisture observations. The validation period was from 6th April 2016 to 4th April 2018. The bias and RMSD were then analyzed with respect to landcover and soil texture to evaluate the probable causes of error/uncertainties. This was followed by SMDD identification where the focus was on rain-free days. Using the least squares method, the exponential curve fitting was done to obtain the

model parameters. This was done for Twente, Raam and The Netherlands using both SMAP 36 km and SMAP-E 9 km SM estimates. A summary of the research methodology is shown in Figure 1.1.
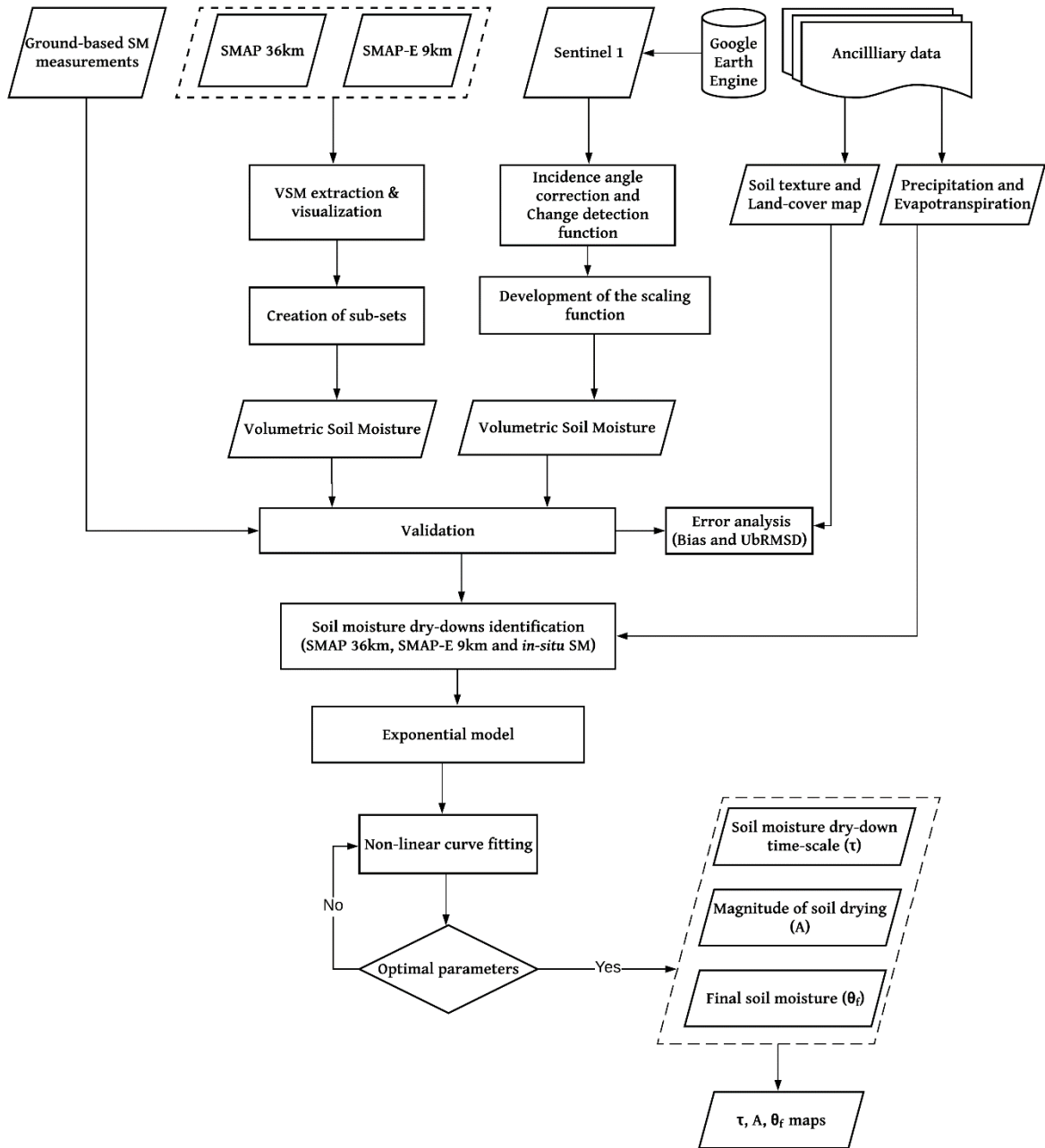
Figure 1.1: Schematic representation of the research methodology

2.   STUDY AREA AND IN-SITU DATA

2.1.   The Netherlands

The study is based in the Netherlands with a pivotal focus on three soil moisture monitoring networks as shown in Figure 2.1. They include Twente, Raam and Flevoland networks. The Netherlands is situated along the North Sea in North-west Europe with an area of approximately 34000 km².
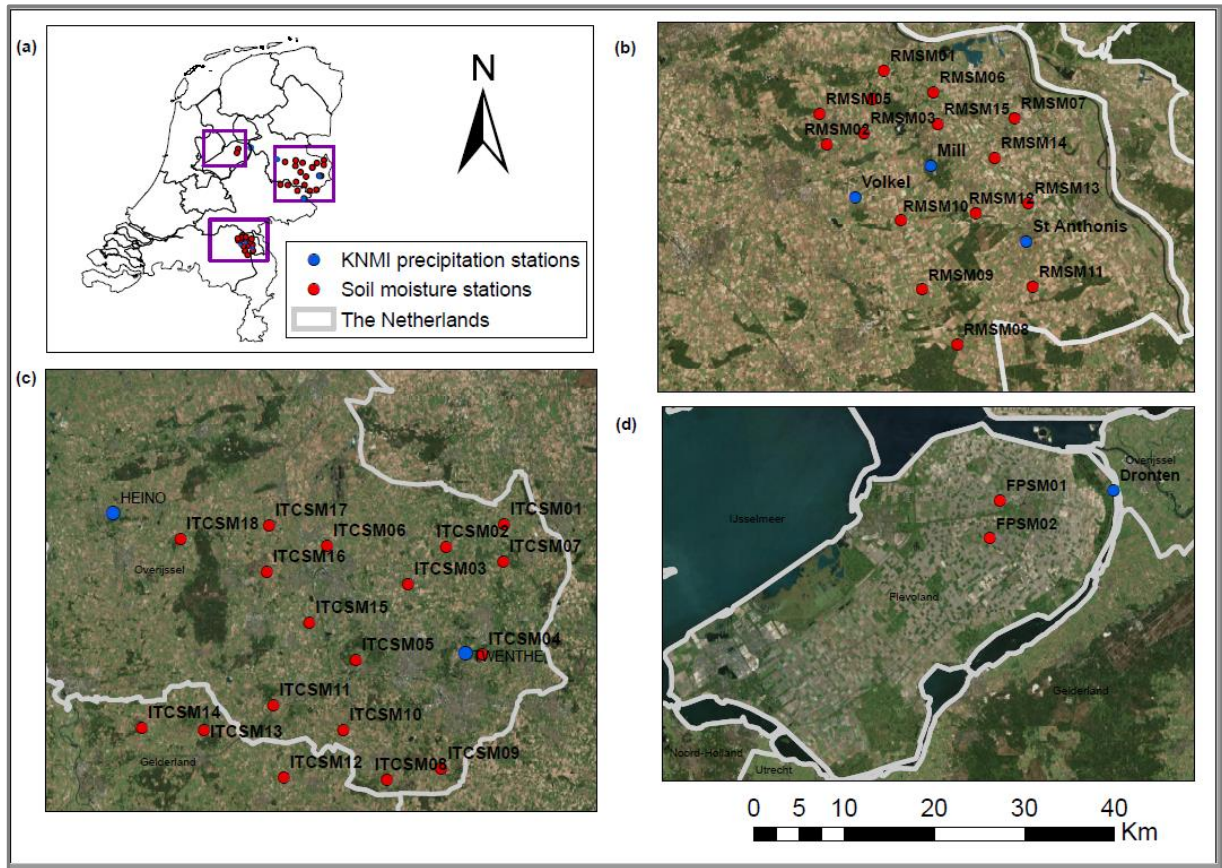
Figure 2.1: Google earth image showing (the Netherlands, the purple boxes showing the study areas i.e., (b) Raam, (c) Twente, (d) Flevoland networks and the red dots showing the soil moisture stations. The blue dots show some of the KNMI rainfall stations (https://www.knmi.nl/nederland-nu/klimatologie).

The Netherlands experiences a temperate climate according to the Köppen classification system. Precipitation is spread equally over the year with average annual precipitation of 760 mm. The potential evapotranspiration in the Netherlands has a seasonal trend with the highest amount recorded in July and August, and with a yearly potential of 525 mm. Due to the uneven distribution of ET, there are probabilities of drought in the summer. To mitigate droughts during summer, other sources of water such as surface and groundwater are sought when the need arises. The monthly average air temperature ranges from 3 °C in January to approximately 17 °C in July.

Tertiary and Mesozoic deposits are found within great depths of the country and nearly everywhere these formations are covered by Pleistocene and Holocene deposits. At shallow depths, only outcrops are observed in the south-eastern and eastern areas. Marine clay layers of tertiary age exist at a depth of about

400 meters acting as an impermeable base to the groundwater aquifer system. The soils in the eastern and southern parts of the Netherlands mainly consist of fine loamy sand, medium, and coarse sand. In the south, silt and silt loam (Loess) soils occur.

2.2. Soil moisture monitoring networks

Ground-based observations from three SM monitoring networks as shown in Figure 2.1 were used for assessment of the satellite products at 5 cm depth. These are Twente, Raam, and Flevoland. These 3 networks were chosen because they have readily available SM data with a few gaps. The SM and temperature data for Twente and Flevoland networks were provided by ITC while data for Raam network, was retrieved from 4TU.research data center at https://data.4tu.nl/repository/uuid:dc364e97-d44a-403f-82a7-121902deeb56(Benninga et al., 2018). Twente SM data is available from 2009 to present, Raam network data is available from April 2016 to present while Flevoland network has data from 2016 to June 2018. The validation period chosen was from April 2016 to April 2018 in accordance with the Raam network data span to obtain a standard set.

The regional networks provide SM information over a range of land covers and soil types with well-calibrated probes as described in Table 2.1 for the Twente network and Table 2.2 for the Raam network. Flevoland description is not displayed in a table format because it has very few stations. Its description is on section 2.2.3.

Table 2.1: Twente Regional SM network soil texture and land cover characteristics (adapted from Dente et al., (2011).

SMAP grid	*In-situ* stations	Soil texture	BOFEK 2012	Landcover
1,0	ITCSM15	Sand	Fine Sand	Grassland
	ITCSM16	Sand	Sandy topsoil on peat on sandy soil mineral subsoil	Grassland
	ITCSM17	Sand	Fine Sand	Grassland
	ITCSM18	Loamy Sand	Loamy fine sand	Grassland
1,1	ITCSM5	Loamy Sand	Man-made sandy thick earth soil	Grassland
	ITCSM10	Sand	Fine Sand	Grassland
	ITCSM12	Sand	Sandy clay loam on a subsoil of fine sand	Grassland
	ITCSM13	Sand	Fine Sand	Grassland
	ITCSM14	Loamy Sand	Loamy fine sand	Grassland
2,0	ITCSM1	Sand	Sandy clay loam on a subsoil of fine sand	Grass bush
	ITCSM2	Sand	Man-made sandy thick earth soil	Grassland
	ITCSM3	Loamy Sand	Loamy fine sand	Grassland
	ITCSM7	Loamy Sand	Sandy clay loam on a subsoil of fine sand	Corn
2,1	ITCSM4	Loamy Sand	Loam	Grassland
	ITCSM8	Sand	Sand	Corn
	ITCSM9	Sand	Man-made sandy thick earth soil	Corn

Table 2.2: Raam Regional SM network soil texture and land cover characteristics (adapted from (Benninga et al., 2018)

SMAP grid	Station	Landcover type	Adjacent landcover	Soil order	BOFEK Code	Sand (>50mm) %	Silt(>50-2mm) %	Clay (<2mm) %	Organic matter (%)
(1,0)	Rm10	grass	grass	podzols	304	96.3	0.8	0.7	2.2
	Rm11	grass	grass and corn	Podzols	304	94.8	1.7	1.6	1.9
	Rm14	grass	grass	podzols	312	90	4.7	2.3	3
	Rm15	grass	grass	Anthrosols	311	88.6	5.5	2.8	3.1
(1,1)	Rm5	Grass fallow	onions	Anthrosols	311	93.1	2.3	1.1	3.5
	Rm12	grass	grass	Podzols	304	92	2.5	1.7	3.9
	Rm13	grass	corn	Podzols	309	96.7	1.1	0.8	1.4
(2,0)	Rm1	grass	grass	Podzols	305	91.3	1.9	3.5	3.3
	Rm2	grass	Sugar beets	Podzols	305	90.4	3.7	2.1	3.8
	Rm3	grass	grass	podzols	304	93.3	2.4	1.9	2.4
	Rm7	Grass fallow	Corn and chicory	Podzols	317	82.1	10.5	5.2	2.2
(2,1)	Rm4	grass	grass	Podzols	305	90	2	2.9	5.2
	Rm8	grass	Sugar beets	Podzols	304	92.8	1.6	1.4	4.1
	Rm9	Grass fallow	Sugar beets	Podzols	304	95.4	1.1	0.8	2.6

2.2.1. Twente regional soil moisture monitoring network

Twente region is situated in the Overijssel province, the eastern part of the Netherlands (52° 05'–52° 27'N and 6° 05'–7° 00'E). It consists of 20 stations that have been installed at ≈40 km * 50 km large area. The *in-situ* probes installed collect SM data at 5 and 10 cm depth, and only for four stations SM is recorded at depths (5, 10, 20 and 40 centimeters) while for eight sites three different depths are monitored (5, 10 and 20 centimeters). Out of the 20 monitoring stations, 16 stations are installed on grassland, 3 in a cornfield and 1 in a forest (Dente et al. 2012). The most extensively occurring land cover is grassland for pasture which is harvested and fertilized several times in a year. The land use of this region consists of a mosaic of agricultural fields, forest patches and several urban areas with corn growing as the major crop type where planting and harvesting are done on April and September, respectively (Dente et al. 2012). The area has four main soil types namely sand, loam, man-made sandy thick soils and peat soils covered by a layer of peat or sand (Dente et al. 2011). Generally, 13 and 7 stations are installed on sandy and loamy soils, respectively. Twente network is characterized by very low clay contents. To understand the SM variation trends, a time series comparison of the daily mean for all the stations were calculated. A figure showing the driest and wettest stations at Twente network for ITCSM4 and ITCSM13 which represent the wettest and driest stations respectively within the networks is shown in Figure 2.2. ITCSM04 has the highest daily mean of 0.508 m^3m^{-3} while ITCSM13 has the lowest daily mean of 0.136 m^3m^{-3} during the validation period. ITCSM13 is dominated by sandy soils while ITCSM04 is dominated by loamy sandy soils and both have grassland type of land cover. This could explain why they have a big difference in the observed means.
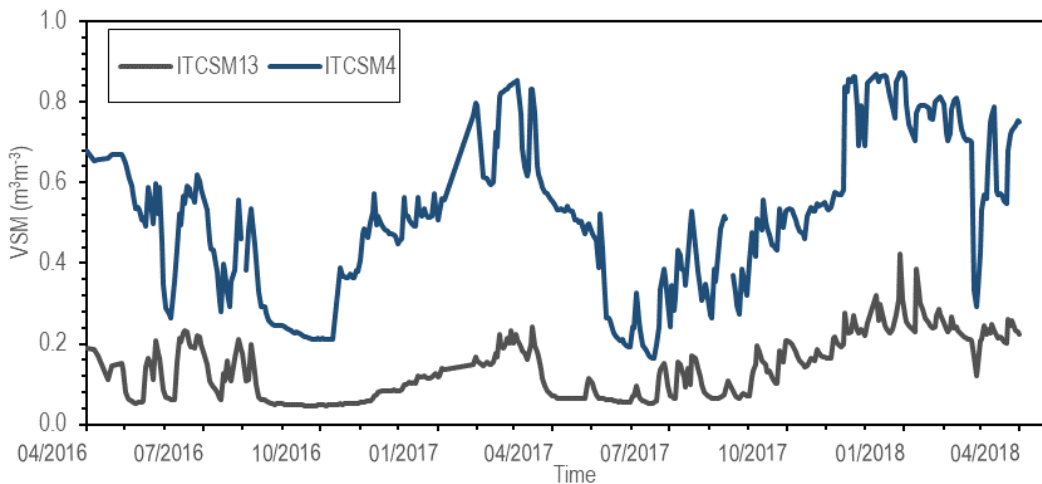
Figure 2.2: Time-series of VSM at 5 cm depth on-site ITCSM13 representing the driest station and ITCSM4 representing the wettest station

2.2.2. Raam regional soil moisture monitoring network

The Raam regional soil moisture monitoring network is located between the Dutch city Den Bosch and the German border in the South-east of the Netherlands. Currently, the network consists of 15 stations. The theta-probes are installed at the depths of 5 cm, 10 cm., 20 cm, 40 cm, and 80 cm depth. The Raam network has generated data since April 2016. Raam catchment consists of a closed sub-catchment called Hooge 'The High Raam' where stations 1 to 5 are located whereas the rest including 1 to 7, 10 and 12 to 15 are within the Raam catchment (Benninga et al., 2018). The region mainly holds sandy soils. 13 stations installed on coarse sand while stations 6 and 7 in clayey sandy and loamy sand respectively. Nearly all the stations are within the agricultural land apart from station 6 which is located on natural grassland. A time series plot showing the wettest and driest station at the Raam network was plotted to understand the soil moisture variation trend in this network as shown in Figure 2.3

Rm09 has the lowest daily mean VSM with a mean of 0.128 m^3m^{-3} while the highest daily mean is Rm01 with a mean of 0.314 m^3m^{-3} respectively. The difference in the VSM content is not very high. This could be because the two stations are covered with similar landcover and soil texture. The adjacent fields to Rm01 have grass while at Rm09, there are sugar beets.
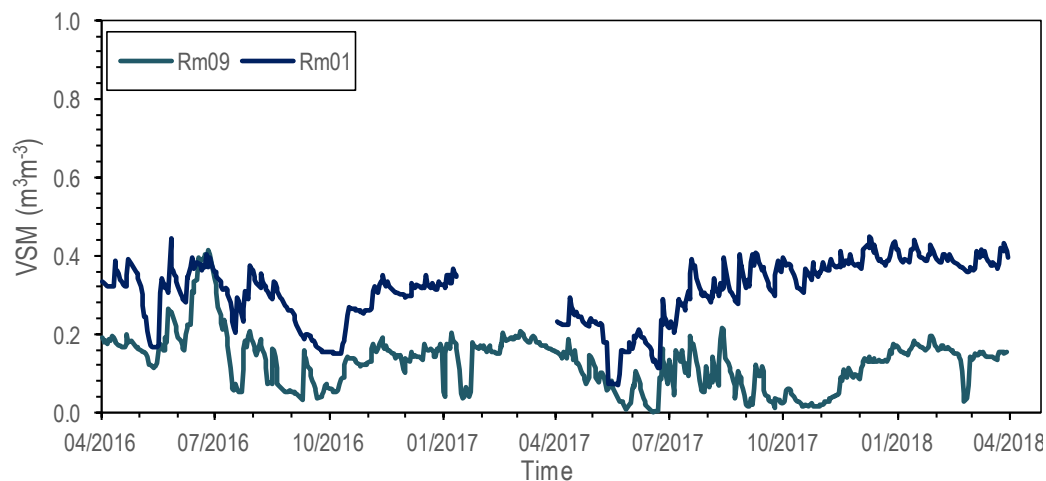
Figure 2.3: Time series of VSM at 5 cm depth on-site Rm09 representing the driest station and Rm01 representing the wettest station at Raam network

2.2.3. Flevoland soil moisture monitoring network

Flevoland is in the center of the Netherlands at $52^0,26'$N and $5^033'$E. It is a flat agricultural site characterized by marine clay pedology (Lievens and Verhoest, 2012). It consists of two *in-situ* SM monitoring stations. The field consists of a flat topography and homogeneous soil texture (Hans and Verhoest, 2012). A time series comparison of the wettest and driest station at Flevoland is shown in FP01 at Flevoland has the lowest mean of 0.307 m³m⁻³ while FP02 has a mean of 0.295 m³m⁻³ . The difference observed in the in their daily mean VSM is minor.
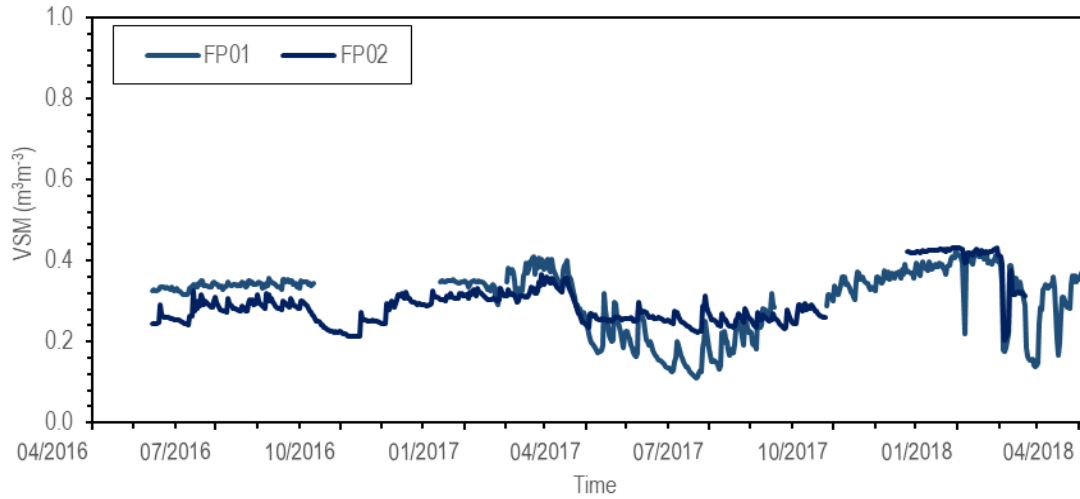
Figure 2.4:Time series of VSM at 5 cm depth on site FP02 representing the driest station and FP01 representing the wettest station at Flevoland network.

2.3. Soil moisture monitoring networks instrumentation

At Twente, Raam and Flevoland networks, capacitance sensors have been installed but of varying types. For Twente network, 5TM sensors have been installed with only one station (ITCSM15) having EC-TM ECH$_2$O sensor installed for 5 cm to 20 cm depth. The calibration coefficients for the 5TM sensor are 1.758 and 0.020 while for EC-TM are 0.775 and 0.071 for *a* and *b* respectively. At Raam network, Decagon 5TM sensors in all the 15 SM stations have been installed. For Flevoland, 5TM sensors have been installed with *a=1* and *b=0* as the calibration coefficients. All employ Em50 ECH$_2$O data loggers to monitor and record soil moisture. The sensors are usually placed on a horizontal level while the prongs are vertically placed to minimize problems related to ponding. They employ an oscillator at 70MHz to measure soil capacitance which translates to the dielectric permittivity of the soil. The dielectric permittivity of the soil is then used to infer volumetric soil moisture (Dean et al. 1987). Soil temperature is also detected using thermistors installed on the same probes and therefore both soil moisture and soil temperature measurements are recorded at intervals of 15 minutes (Benninga et al., 2018; Dente et al., 2011). Figure 2.5 is created with selected images to show the cross-section of a data logger and location of some stations Twente, Raam, and Flevoland.
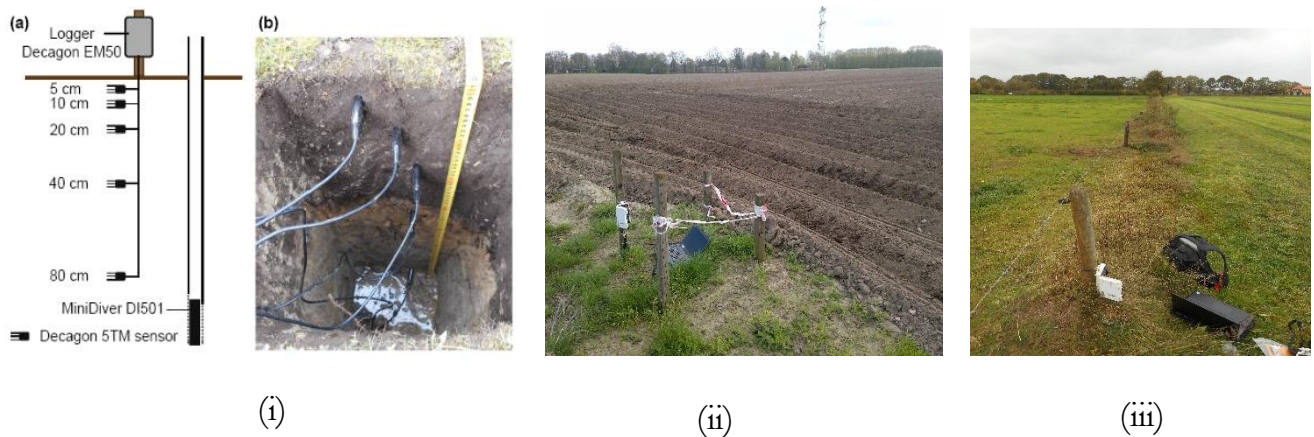
Figure 2.5: Selected images to show soil moisture instrumentation in the Netherlands: (i (a)) Schematic cross-section of soil moisture data logger and a nearby well (i (b)) soil moisture sensors at 5 different depths for an installation pit at Flevoland (FP01) network (source: Benninga et al. (2018), (ii) Raam network station Rm07 and (iii) Twente network station ITCSM13.

2.4.   Ancillary information

2.4.1.   Evapotranspiration and rainfall

Figure 2.6 shows the average time series of precipitation and evapotranspiration of *in-situ* measurements for Twenthe, Heino and Hupsel KNMI stations for 2016 to 2018 (https://www.knmi.nl/nederland-nu/klimatologie). The black lines represent evapotranspiration while the blue bars represent rainfall. There is a good agreement of the rainfall measurements with evapotranspiration in both summer and winter. With 366, 365 and 273 dataset points, for the years 2016, 2017 and 2018, daily mean averages of 2.37 mm, 2.42 mm and 1.87 mm were obtained. The values are closely related to the cumulative frequency plot in Figure 2.7 which shows reduced rainfall amounts in 2018 as compared to 2016 and 2017. This relates to the reported 2018 extremely hot spring season which then transitioned into the summer period (https://nos.nl/artikel/2257169-net-geen-droogterecord-in-2018-in-1976-viel-nog-minder-regen.html).   It is reported that a similar incident worse than 2018 had occurred 40 years ago in the year 1976.
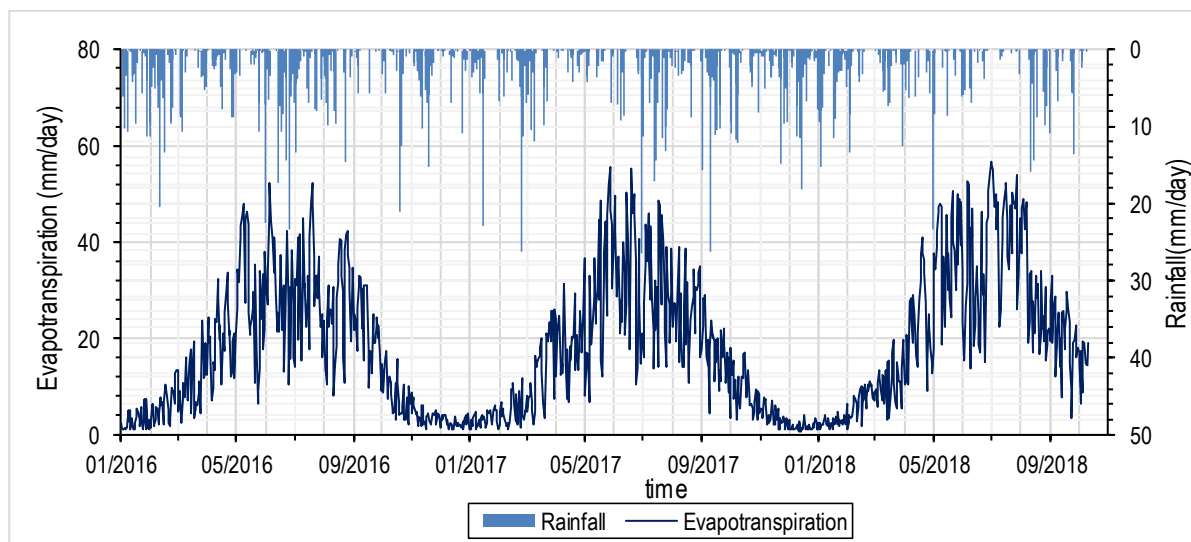
Figure 2.6: Schematic representation of evapotranspiration and rainfall time series for Twenthe, Heino and Hupsel on average basis from 2016 to 2018.
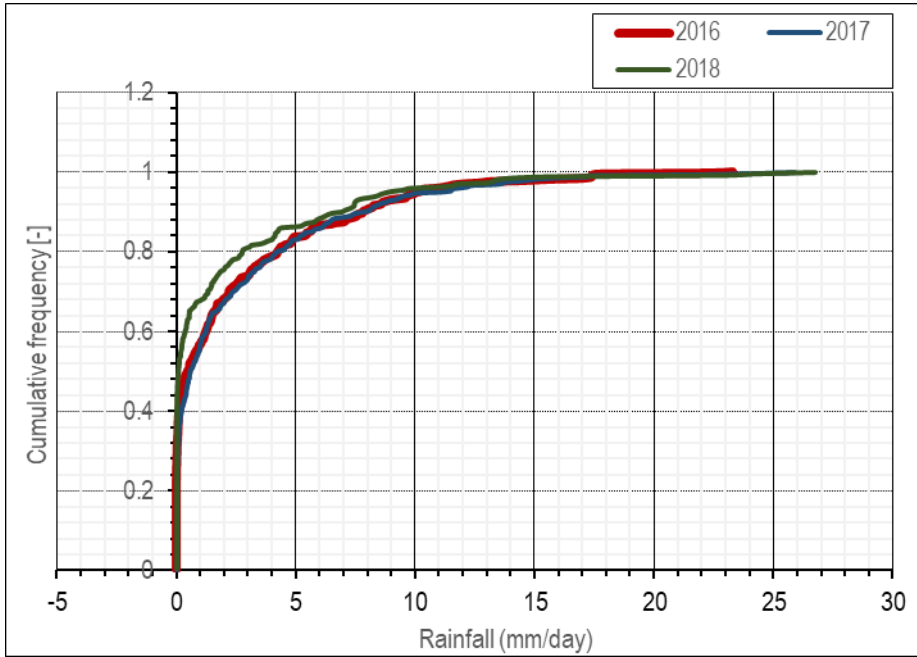
Figure 2.7: Cumulative rainfall distribution for the Netherlands for the years 2016, 2017 and 2018 based on an average of seven KNMI rainfall stations

2.4.2. Description of the soil properties data

There are two nationwide soil maps in the Netherlands; one with a scale of 1:250,000 and another one with a scale of 1:50,000. They both provide information about the soil characteristics at a meter depth. BOFEK2012 comprise one or more types of soils with a matching hydrological behavior, soil type, and profile structure. It dispenses information on soil physical characteristics including soil texture, water retention curve and hydraulic conductivity curve for the Netherlands soil units based on the Staring series, the Dutch class pedotransfer functions (Wösten et al., 2001). The units are coded in such a way that the hundreds indicate the soil type, i.e., 101,102 (peat soil), 201, 202 (peat moors), 301, 302 (sandy soils), 401, 402 (clay soils) and 501, 502 (loamy soils) (Wösten et al., 2001). The saturated soil moisture content and the wilting point is the soil moisture given at a pF of 4.2. The saturated soil moisture content is a parameter in BOFEK2012, as indicated in Eq. (2-1) (Vereecken et al., 2010). The soil properties map adopted from BOFEK2012 and the saturation and wilting point maps both at 5 cm depth are shown in Figure 2.8

$$S = \frac{\theta - \theta_{rs}}{\theta_{st} - \theta_{rs}} = [1 + (\alpha h)^n]^{-m} \tag{2-1}$$

where S is effective saturation [-], θ is the volumetric soil moisture (m³m⁻³), θ_{rs} is the residual moisture content [-] and θ_{st} is the saturated moisture content [-], α is the inverse of the air-entry value (cm⁻¹), h is the pressure head (cm), while n and m are shape parameters, respectively.
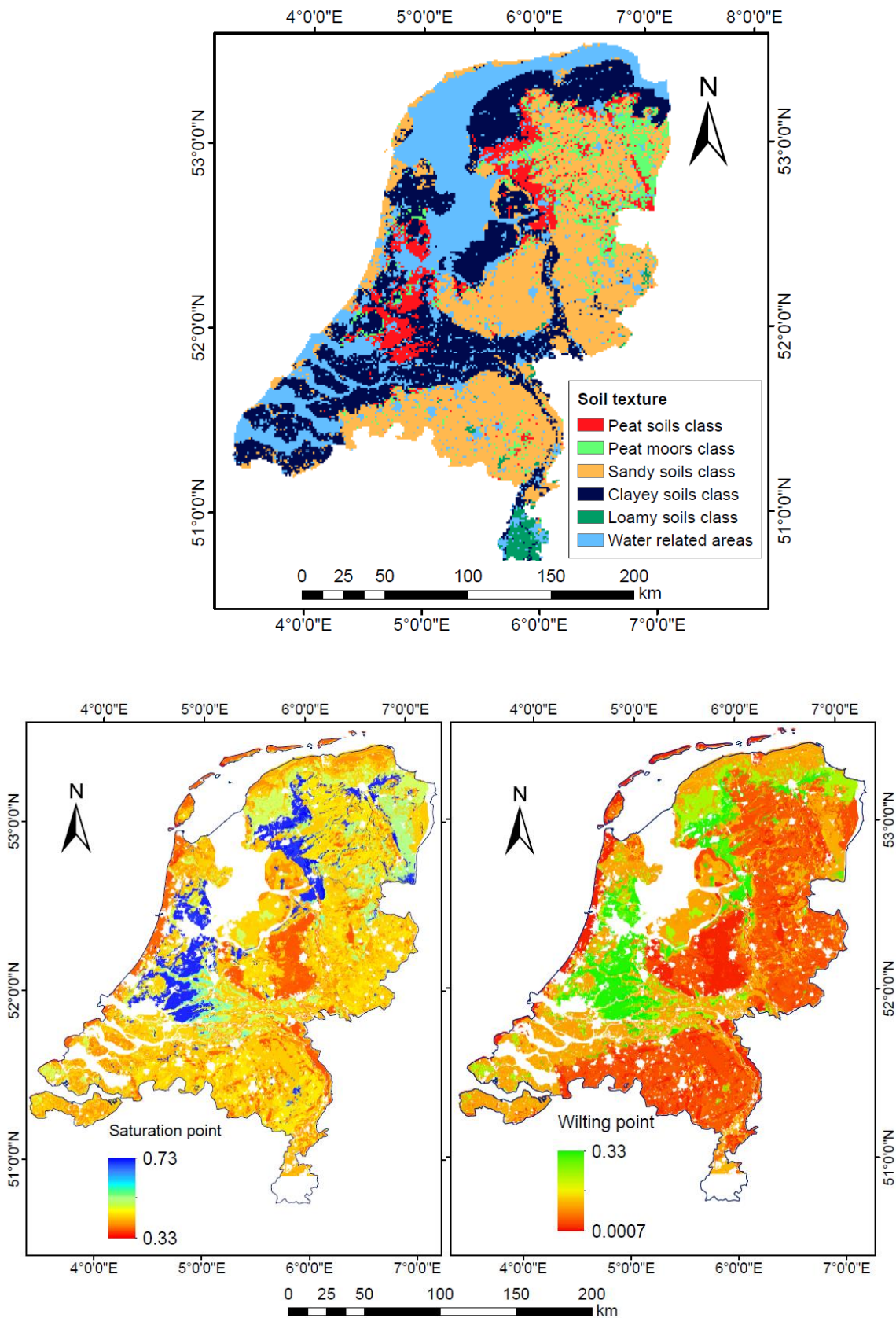
Figure 2.8: Top: Soil properties map adopted from BOFEK2012 (https://www.wur.nl/nl/show/Een-nieuwe-bodemfysische-schematisatie-van-Nederland.htm) and Bottom: Soil moisture saturation point and wilting point map at 5 cm depth source:(https://www.pdok.nl/geo-services?articleid=1948958)

2.4.3. Land cover data

Figure 2.9 shows the landcover map for the Netherlands with 15 different landcover classes demonstrating high land surface heterogeneity. More than four-fifths of the Netherlands surface area is utilized for agriculture, recreation, woodlands and nature as seen through the green color patches. Agriculture is the main land-use activity for the Dutch, mainly growing corn, sugar beets, potatoes, wheat, fruits and flowers and a vast of various forests. The red color represents built-up areas where large concentration lies on the western side, with substantially less urban land use in the Northern and Eastern part of the Netherlands.
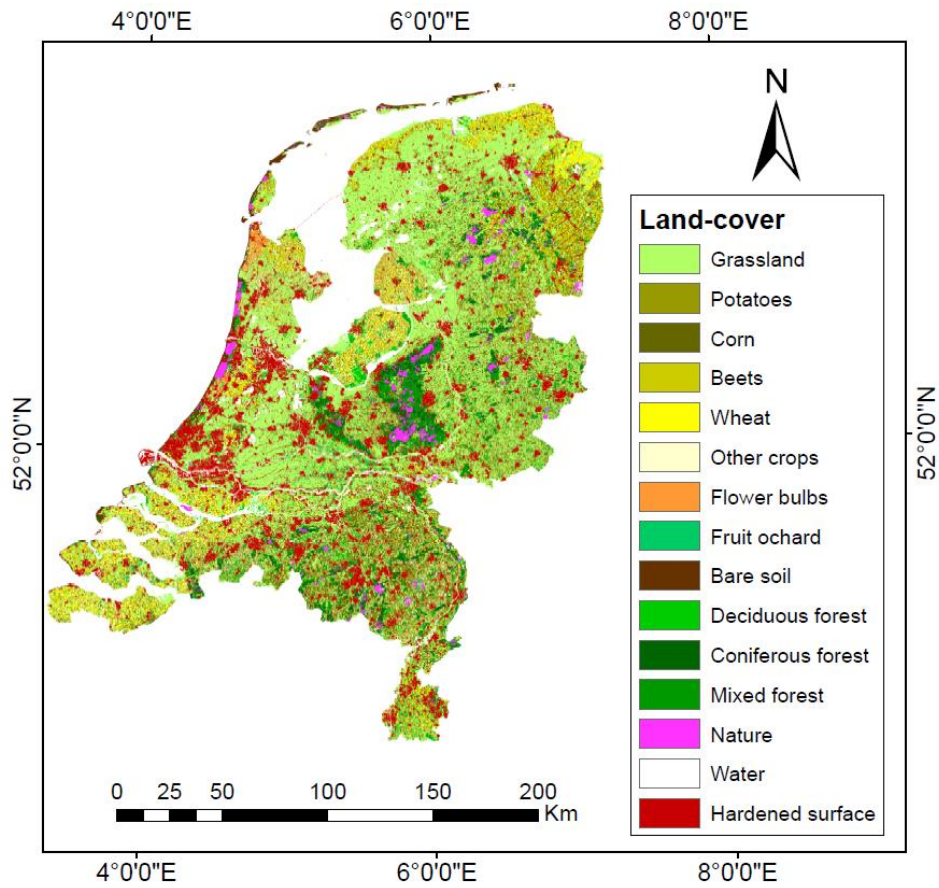
Figure 2.9: Landcover map for the Netherlands (https://www.clo.nl/node/20807)

3. SATELLITE DATA

3.1. SMAP Mission

SMAP is the latest L-band satellite mission providing global-scale SM and freeze/thaw state measurements (Cui et al., 2018). It incorporates an L-band radar and an L-band radiometer that share a single feedhorn and parabolic mesh reflector (Entekhabi et al., 2014). This becomes the third mission after SMOS and Aquarius to employ L-band radiometry for global SM monitoring from space (Chan et al., 2018). The reflector is usually offset from nadir and rotates about the nadir at 14.6 rpm and a surface incidence angle of approximately 40°. Constant incidence angle simplifies data processing and enables accurate repeat pass estimates. The reflector's diameter is 6m, producing 3dB footprint of 40km. The real aperture radar has a 30km footprint and two-way antenna beam width. This enables global data collection during ascending and descending passes. The SMAP baseline orbit parameters include:

   i.   685 km orbit altitude with 2-3-day average revisit time globally,
   ii. 98° inclination angle, sun-synchronous, and
   iii. Local time of ascending node 6 pm and 6 am descending local overpass time.

SMAP mission generates 22 different distributable data products with 4 levels of data processing. Level 1 contains instrument related data, Level 2 is half orbit geophysical retrievals, L3 consist of daily geophysical retrievals and L4 contains modeled geophysical retrievals (Entekhabi et al., 2014). SMAP standard products are in Hierarchical Data Format version 5 (Menzel, 2001). SMAP radar and radiometer uses unique design features to mitigate the effect of radio frequency interference (RFI) and therefore stands at a better position than earlier missions like SMOS. However, the SMAP radar malfunctioned on July 7, 2015, leaving behind the SMAP radiometer in operation.

In December 2016, the SMAP mission launched two new products with the aim of fulfilling the mission objective that was linked with the capabilities of high-resolution radar. Among them are SMAP Level 2 Enhanced Passive Soil Moisture Product (L2_SM_P_E) in December 2016 and the SMAP/Sentinel-1 Active-Passive Soil Moisture Product in April 2017 (Kim et al., 2018).

For this study, the SMAP products were retrieved from the NSIDC website accessible at https://search.earthdata.nasa.gov/ for the year 2016 to 2018. The descending overpass time at 6:00 am was used to evaluate L2_SM_P and L2_SM_P_E SMAP products' accuracy (Colliander et al., 2017). This is the time of the day, during which the air, vegetation, and near-surface temperature is in equilibrium with the topsoil temperature at that time of the day according to Entekhabi et al. (2014) and was therefore chosen. All the images were geographically projected to RD new projection, and band sub-setting was done using centroid longitude and latitude of the regions of interest. An IDL code was then created to retrieve soil moisture content from the SMAP images. SMAP parameters are as summarised in Table 3.1.

Table 3.1: SMAP parameters.

Parameters	Values
Frequency	1.41 GHz
Polarization	H, V, 3rd and 4th Stokes parameter
Instrument native resolution	38 km by 49 km (3-dB IFOV)
Antenna diameter	1.3K
Antenna rotation rate	14.6 rpm

Beam efficiency	~90%
Incidence angle	~40° (from Nadir)
Orbit type	Near-polar, sun-synchronous
Orbit repeat period	8-day exact repeat every 117 orbits
Orbit altitude	685 km
Orbit period	98.5 minutes
Swath Width	~1000 km
Local time des/asc node	6:00 am/6:00 pm
Complete global coverage	Every 2-3 days

3.1.1. SMAP level-2 passive soil moisture product (L2-SM-P)

The L2-SM-P product is derived with the SMAP L-band radiometer time-ordered observations (L1B-TB) as the input data (Chan et al., 2018). It provides SM estimates on a 36 km earth fixed grid produced using T_B observations from descending passes at 6:00 a.m. The 36 km grid resolution is close to the 3-dB native spatial resolution of the instrument observations, but the two measures of resolution are not necessarily identical. At Twente SM network, four SMAP 36 km pixels cover the network while at Raam and Flevoland, one grid covers the entire network as shown in Figure 3.1.
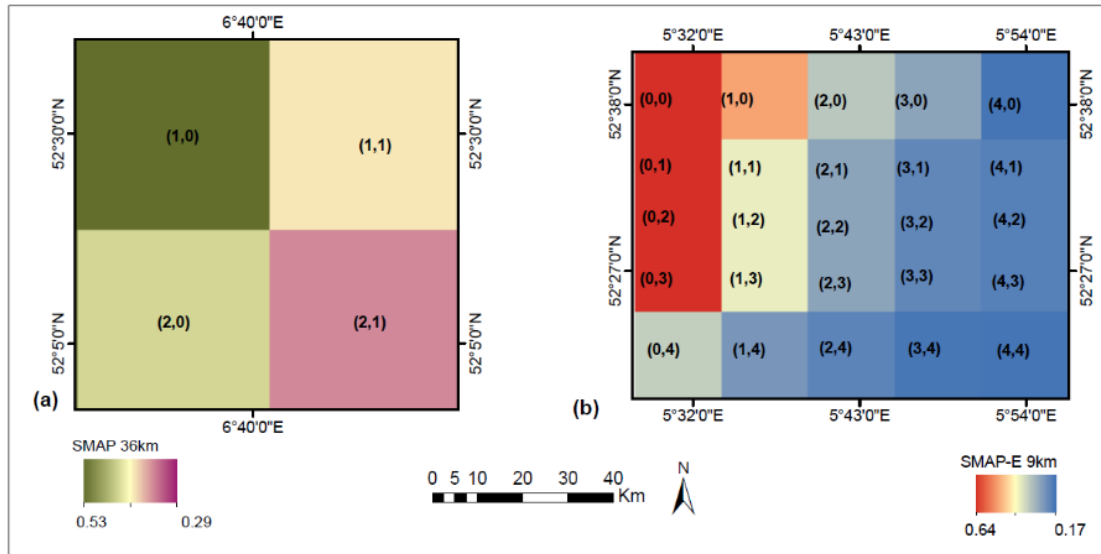
Figure 3.1: SMAP 36 km grid at Twente and SMAP-E grids at Flevoland SM networks showing the pixel index

3.1.2. SMAP level 2 Enhanced soil moisture product (L2-SM-P-E)

The SMAP level 2 Enhanced passive SM product was released in December 2016 (Cui et al., 2018). The L2-SM-P-E estimates SM at a resolution of 9 km. The grid is based on NSIDC EASE 2.0 grid specifications for SMAP. This nesting feature gives SMAP products a unique and common projection capability as well as their geophysical products. The product was created through the use of the Backus-Gilbert optimal interpolation technique to the antenna temperature (TA) data in the original SMAP level 1B brightness temperature product to make use of the overlapped radiometer footprints on orbit (O'neill et al., 2016). The interpolated TA data is corrected and calibrated to yield SMAP level 1C Enhanced Brightness Temperature product (L1C-TB-E). The L1C-TB-E is then updated to the current L2-SM-P-E using the SMAP baseline soil moisture retrieval algorithm. Imageries of this product show enhanced visual features that miss out on the standard SMAP 36 km (Bindlish et al., 2016). At Twente SM network, eighteen L2-SMAP-E grids cover the entire network while at Raam and Flevoland, six and two grids cover the networks, respectively.

3.2. Sentinel-1 characteristics

3.2.1. Sentinel-1 mission

The SAR instrument onboard Sentinel-1 satellite operating at C-band. Sentinel-1 is the first operational SAR satellite mission (Kornelsen and Coulibaly, 2013). It is the SAR constellation of two satellites orbiting 180° apart at an altitude of almost 700 km, imaging the entire earth every six days (Lievens et al., 2017). The Sentinel-1A was launched on 3 April 2014 and Sentinel-1B on 25 April 2016. Sentinel-1 uses advanced radar instrument to provide an all-weather, day-and-night earth's surface data (Martinis et al., 2018). It operates in four modes: Interferometric Wide Swath (IW), Extra Wide Swath (EW), Wave (WV) and Strip map (SM). Some of the modes operate in either single or dual polarization schemes; Wave mode has a single polarization, while the other modes have a dual polarization scheme; VV, VH, VV+VH, and HH+HV as depicted in Figure 3.2.
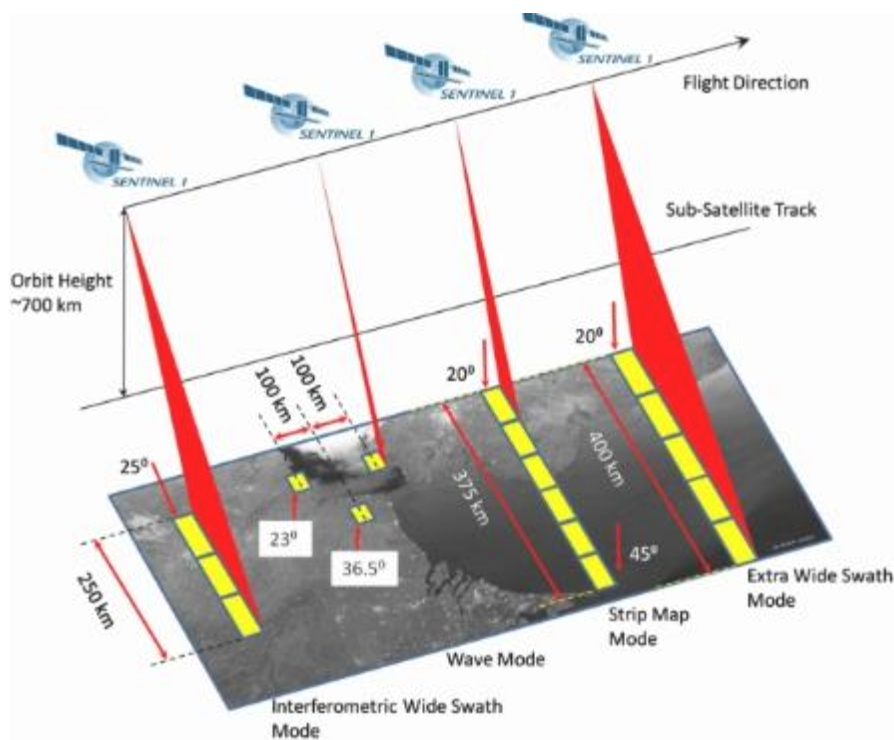
Figure 3.2: Sentinel-1 mission operational modes (https://sentinel.esa.int/web/sentinel/user-guides/sentinel-1-sar/acquisition-modes)

Sentinel-1 data can be accessed from, among other platforms, Sentinel-hub.com, EODIAS.eu, National collaborative ground segment, Alaska SAR facility, Google Earth Engine (G.E.E), and Copernicus. For the current study, Google Earth Engine was used to derive soil moisture from Sentinel-1 by applying a change detection concept as described in 4.1.1.

3.2.2. The Google Earth Engine platform

This is a cloud-based geoprocessing platform for scientific computation of large geospatial datasets (Gorelick et al., 2017). It allows for global time series processing of images integrating information communication technology (ICT) with remote sensing. It consists of a powerful Application programming interface (API) with a huge archive of datasets such as Landsat, MODIS, Sentinel-1, and Sentinel-2 where execution of processes is done with a few lines of code. It works with 'image collections' that makes it easy to create a time series of images (Kennedy et al. 2018). It has been applied in various disciplines such

as global surface water change, flood mapping, crop yield estimation, among others, as outlined by Gorelick et al. (2017) (see 4.1.2).

4. METHODS

4.1. Soil moisture estimation using Sentinel-1

4.1.1. Description of the Change detection algorithm

Radar backscatter (σ^o) experiences low sensitivities to SM in areas that are vegetated because it is usually affected by surface roughness, vegetation canopy structure and water content (Link et al., 2018). Sentinel-1 radar falls in this category and therefore retrieval procedures are applied. The popular retrieval algorithms are change detection (CD), Neural Network (NN) and Support Vector Regression (SVR). In this study, the CD algorithm was applied. CD is a linear time-invariant model used to estimate soil moisture at point and local scales. Based on radar observations, at short time scales, changes occur on account of soil moisture variations while changes in surface roughness and vegetation are assumed to be constant or to vary insignificantly (Kim and Van Zyl, 2009) as indicated in Eq. (4-1). CD makes use of extensive time series of SAR measurements to obtain soil moisture from the relationship between the measured SAR backscatter and two backscatter coefficients which are based on wilting and saturation soil moisture levels (Musial et al., 2016). The change detection algorithm assumes incident angles, frost and snow detection and σ^o variation represent completely wet and dry environments.

$$VSM = \frac{\sigma^0(30,t) - \sigma^0_{dry}(30)}{\sigma^0_{wet} - \sigma^0_{dry}(30)} \qquad (4\text{-}1)$$

where, σ^0 is the backscatter measurement to be inverted, σ^0_{dry} and σ^0_{wet} are the backscattering measurements representative of a dry and a wet surface, respectively.

The σ^0 values given in decibels (DB) were converted to m^2m^{-2}. The dry reference backscatter at the local incidence angle of 30° which varies in space and time corresponds to soil wilting point and the wet reference corresponds to the soil saturation point. The VSM is usually a number between 0 and 1 but in the form of percentages. The assumption is that during no rain periods (σ^0_{dry}) and completely wet periods (σ^0_{wet}), saturation is reached and converted to volumetric Soil Moisture (VSM) content in m^3m^{-3} as indicated in Eq. (4-2).

$$VSM = (SAT - WP) * SMC + WP \qquad (4\text{-}2)$$

where VSM is used to refer to volumetric soil moisture, SAT is the saturation point at 5 cm depth representing maximum SM, WP is the wilting point at 5 cm depth representing the minimum SM, denoting the degree of saturation, SMC denotes the reference image (index).

Sentinel-1 SAR data has varying incidence angles (20 – 46°) which can alter the backscattering effect (Esa, 2012). Normalization to a reference angle to account for these effects of backscatter due to varying incidence angles, therefore, was done. By applying a simple cosine correction function related to Lambert's scattering law by Mladenova et al. (2013) as in Eq. (4-3), normalization was achieved. Scaling of the σ^o between the driest and the wettest value was done using quartile statistics of 97.5% percentile to obtain the maximum pixel value and 2.5% percentile to obtain the minimum value in the pixel. These median quartiles were chosen to ensure that any outlier was exempted from the analysis.

$$\sigma^0_{ref} = \sigma^0 \frac{cos^n(\theta_{ref})}{cos^n(\theta_{inc})} \qquad (4\text{-}3)$$

where σ^0_{ref} refers to backscatter coefficient normalized to a reference angle [m^2m^{-2}], σ^0 is the measured backscatter [m^2m^{-2}], n is the roughness coefficient taken as 1, θ_{ref} is taken as 30^0 and θ_{inc} is the incidence angle.

4.1.2. Implementation of the change detection algorithm in the Google Earth Engine platform

Using Earth Engine collection ID, Sentinel-1 Image collections from 'Copernicus/S1-GRD' were loaded and constrained to the date range from April 2016 to April 2018. The execution of the script was based on the CD algorithm discussed in 4.1.1. The image correction function was defined with a reference angle of 30^0 and a roughness coefficient of 1 (see Eq. (4-3)) after which conversion to decibels via log scaling ($10*log10(\sigma^0_{ref})$) was done. Figure 4.1 shows the Google Earth Engine interface with an image for Flevoland network captured on 22nd July 2018. An Example of sentinel-1 time series for the Raam network are shown in Appendix F.
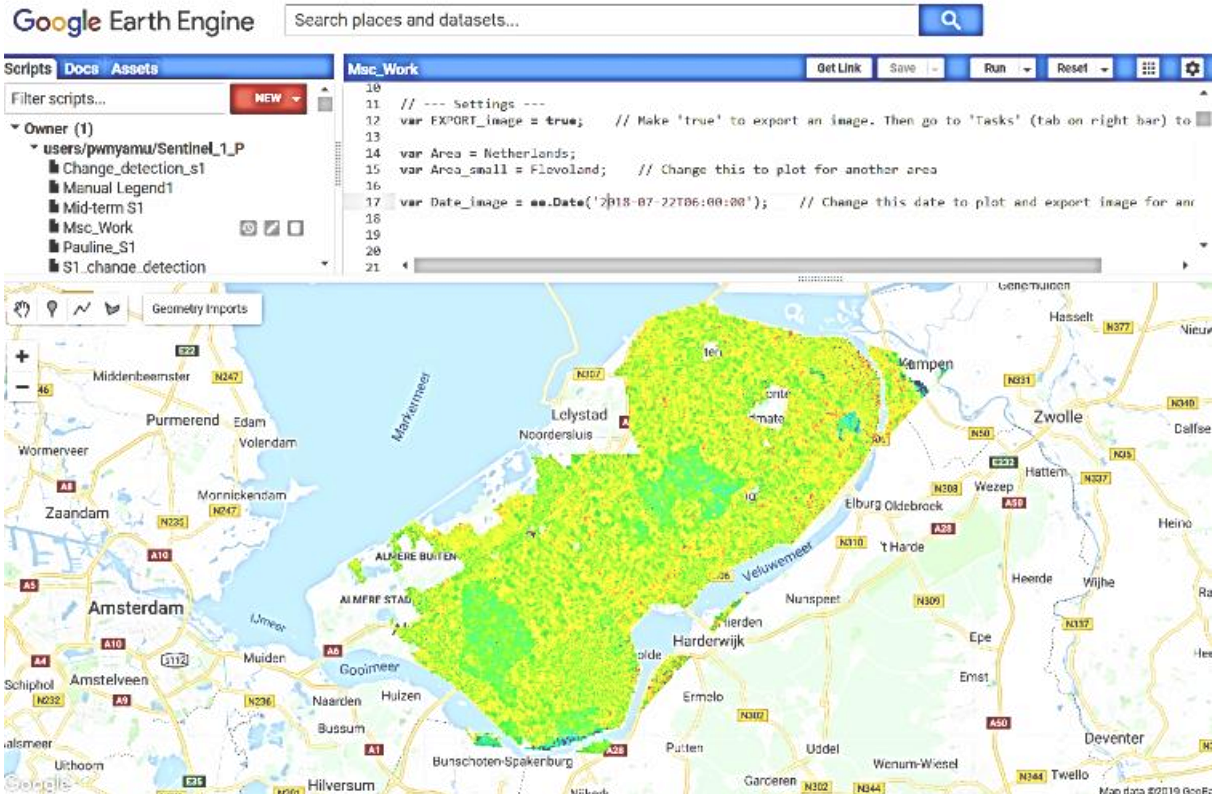
Figure 4.1: Pictorial representation of the Google Earth Engine interface showing an image for Flevoland network dated 22/07/2018.

Thresholding was performed by masking Sentinel-1 observations using the reducer functions (min and max) to obtain the dry (2.5%) and wet (97%) references. The wilting point and saturation point maps were added as layers (see Figure 2.8) and by scaling between the two, the volumetric soil moisture time series for S1 was obtained. The VV polarized images were selected for use in this study. VV polarized images are more suitable for soil moisture estimation because they suffer less from the masking effects of vegetation (Paloscia et al., 2013). The resulting VSM from Sentinel-1 were validated against *in-situ* measurements and

compared with SMAP 36 km and SMAP-E soil moisture products to assess the products' respective accuracies.

4.2. Soil moisture dry-down characterization

4.2.1. The Exponential model

Dry-downs refer to temporal evolution of surface soil moisture during rain-free days after a precipitation event (Salvia et al., 2018). Soil moisture dry downs were modeled as exponential decay functions (Shellito et al., 2016). Equation (4-4) was used to model the dry down episodes.

$$\theta_v = A * exp\left(-\frac{t}{\tau}\right) + \theta_f \qquad (4\text{-}4)$$

where θ_v is the volumetric soil moisture content at time t (m^3 m^{-3}), t is the time since the beginning of the dry-down in days, A is the amplitude representing the magnitude of SM drying in m^3 m^{-3}, τ is the dry down time scale (days) and θ_f is the final soil moisture content (m^3 m^{-3}).

The exponential decay function consists of three empirical parameters (A, τ, and θ_f) that were modelled for each dry down event. A parameter is equivalent to the difference between the moisture content observed on the first day after a rainfall event and the final moisture content at the end of the dry-down episode. Parameter A was used to determine the intensity of drying, τ to determine the drying time-scale in days and θ_f calculates the final soil moisture residual in m^3 m^{-3}. It is taken as the wilting point but depends on the length of the dry-down and whether the wilting point is achieved or not. The rate of soil drying depends upon the time window used, so the dry down events were modelled per season (Shellito et al., 2016). θ_f was constrained to 0.02 m^3 m^{-3} and above. It is worth noting that modelled θv cannot be equivalent to θ_f but the values are closer to each other.

The coefficient of determination (R^2) was calculated for each dry-down to evaluate how well the model estimates can represent the measurements. Similar to McColl et al. (2017), all the SMDD episodes with R^2 of 0.7 or more were considered for analysis. The exponential model fitting was based upon the least squares fitting method. The model parameters were chosen to minimize the sum of the squared errors between the calibrated soil moisture and SMAP 36 km, SMAP-E 9 km and *in-situ* SM. The targeted calibration parameters were fitted τ value above zero *(0)*, an A parameter corresponding to the maximum soil moisture content in the SMDD event and θ_f parameter value corresponding to the minimum value within the dry down. The study prioritized on τ parameter because it is comparable with other different data sources besides correlating well with the changing aspects of the soil moisture drying process in terms of velocity.

4.2.2. Identification of soil moisture dry down episodes

Pixel matchups between SMAP 36 km, SMAP-E and *in-situ* measurements were used for soil moisture dry-downs identification at Twente and Raam. This was done with regards to the SMAP 36 km by 36 km grid i.e., spatially averaging four SMAP-E 9 km grids and *in-situ* measurements within the 36 km. Dry downs using SMAP 36km and SMAP-E 9 km products were also modelled for the Netherlands.

Soil moisture dry-down process takes place after a rainfall event and therefore rainfall measurements were considered. So, local rainfall data from Koninklijk Nederlands Meteorologisch Instituut (KNMI) were used. To ensure a homogenous representation of rainfall, stations within or surrounding the individual networks were selected for this study analysis. For the Twente network, an average of Heino, Hupsel and

Twenthe rainfall measurements was utilized. At Raam, an average rainfall from Mill, St. Anthonis and Gemert stations were determined. An average of seven rainfall stations, which are close to the three monitoring networks facilitated dry-down identification for the Netherlands.

Similar to Shellito et al. (2016), the respective rain gauge measurements were used as a preliminary method for identifying rain-free days that coincided with the soil moisture dry-downs. The maximum soil moisture observation within the dry-down event was considered as the starting point whereas the minimum soil moisture was taken as the endpoint during rain-free events. These dry-down events were not uniform in length and therefore a threshold of at least four time-steps per event was considered. The assumption made is that for any truncation of a dry-down because of increased soil moisture could be as a result of a rainfall occurrence that had not been captured and therefore not unless the increase was more than double the UbRMSD acceptable for the SMAP mission, the time-step was considered. τ, A and θ_f values were computed for different years for each pixel based on winter and summer seasons between January 2016 and September 2018. October to May and June to September constituted the Winter and Summer seasons, respectively. Using median and mean statistical analysis, τ, A and θ_f maps were created for the Netherlands. The maps of median and mean τ were plotted with exceptions of τ values equivalent to zero (0), τ values more than 20 days, correlation coefficient >0.7, RMSD more than 0.04 m³m⁻³ and any other outliers. The maps are for the Netherlands created using SMAP 36 km and SMAP-E 9 km.

4.3. Validation matchups and evaluation metrics

4.3.1. Evaluation metrics

To carry out assessment between *in-situ* and L2-SMAP, L2-SMAP-E and Sentinel-1 data, four metrics were calculated: the coefficient of determination (R^2), Unbiased Root Mean Square Difference (UbRMSD), Root Square Mean Difference (RMSD) and the mean Difference (Bias). Though these metrics are taken as complementary, they are strongly interrelated. The Bias and RMSD are used to measure the difference between the *in-situ* soil moisture estimates and the satellite SM estimates (Entekhabi, et al., 2010). The bias is used specifically to evaluate the trend of the satellite data to show if it is a dry or a wet bias. A wet bias means that the satellite product is overestimating SM amounts, otherwise underestimating with reference to the *in-situ* measurements (Al-Yaari et al., 2014).

For the RMSD and bias indices, the closer the value obtained is to zero, then the better the performance. The magnitude of the RMSD is also affected by the bias between the satellite product and the *in-situ* measurements. This means that even though relative temporal soil moisture dynamics are reproduced perfectly if both the products being assessed have a large bias, the RMSD value will still be high (Loew et al., 2017). Globally, the user requirement for satellite soil moisture products using UbRMSD is ≤0.04m³m⁻³. The statistical scores listed in Eq. (4-5) to (4-8) are calculated and used for assessing the errors. The resulting UbRMSD was further evaluated with respect to the prevailing physical characteristics (Kolassa et al., 2018).

Bias

$$Bias = \frac{1}{n}\sum_{i=1}^{N}(\theta_s(i) - \theta_m(i)) \tag{4-5}$$

Root Square Mean Difference

$$RMSD = \sqrt{\frac{\sum_{i=1}^{N}(\theta_s(i) - \theta_m(i))^2}{N}} \tag{4-6}$$

Unbiased Root Square Mean Difference

$$ubRMSD = \sqrt{\frac{1}{N}\sum_{i=1}^{N}\left(\theta_s'(i) - (Bias) - \theta_m(i)\right)^2}$$

(4-7)

Coefficient of Determination

$$R^2 = \left(\frac{\sum_{i=1}^{N}(\theta_s'(i) - \mu_s) - (\theta_m(i) - \mu_m)}{(N-1)*\sigma_s*\sigma_m}\right)^2$$

(4-8)

where, θ_m is the *in-situ* SM observations in m³ m⁻³, N is the total number of time steps, i represent the specific time steps, θ_s is estimated VSM, θ_s' is the mean estimated SM, θ_s' is the estimated soil moisture in m³ m⁻³, σ_s is the standard deviation of estimated soil moisture in m³ m⁻³, σ_m is the standard deviation of *in-situ* observations in m³ m⁻³, μ_m is the mean value of *in-situ* observations in m³ m⁻3 and μ_s is the mean value of estimated soil moisture in m³ m⁻³.

4.3.2.   Validation matchups

Validation of the satellite products was categorized into (i) pixel matchup, (ii) network matchup. and (iii) station matchup. By pixel matchup validation process, a match of the satellite soil moisture processing extent with the location of the *in-situ* SM stations is created. In this study, SMAP 36 km by 36 km grid was taken as the reference to make a fair comparison with the other products. In network matchup validation procedure, both the satellite estimates and the *in-situ* SM estimates within each network are aggregated. Finally, station matchup involves comparing estimates from the SM-satellite products with individual stations measurements within each grid.

Spatial upscaling of the *in-situ* measurements to the satellite footprint was done using arithmetic averaging by considering the stations with complete data and those missing a few SM time series. Time series of averaged SMAP 36 km, SMAP-E 9 km, and Sentinel-1 were plotted against averaged *in-situ* measurements from each SM network. The matchups of SMAP 36 km, SMAP-E 9 km and Sentinel-1 based on the four SMAP 36 km pixels within Twente i.e., pixel (1,0), pixel (1,1), pixel (2,0), and pixel (2,1) was carried out as indicated in Figure 3.1.

5.   VALIDATION

5.1.   Pixel matchup comparison

Matchup validation metrics of the SMAP 36 km and SMAP-E 9 km with reference to the *in-situ* SM based on SMAP 36 km by 36 km grid were computed and presented in Table 5.1 for the Twente network, Table 5.2 for the Raam network and Table 5.3 for the Flevoland network. For SMAP 36 km, 356, 364, 256 and 373 data points were used while for SMAP-E 9 km 507, 441, 434 and 373 data points were used for pixel (1,0), (1,1), (2,0) and (2,1) respectively to analyze the accuracy. The number of points per pixel depends on the data latency of the *in-situ* observations. The analysis is done using performance metrics in Table 5.1 and Figure 5.1. Other scatter plots for the other pixels are shown in Appendix .

Table 5.1: Bias, UbRMSD, and R² computed for Twente SMAP 36 km and SMAP-E 9 km matchups available from April 2016 to April 2018

Stations and SMAP grids		Bias [m³ m⁻³]		UbRMSD [m³ m⁻³]		R²[-]	
Twente SM stations	SMAP grid	SMAP 36 km	SMAP-E 9 km	SMAP 36 km	SMAP-E 9 km	SMAP 36 km	SMAP-E 9 km
ITCSM15,16,17,18	(1,0)	0.021	0.012	0.074	0.074	0.67	0.632
ITCSM5,10,12,13,14	(1,1)	-0.032	0.022	0.067	0.096	0.657	0.537
ITCSM1,2,3,7	(2,0)	0.021	-0.004	0.056	0.056	0.751	0.744
ITCSM4,8,9	(2,1)	-0.101	-0.061	0.073	0.07	0.618	0.621
Average		-0.023	-0.006	0.068	0.074	0.674	0.633

The accuracy in terms of the UbRMSD in all the pixels is not within the SMAP acceptable requirement of ≤0.04 m³ m⁻³ but closer. Both SMAP products reported the best SM estimates in pixel (2,0) with an accuracy of 0.056 m³ m⁻³ and R² of 0.751 and 0.744 in SMAP 36 km and SMAP-E 9 km, respectively. The SMAP 36 km and SMAP-E were found to over-estimate the SM measurements in pixel (2,1) by -0.101 and -0.061 m³ m⁻³, respectively. SMAP-E had the least bias at pixel (2,0) compared to the rest of the pixels. On average, SMAP 36km performs better than the rest of the products.

The accuracy levels witnessed could be due to the poor spatial representation of stations (for example, the highest number of stations of up to 5 number are in pixel 1,1 at Twente network. This does not meet the threshold argued in Brocca et al. (2017) that each pixel should contain 8 stations for SMAP 36 km and 5 stations for SMAP-E 9 km in order to obtain a good accuracy level. This sparsity of the *in-situ* stations in relation to the SMAP footprint scale could also contribute to the mismatch in performance as observed in Crow et al. (2012). The results are, however, comparable to those of O'neill et al. (2016) who carried out validation of the SMAP level 2 version 5 and SMAP-E level 2 version 2 and obtained accuracies of between 0.5 and 0.7 m³ m⁻³ and R² of between 0.7 and 0.8 at Twente network.

The satellite retrievals per individual pixel are plotted against the *in-situ* observations located within the pixel in Figure 5.1. The slope for SMAP (pixel 2,1) shows less correlation at only 0.508 and a y-intercept of 0.059 translating to reduced UbRMSD and R² compared to the other plotted pixels. Most of the data points are away from the 1:1, leaning towards the *in-situ* SM measurements. The rest of the plots show that both the *in-situ* and the satellite estimates are centered on the 1:1 line with a few outliers. Scatter plots for pixel 1,0 and 1,1 as shown in Appendix A.
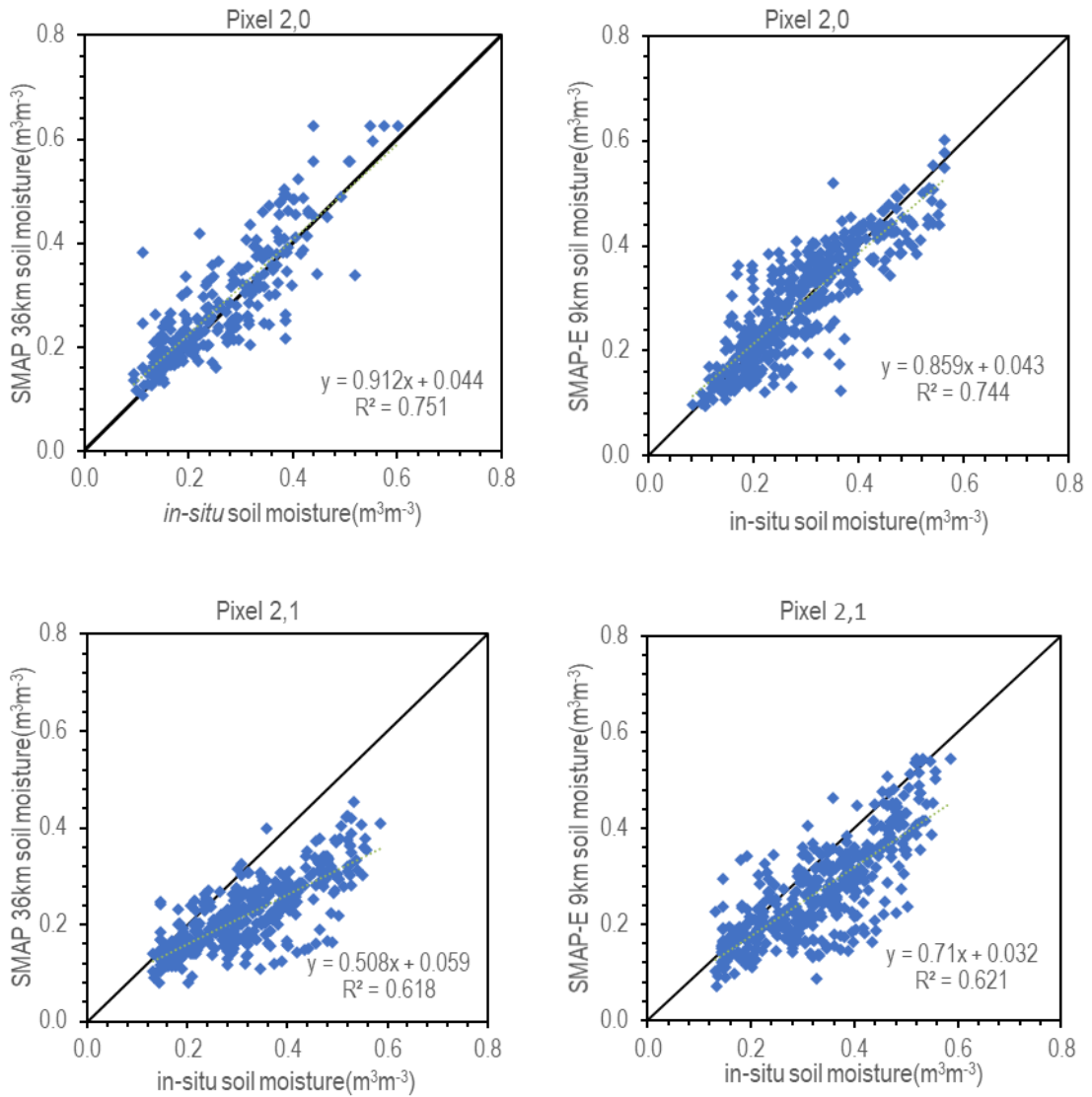
Figure 5.1: Scatter plots of SMAP 36 km and SMAP-E 9 km versus the *in-situ* soil moisture measurements at Twente network. at. pixel (2,0) and b. pixel (2,1).

At Raam SM network, one SMAP 36 km pixel and six SMAP-E 9 km cover the entire network. The matchup was based upon SMAP 36 km grid (pixel 0,0) as presented in Table 5.2. For SMAP 36 km, 269 data points were used while for SMAP-E 9 km, 302 data points were used instead.

Table 5.2: Bias, RMSD, UbRMSD, and R^2 computed for SMAP 36 km and SMAP-E 9 km matchups available from April 2016 to April 2018 for all Raam stations.

Stations	SMAP grid	Bias [$m^3 m^{-3}$]		UbRMSD [$m^3 m^{-3}$]		R^2[-]	
All	(0,0)	SMAP 36 km	SMAP-E 9 km	SMAP 36 km	SMAP-E 9 km	SMAP 36 km	SMAP-E 9 km
	(0,0)	0.094	0.094	0.069	0.060	0.681	0.694

The ubRMSD of SMAP-E at 0.06$m^3 m^{-3}$ and R^2 of 0.694 is slightly better than that of SMAP 36 km which is 0.069m^3m^{-3} and R^2 of 0.681 at the Raam SM network. The UbRMSD for both products were close to the SMAP acceptable accuracy requirement of ≤0.04$m^3 m^{-3}$. The R^2 for SMAP-E was better than that of

SMAP 36 km. Visually inspecting the plots in Figure 5.2, it can be observed that both SMAP 36 km and SMAP-E are over-estimating SM amounts. Even though this is the first attempt when these products are being validated for the Raam SM network, the obtained performance seem quite promising. The scatters at for both SMAP 36 km and SMAP-E 9 km do not fall exactly on the 1:1 line which simplifies the slope but leans more towards the SMAP products. This represents a wet bias being observed at Raam.
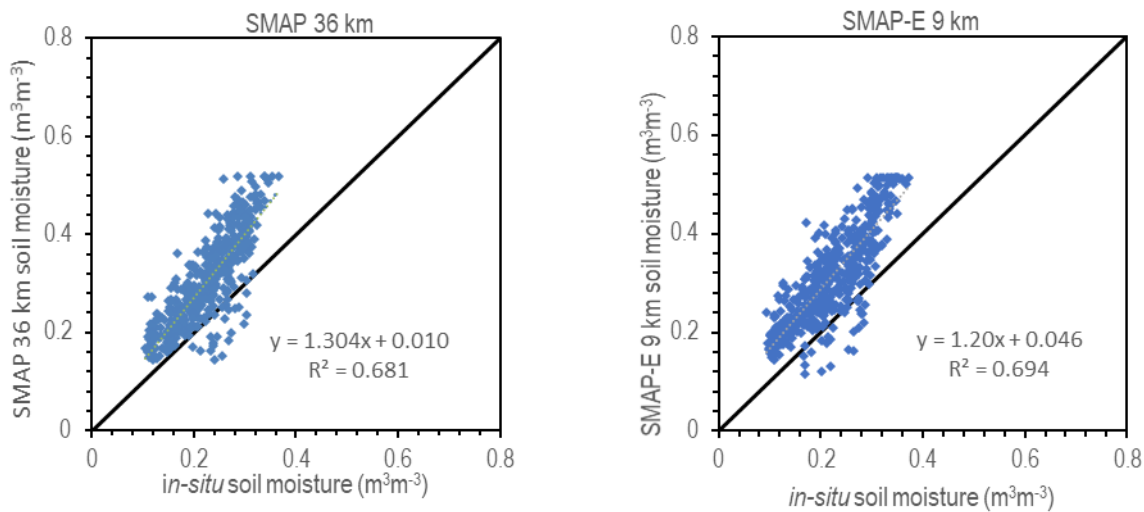
Figure 5.2: Correlation between *in-situ* SM and SMAP 36 km and SMAP-E 9 km at Raam SM network

For Flevoland SM network, one SMAP 36 km grid and two SMAP-E 9 km covers the entire network. The matchup consisted of one SMAP 36 km pixel by which through spatial averaging of the satellite estimates and the *in-situ* measurements, the accuracy was evaluated with resulting metrics presented in Table 5.3. For SMAP 36 km, 334 data points were used while for SMAP-E 9 km, 183 data points were used instead. SMAP-E 9 km with an UbRMSD of 0.048m^3 m^{-3} performs slightly better than SMAP 36 km which has an UbRMSD of 0.058 m^3 m^{-3}. The R^2 is below the acceptable limit of 0.6 with SMAP 36 km showing a better trend. Though the SMAP-E 9 km accuracy is better than that of the SMAP 36 km, its bias at 0.1 m^3 m^{-3} and R^2 at 0.167 are poor compared to SMAP 36 km. This could be attributed to the data gaps within the *in-situ* data set and the satellite products. The SM time series had erroneous data entries that had to be flagged mostly during summer and winter periods of 2016 and 2017. The time series had almost constant values of about 0.5m^3 m^{-3} causing inconsistencies. Scatter plots between SMAP and SMAP-E with *in-situ* SM measurements at Flevoland are indicated in Figure 5.3. The slope for the SMAP 36km and the *in-situ* SM is quite good almost falling exactly with the 1:1 line but falling more towards the SMAP side. For the SMAP-E 9km, an over-estimation is quite spontaneous. The scatters are towards the SMAP-E more than on the *in-situ* side, showing that generally, the products are over-estimating SM in this network.

Table 5.3: Bias, ubRMSD, and R^2 computed for Flevoland SM measurements and SMAP 36 km and SMAP-E 9 km matchups available from April 2016 to April 2018.

Stations	SMAP grid	Bias [m^3 m^{-3}]		UbRMSD [m^3 m^{-3}]		R^2[-]	
All	(0,0)	SMAP 36 km	SMAP-E 9 km	SMAP 36 km	SMAP-E 9 km	SMAP 36 km	SMAP-E 9 km
	(0,0)	0.053	0.088	0.058	0.048	0.508	0.167
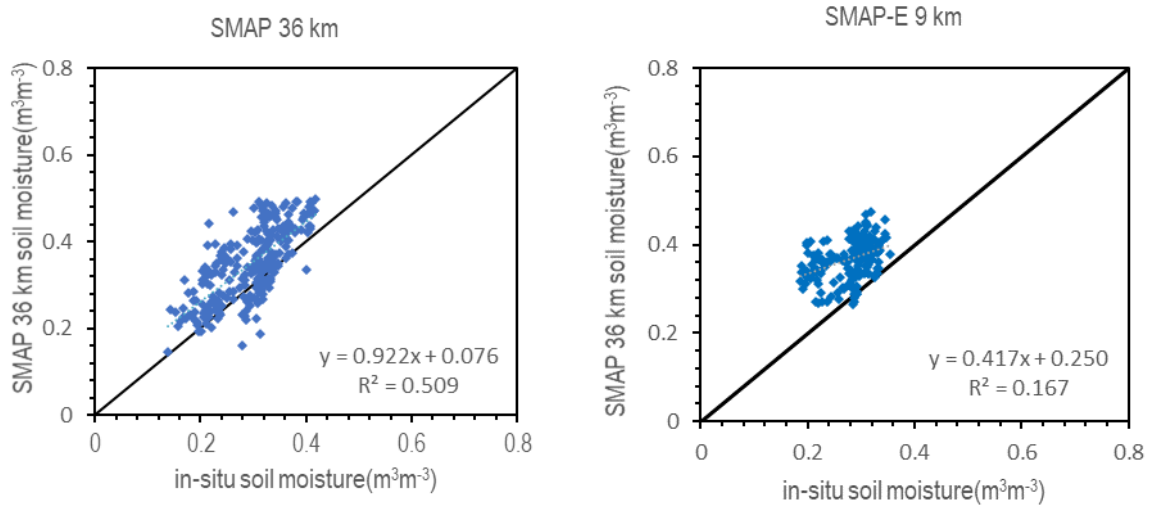
Figure 5.3: Correlation between SMAP 36 km and SMAP-E 9 km with the *in-situ* soil moisture measurements at Flevoland network.

5.2. Soil moisture network matchup validation

Comparisons were also done based on spatial averaging of all the *in-situ* measurements and the satellite estimates within each network. In this section, both SMAP products and sentinel-1 SAR are validated. against *in-situ* measurements. Time series plots for each product and each network are presented to show the correlations and the trends of the satellites with the *in-situ* measurements (see Figure 5.4, Figure 5.5 and Figure 5.6. Soil moisture content depends on the spatial precipitation patterns and therefore the plots were built using the average precipitation from Heino, Twente, and Hupsel stations that lie within the vicinity of the Twente network. High moisture content is generally experienced during the winter periods (December to March) while lower levels are seen in summer (July to September) observed from Figure 5.4. From the plots, there is a good agreement of the satellite estimates with the *in-situ* measurements apart from sentinel -1 product roughly between January and March where there is a larger difference.

SMAP 36 km outperformed the other two SM products at Twente network with an accuracy of 0.047m^3 m^{-3}. Accuracies of SMAP-E 9 km and Sentinel-1 were 0.053 and 0.095 m^3 m^{-3}, respectively. R^2 for both SMAP 36 km and SMAP-E 9 km were quite good but drastically deteriorated for Sentinel-1 product (see Table 5.4). The Sentinel-1 largely under-estimates the moisture content, with respect to the *in-situ* measurements for Twente network. Both SMAP 36 km and SMAP-E 9 km reported the least bias. On the contrary, Sentinel-1 had the largest bias emanating from the months of October 2017 to March 2018. Snow accumulations could be a probable cause of low prediction accuracy as depicted between in the months of January and February in Figure 5.4. Both SMAP 36 km and SMAP-E 9 km reported the least bias. On the contrary, Sentinel-1 had the largest bias emanating from the months of October 2017 to March 2018. The three satellite products show a good agreement with the prevailing meteorological conditions in all the seasons in the Netherlands.

During the analysis, no ancillary information either from optical remote sensing or landcover was used to correct for the vegetation and roughness effects. The underlying conditions on this network in terms of vegetation and soil texture are highly variable and this could have contributed to the poor performance exhibited by Sentinel-1 SM estimates, a similar finding by Paloscia et al. (2013). Snow accumulations could be a probable cause of this low prediction accuracy as depicted between the months of January and February in Figure 5.4.

During the analysis, no ancillary information either from optical remote sensing or landcover was used to
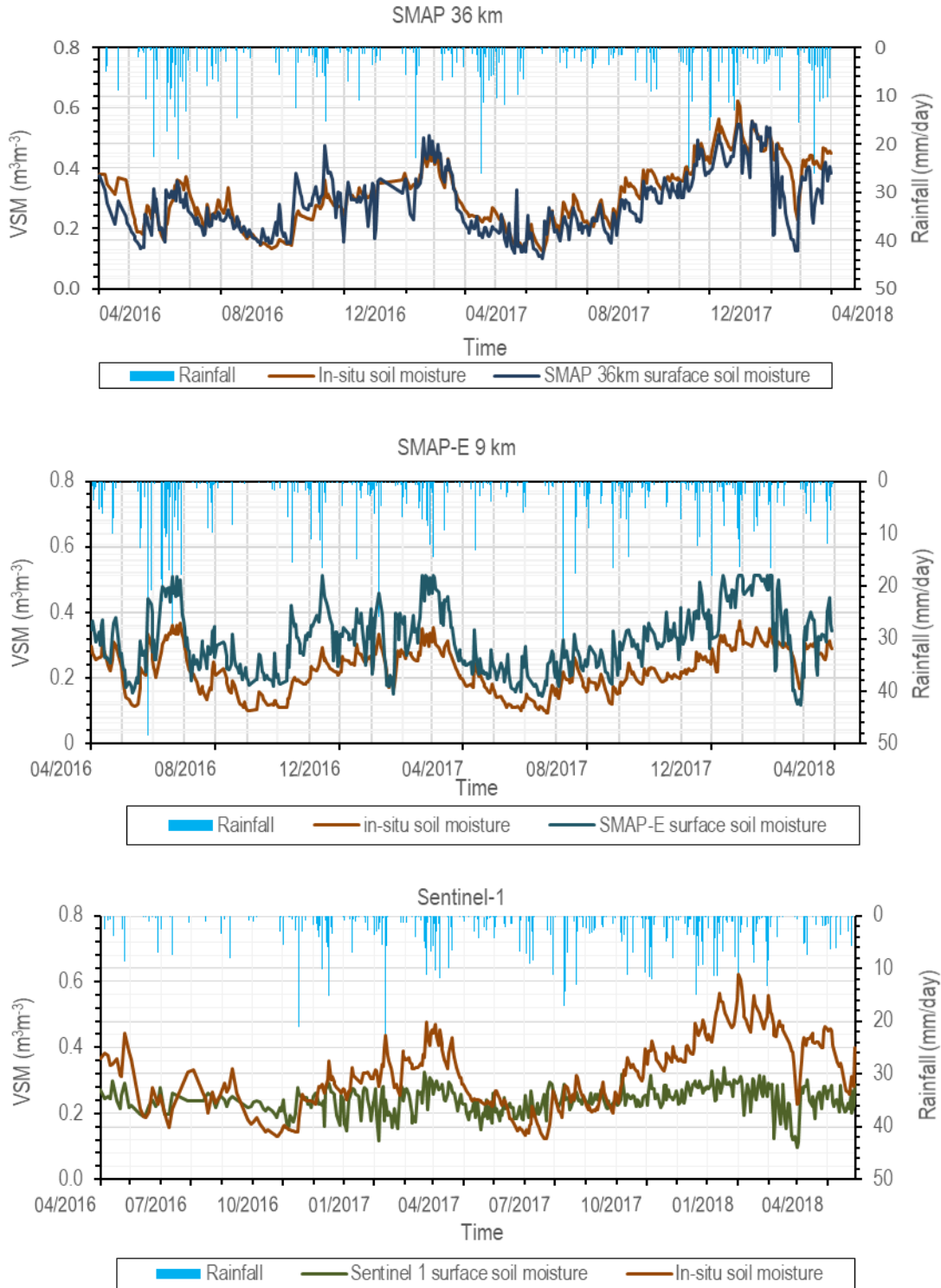
Figure 5.4: Time series showing the averaged satellite products soil moisture and averaged *in-situ* SM Twente SM network and rainfall data for Twente KNMI station.

Table 5.4: Bias, UbRMSD, and R2 computed for Twente, Raam and Flevoland SM networks to show the accuracy between SMAP 36 km, SMAP-E 9 km and Sentinel-1 for the period between April 2016 to April 2018.

SM network	Bias [$m^3 m^{-3}$]			UbRMSD [$m^3 m^{-3}$]			R^2[-]		
	SMAP 36 km	SMAP-E 9 km	Sentinel-1	SMAP 36 km	SMAP-E 9 km	Sentinel-1	SMAP 36 km	SMAP-E 9 km	Sentinel-1
Twente	-0.003	-0.002	-0.081	0.047	0.053	0.095	0.795	0.775	0.216
Raam	0.079	0.093	0.011	0.054	0.050	0.064	0.681	0.694	0.174
Flevoland	0.047	0.085	-0.024	0.056	0.060	0.053	0.472	0.246	0.495
Average	0.038	0.045	-0.031	0.052	0.054	0.095	0.650	0.570	0.290

For Raam SM network, the time series of average rainfall measurements from Mill, Gemert, St Anthonis were used. From the graphs (Figure 5.4), a good agreement between the SM *in-situ* measurements and the satellite estimates prevails. There is a matching response between the soil moisture and the rainfall measurements. A better match is seen with SMAP 36 km as compared to the rest two. SMAP-E retrievals are good but highly over-estimated.

SMAP-E 9 km at this network slightly outperformed the other two SM products with UbRMSD of 0.054m³ m⁻³ but indicated the largest bias of 0.108 m³ m⁻³ as summarised in Table 5.4. This is a wet bias which through the application of the bias correction techniques, the accuracy would improve. R² for Sentinel-1 lagging behind that of SMAP-E and SMAP 36 products at only 0.174, which is a similar observation also made at the Twente SM network. Their UbRMSD are all close to the SMAP accuracy requirement but SMAP-E 9 km performs better in this network. Every SM satellite product assessed for this SM network overestimated SM amounts. The imprecise detection of SM estimates could be explained by the presence of different agricultural areas. In Colliander et al., (2017), SMAP 36 km sensor is reported to have difficulties in precisely detecting SM over agriculturally-based areas. Further, resulting bias can be attributed to retrieval issues during crops emergence and insensitivities during the growing period; thus, leading to overestimation of SM amounts by the products witnessed. The SMAP grid in this network is dominated by grass in most of the stations but in some of the stations the adjacent crops are different, for example, in station Rm2, Rm8 and Rm9 there are sugar beets while at stations Rm5, Rm7, Rm11, and Rm13 there are a mixture of corn, grass, onions and chicory vegetation whose growing trends are different and therefore could affect the amount of VSM being detected by the sensor.
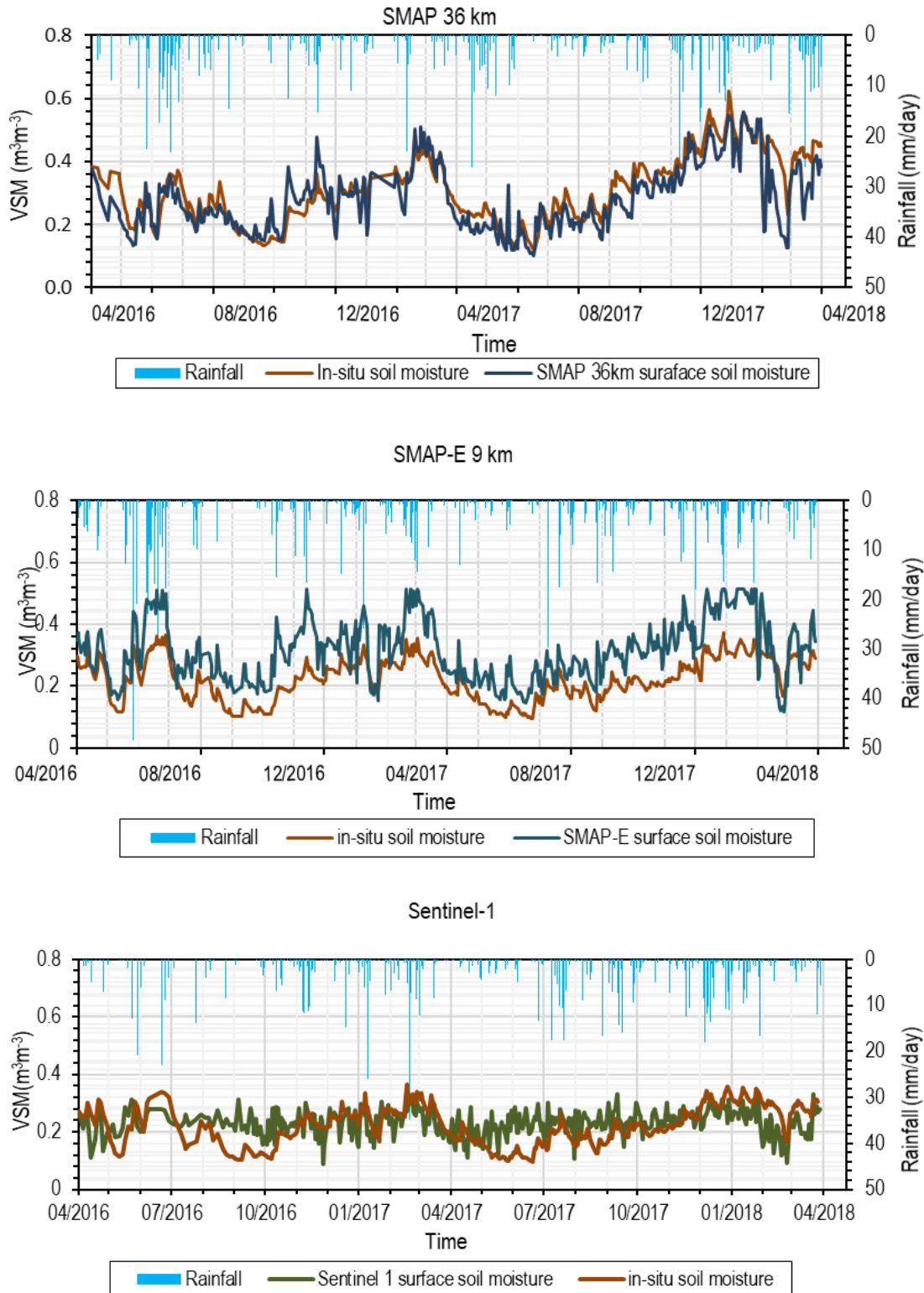
Figure 5.5: Time series showing the comparison of SMAP 36 km, SMAP-E 9 km, and Sentinel-1 SM satellite estimates and averaged *in-situ* SM at Raam SM network and rainfall estimates for Mill, Gemert and St Anthonis stations.

For the Flevoland network, Dronten station rainfall measurements from KNMI were used to show the trend between rainfall and soil moisture. The time series plots in this network show a good agreement with *in-situ* SM measurements although there are small over-estimations and under-estimations seen at
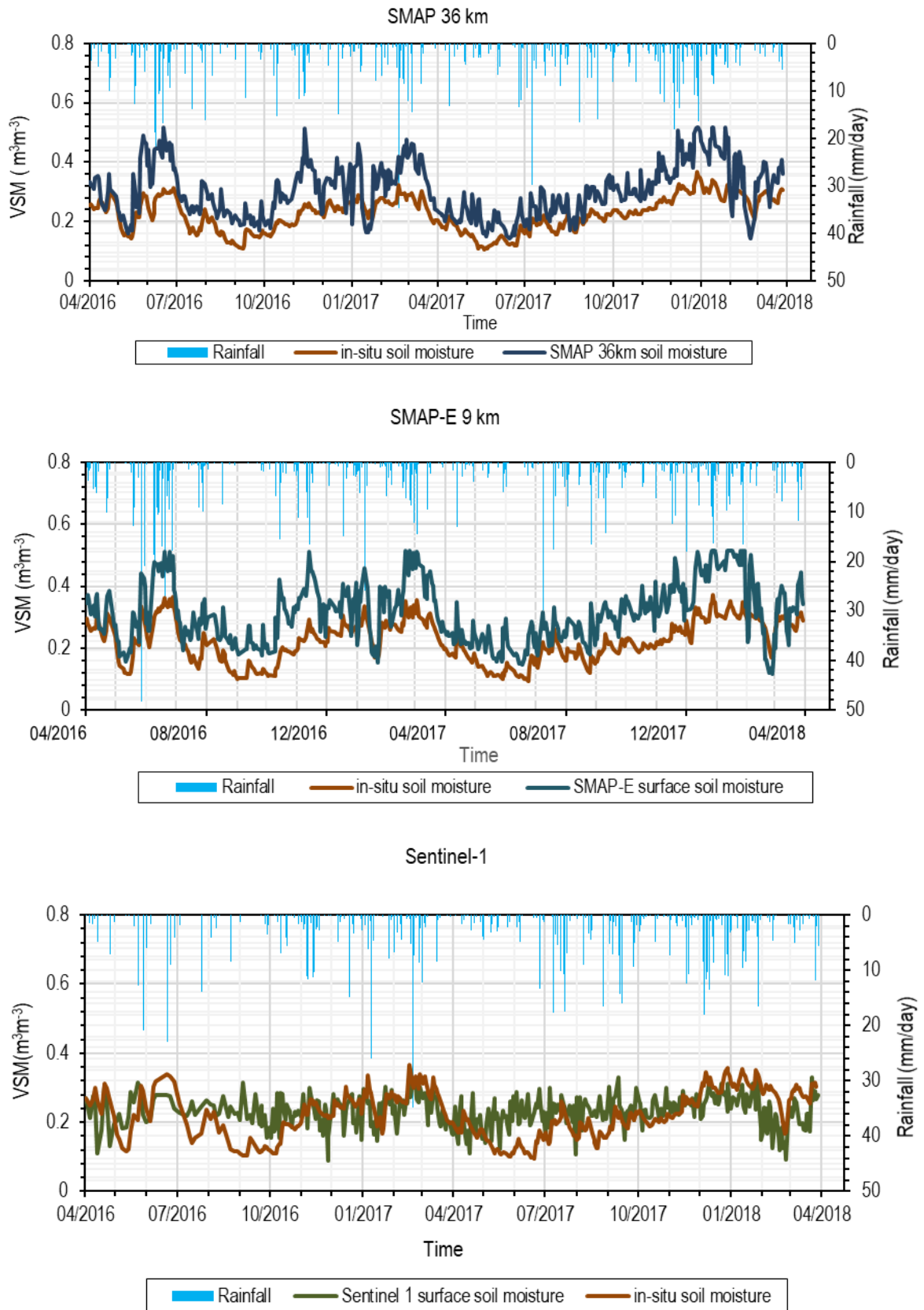
Figure 5.6: Comparison of SMAP 36 km, SMAP-E 9 km and Sentinel-1 SM satellite estimates and averaged *in-situ* SM for Flevoland network and rainfall data for Dronten KNMI station.

different times of the year. This scenario is not so different from other networks. Based on UbRMSD, Sentinel-1 performed better than SMAP and SMAP-E. The SMAP accuracy obtained fell short of SMAP mission target exceeding the 0.04 m3 m-3 limit but remained within a close range. SMAP-E had the least R2 (0.246) compared to the other two products as summarised in Table 5.4. Both SMAP and SMAP-E overestimated SM measurements while Sentinel-1 reported an underestimate for this SM network. In the month of January and February of 2018, the satellite estimates portrayed a very good agreement with the in-situ measurements (Figure 5.6). The surface roughness at Flevoland in terms of vegetation seems to be moderate. This could have contributed to the better accuracy reported by Sentinel-1 product.

The UbRMSD and R^2 of the three SM products were graphically generated (in Figure 5.7) to investigate the best performing product per network. Results indicate that SMAP 36km, SMAP-E, and Sentinel-1 outperformed other products at the Twente, Raam and Flevoland SM networks, respectively - their respective UbRMSD were 0.047, 0.05 and 0.053 m^3m^{-3} while R^2 are 0.79, 0.69 and 0.5. There is a variation in performance of each product per SM network that can be attributed to underlying soil moisture variability in terms of vegetation cover and surface roughness. For example, Flevoland network is dominated by similar grassland and clay soil texture where Sentinel-1 is the best performing product out of the three assessed. In general, the product in decreasing order of performance was found to be SMAP 36 km (UbRMSD of 0.52 m^3 m^{-3} and R^2 of 0.65), SMAP-E 9 km (UbRMSD of 0.054 m^3 m^{-3} and R^2 of 0.57), and lastly Sentinel-1 (UbRMSD of 0.095m^3 m^{-3} and R^2 of 0.29). These results were determined by averaging the performance of each product at all the sites. This average-based SM validation has captured the soil moisture variations (both wetting and drying) better than the average resulting from individual stations in Table 5.5.
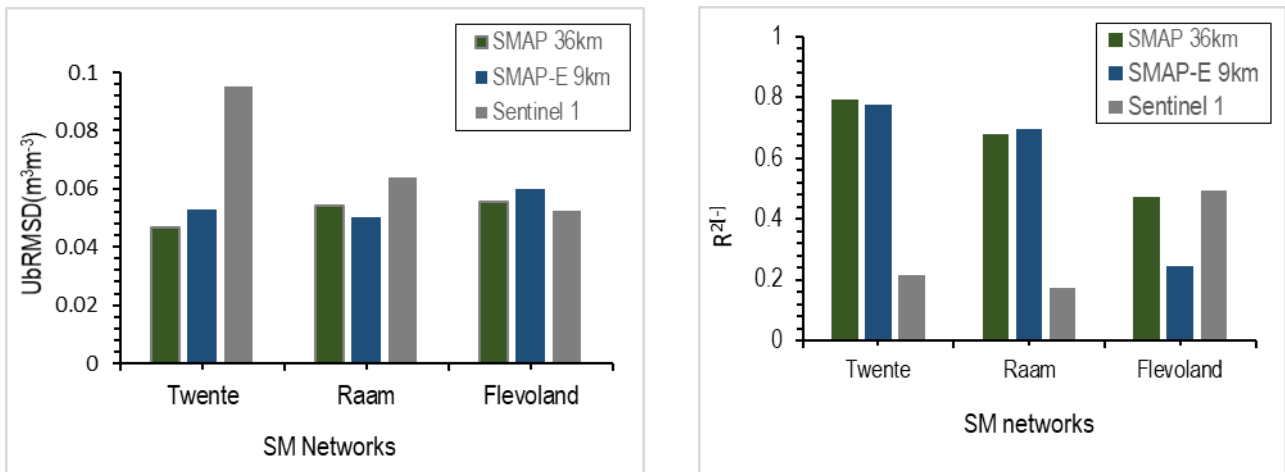
Figure 5.7: Statistical comparison based on aggregated UbRMSD and R^2 for Twente, Raam, and Flevoland SM networks.

5.3. Soil moisture station matchup comparison

Each individual station SM time series from the three networks considered was compared with the satellite estimates to check their performance on an individual basis. N in Table 5.5 represents the number of data points used to calculate the accuracy. For Twente network, the best performing station was ITCSM7 for both SMAP 36 km and SMAP-E 9 km while for Sentinel-1, ITCSM13 was the best in performance although the accuracy was less than the expected target of 0.04 m^3 m^{-3}. Based on averages, SMAP 36 km with an accuracy of 0.070 m^3 m^{-3} and R^2 of 0.69 outperformed the other products as summarised in Table

5.5. For Raam network, Raam15 performs best in both SMAP 36 km and SMAP-E 9 km at 0.057m³ m⁻³ and 0.06m³ m⁻³, respectively, while Raam7 performs the best for Sentinel-1 at 0.046m³ m⁻³ as shown in Table 5.6. On average, SMAP-E 9 km at 0.077m³ m⁻³ and R^2 of 0.488 outperformed the other SM products at Raam network. For Flevoland, out of the two SM networks, both FP01 and FP02 have similar accuracy for SMAP 36 km (0.081 m³ m⁻³), while FP02 performs the best in both SMAP-E 9 km (0.067 m³ m⁻³) and Sentinel-1 (0.05 m³ m⁻³) as shown in Table 5.7. On average, Sentinel-1 with an accuracy of 0.057 m³ m⁻³ and R^2 of 0.30 was ranked the best for the network.

The largest bias in decreasing order with respect to SMAP 36 km, SMAP-E 9 km, and Sentinel-1 is shown by stations ITCSM4, ITCSM14, ITCSM5, ITCSM13, ITCSM17 and ITCSM8. The ITCSM2, ITCSM3, ITCSM15, ITCSM16 and ITCSM18 stations show a large bias with Sentinel-1 SM estimates. at Twente network. Rm9 has the largest wet bias while Rm1 has the least bias for all the three products except for Sentinel-1 that had a large dry bias. As found from Figure 2.2, Rm09 the wettest station and Rm01 the driest station, it could be translated to mean that satellite retrievals over wet soils are more than on dry soils. From a keen focus on other stations at the Raam SM network, satellite products are overestimating the SM amounts at most of the stations. A few examples are Rm13, Rm10, Rm3, Rm2, and Rm8. At Flevoland SM network, SMAP 36 km and SMAP-E 9 km overestimated the SM estimates with a huge bias while Sentinel-1 underestimated the SM amounts with a small bias margin. At FP02, SMAP-E had the largest bias of 0.109 m³ m⁻³ while at FP01, the largest bias of 0.076 m³ m⁻³ was reported by SMAP 36 km. From the results based on station matchup comparisons, the UbRMSD is lower compared to the one obtained using network matchup. This can also be seen from the averaged accuracy at each network (station matchup). This could be attributed to the scale mismatch problem.

Table 5.5: Validation based on each individual station and an average of all at Twente network.

Station	UbRMSD [m³ m⁻³]			R^2[-]			N		
	SMAP 36 km	SMAP-E 9 km	Sentinel-1	SMAP 36 km	SMAP-E 9 km	Sentinel-1	SMAP 36 km	SMAP-E 9 km	Sentinel-1
ITCSM1	0.079	0.074	0.072	0.533	0.524	0.114	413	434	426
ITCSM2	0.085	0.084	0.131	0.657	0.664	0.195	413	434	426
ITCSM3	0.088	0.092	0.144	0.670	0.655	0.237	256	404	257
ITCSM4	0.145	0.130	0.166	0.508	0.572	0.159	410	433	257
ITCSM5	0.153	0.152	0.115	0.505	0.490	0.165	382	409	244
ITCSM7	0.064	0.055	0.078	0.695	0.716	0.290	413	434	426
ITCSM8	0.073	0.083	0.080	0.345	0.410	0.156	376	399	409
ITCSM9	0.065	0.064	0.084	0.545	0.622	0.211	413	439	426
ITCSM10	0.076	0.077	0.080	0.495	0.490	0.241	401	423	419
ITCSM12	0.113	0.116	0.155	0.476	0.456	0.117	413	441	426
ITCSM13	0.067	0.071	0.068	0.588	0.553	0.176	413	492	426
ITCSM14	0.110	0.093	0.119	0.303	0.541	0.142	403	518	400
ITCSM15	0.078	0.079	0.099	0.612	0.572	0.141	403	479	400
ITCSM16	0.087	0.091	0.146	0.688	0.651	0.260	369	426	353
ITCSM17	0.135	0.148	0.117	0.152	0.040	0.063	400	508	396
ITCSM18	0.070	0.072	0.115	0.708	0.690	0.198	400	516	396
Average	0.093	0.093	0.111	0.530	0.540	0.179			

Table 5.6: Validation based on each individual station and an average of all at Raam network.

Station	UbRMSD [m³ m⁻³]			R²[-]			N		
	SMAP 36km	SMAP-E 9 km	Sentinel-1	SMAP 36 km	SMAP-E 9 km	Sentinel-1	SMAP 36 km	SMAP-E 9 km	Sentinel-1
Rm1	0.068	0.070	0.082	0.473	0.471	0.107	420	447	125
Rm2	0.065	0.065	0.063	0.499	0.544	0.123	429	456	395
Rm3	0.065	0.068	0.064	0.545	0.525	0.095	238	349	395
Rm4	0.063	0.062	0.062	0.526	0.584	0.110	469	506	232
Rm5	0.104	0.075	0.057	0.018	0.414	0.075	388	416	378
Rm7	0.100	0.066	0.046	0.010	0.613	0.257	452	506	405
Rm8	0.111	0.066	0.086	0.078	0.599	0.125	452	506	405
Rm9	0.076	0.085	0.067	0.334	0.303	0.042	452	528	416
Rm10	0.061	0.071	0.067	0.551	0.526	0.139	469	514	416
Rm11	0.080	0.082	0.072	0.315	0.376	0.085	426	470	374
Rm12	0.134	0.138	0.174	0.417	0.384	0.021	415	465	361
Rm13	0.096	0.102	0.112	0.404	0.341	0.067	415	468	372
Rm14	0.060	0.067	0.071	0.570	0.506	0.122	453	509	400
Rm15	0.057	0.060	0.091	0.682	0.649	0.159	469	528	416
Average	0.082	0.077	0.079	0.387	0.488	0.109			

Table 5.7: Validation results based on each individual station and the average for the two stations at Flevoland.

Station	UbRMSD [m³ m⁻³]			R²[-]			N
	SMAP 36 km	SMAP-E 9 km	Sentinel-1	SMAP 36 km	SMAP-E 9 km	Sentinel-1	
FP01	0.081	0.073	0.065	0.359	0.275	0.408	334
FP02	0.081	0.067	0.050	0.241	0.060	0.394	383
Average	0.081	0.070	0.057	0.300	0.168	0.401	

5.4. Seasonal-based comparisons.

Validation metrics were compared for both summer and winter and on yearly basis at Twente, Raam, and Flevoland as displayed in Table 5.8. Based on each particular year (2016-2018), the performance metrics are shown in Appendix D. In the case of seasonal comparisons, for summer season the months of July to September applied while for the winter season the months of December to March. were adopted. SMAP 36 km shows improved performance in summer attaining SMAP accuracy requirement at Twente network. Its R^2 is also good (above 0.6) apart from Flevoland network. SMAP-E 9 km performance in summer also improves greatly attaining the SMAP mission UbRMSD within 0.04 m³m⁻³ but its R^2 at Flevoland is very low (0.028). For Sentinel-1, the performance is better in winter than in summer at both Raam and Flevoland but at Twente network, UbRMSD is better in summer. Good performance in winter also applies in its R^2. It is also good to note that with Sentinel-1, both winter and summer, a dry bias is recorded.

Generally, an improved performance resulted when the satellite products were compared with their *in-situ* counterparts in summer than in winter. Overall performance for SMAP 36 km in terms of UbRMSD at Twente network was 0.047, SMAP-E 9 km was 0.053 and Sentinel-1 was 0.095 for S1 in Table 5.2 but these results improved to UbRMSD of 0.033, 0.039 and 0.050, respectively, in summer. For Raam and Flevoland SM networks, there is a slight improvement in R^2 in both SMAP and SMAP-E probably imposed by the presence of wet and bare land conditions in winter and presence of vegetation in the fields over summer periods which attenuates the signals. For Sentinel-1, the dilapidation observed in summer at Raam and Flevoland SM networks could be as a result of the vegetation effect.

The performance metrics on yearly basis also slightly improves especially the SMAP 36km. Time series plots based on each individual year for the SMAP products (Appendix D) shows a good agreement.

Table 5.8: The performance of the satellite products in terms of Bias, UbRMSD and R^2 at Twente, Raam and Flevoland for winter and summer periods between 2016 and 2017

product	seasons	Bias [m³m⁻³]			UbRMSD[m³m⁻³]			R²[-]		
		Twente	Rm	FP	Twente	Rm	FP	Twente	Rm	FP
SMAP	Winter	-0.047	0.064	0.037	0.078	0.032	0.050	0.489	0.667	0.624
	Summer	-0.028	0.085	0.082	0.033	0.047	0.053	0.745	0.602	0.205
SMAP-E	Winter	-0.035	0.086	-0.105	0.080	0.077	0.220	0.540	0.722	0.326
	Summer	-0.015	0.081	0.131	0.039	0.030	0.050	0.588	0.700	0.028
S-1	Winter	-0.166	-0.008	-0.043	0.071	0.049	0.043	0.205	0.266	0.608
	Summer	-0.009	0.044	-0.005	0.050	0.050	0.055	0.248	0.172	0.431

6. DRYDOWNS IDENTIFICATION AND CHARACTERIZATION

6.1. Soil moisture dry-downs detection by individual pixel matchups

In this section, the results and analysis of the soil moisture dry downs are presented for the year 2018. Pixel matchup was made with reference to SMAP 36 km by 36 km grid as discussed in 5.1. This is an average of SMAP-E pixels and *in-situ* measurements within SMAP 36 km. Here, we have four pixels at Twente network – pixel (1,0); pixel (1,1); pixel (2,0) and pixel (2,1). A time series of the SMDD and their respective model fits were plotted per pixel.

Figure 6.1 shows two examples of the modeled and observed VSM time series for *pixel 2,0* and *2,1*. A good agreement on the SSM dynamics can be deduced, in that lower minimum values are observed in and towards summer while larger maximum values are observed at the onset of the year. The crosses of different colors represent the VSM while the full lines represent the model fits. For the two pixels, between January and September 2018, each contains three matchup real dry downs i.e., dry downs falling within the same period for the three SM products. On average, the Twente network has six to seven dry-downs which varies per SM product. For instance, *in-situ* soil moisture has a greater number of dry-down events than SMAP products. For pixel 2,1, in the month of March, July and August *in-situ* measurements recorded a dry-down while the SMAP products show no dry-down. In pixel (2,0), SMAP 36 km has not recorded dry-downs equally with the *in-situ* observations and SMAP-E 9 km.

The drying timescale for SMAP 36 km is more rapid as compared to the rest of the products but it closely matches with SMAP-E 9 km. A keen visualization of Figure 6.1 shows that *in-situ* observations tend to dry more rapidly than the satellite-based SM products towards the summer seasons. Also, their dry-down occurrence is more frequent than satellite SM products. According to Shellito et al. (2016), τ decreases as the aridity increases. Soils will lose more water more readily to the atmosphere when the temperatures are increasing because ET by then is hindered by water availability. This observation could also explain why Ford et al. (2015) used *in-situ* measurements to monitor flash droughts in the U.S.A. Though SM dry-downs are spatially and temporally variable, the value of τ is strongly variant in all the pixels throughout all the seasons as summarised in Table 6.1. They are both seasonal and location dependent.
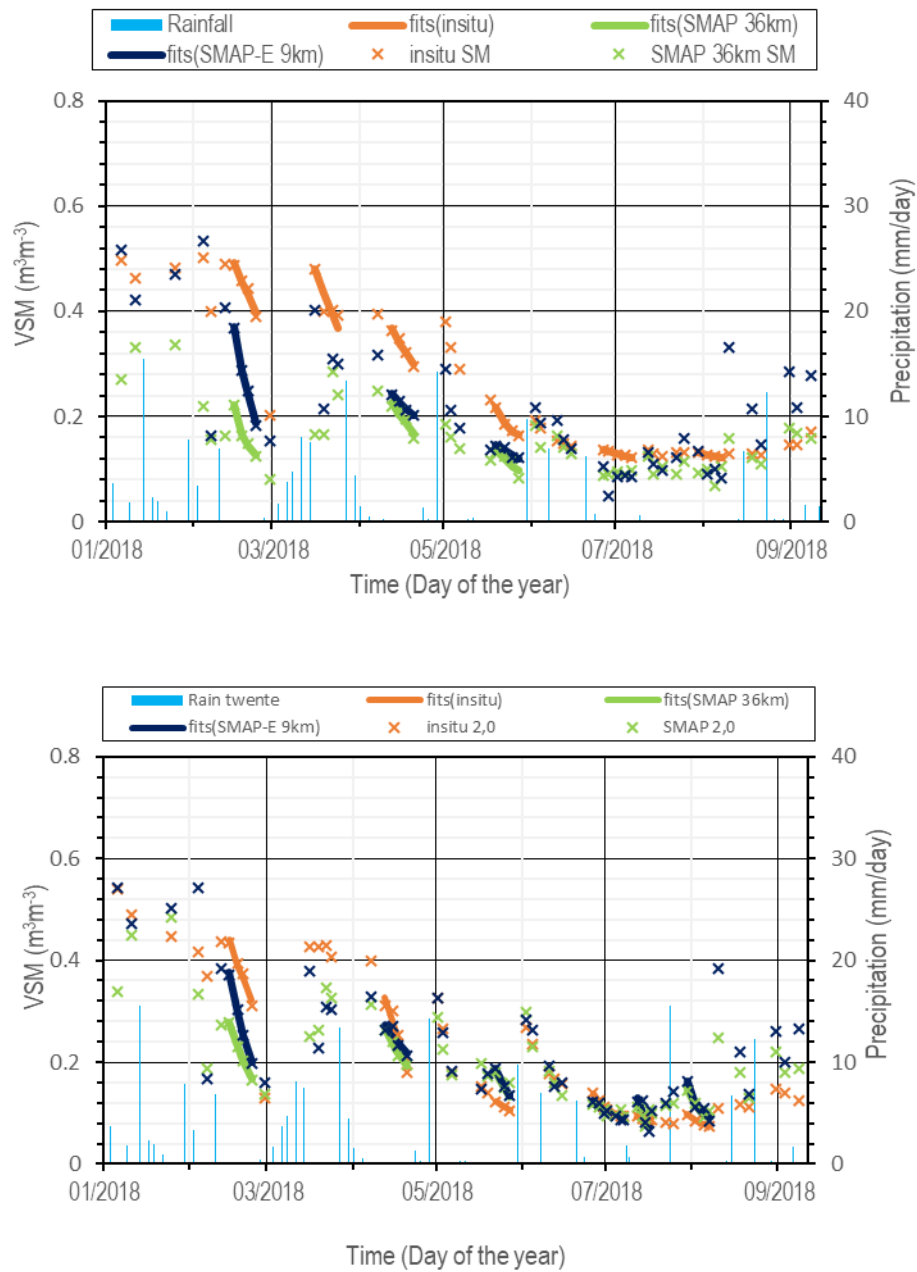
Figure 6.1: A comparison of SMAP 36 km, SMAP-E 9 km and *in-situ* SM observations (crosses) and their model fits (lines) at two pixels (a) pixel 2,0 and (b) pixel 2,1 that cover the Twente SM network. More details are shown on the legend. Rainfall measurements represent an average of 3 rainfall stations i.e., Twenthe, Heino and Hupsel.

SMDD were also investigated between 2016 and 2018 to compare their intensities and the respective plots showing the observed dry-downs against their respective model fits for *in-situ* measurements, SMAP 36 km and SMAP-E 9 km are shown in Figure 6.2. As depicted in the plots, *in-situ* measurements have a higher number of dry-downs from 2016 to 2018. θ_f as in Table 6.1 being a function of static soil properties varies less from one product to the other.
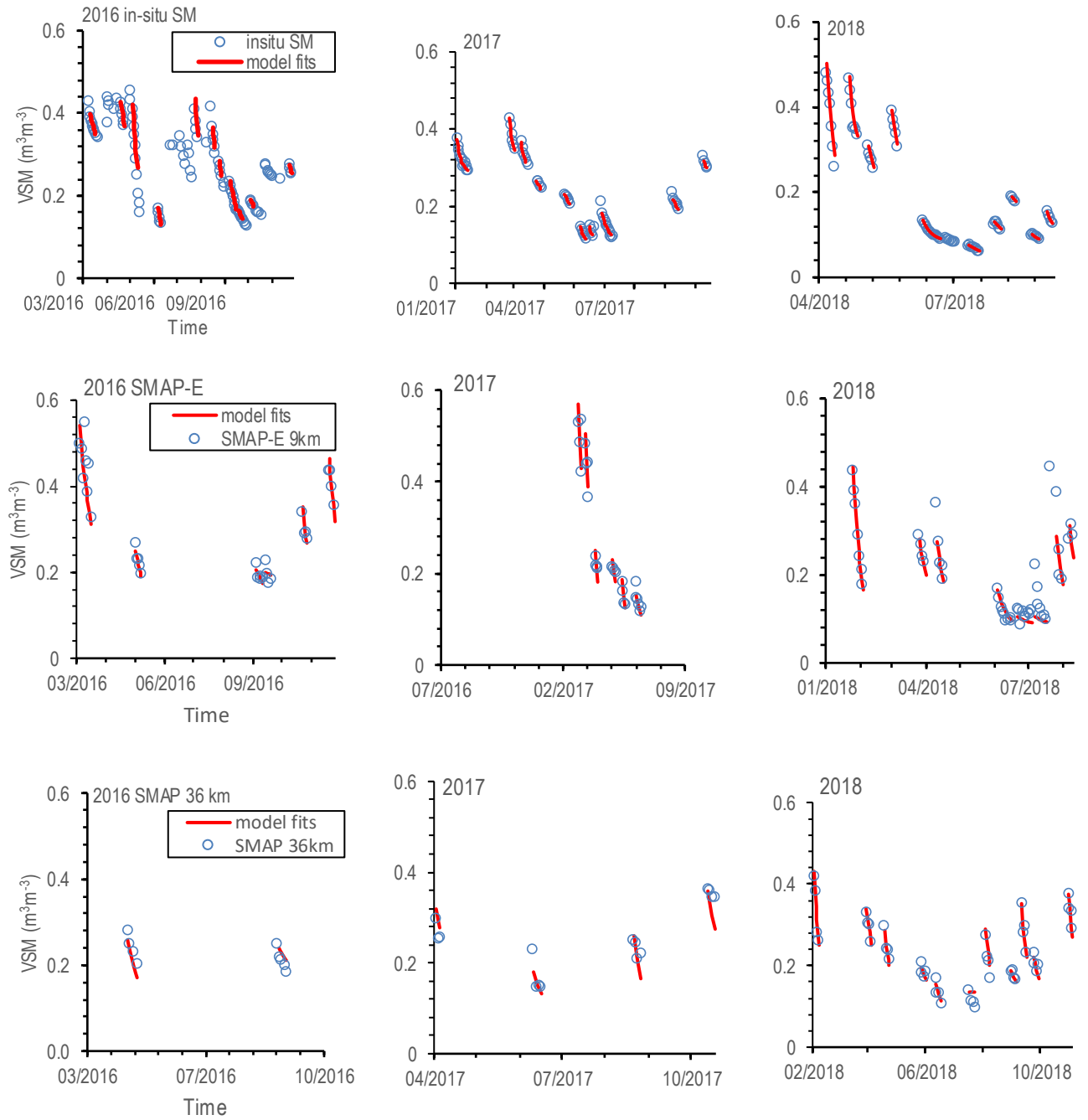
Figure 6.2: Representation of observed soil moisture dry downs since the start of the event and their respective exponential model fits for *in-situ* SM, SMAP 36 km and SMAP-E 9 km for the Twente network.

6.2. Exponential timescales of soil drying

6.2.1. Soil moisture dry-down time scale (τ)

The exponential model fits for SMAP 36 km, SMAP-E 9 km estimates and *in-situ* SM measurements were obtained during rain-free days at Twente and Raam network as presented in Figure 6.3 and Figure 6.4. SMAP 36 km, SMAP-E 9 km estimates and *in-situ* SM τ values in days were compared using cumulative frequency graphs to evaluate τ at different scales. N represents the number of points used in the

computation of the frequency cumulative plots and Appendix G shows the median, mean, minimum and maximum model parameters at Twente and Raam SM network classified into all seasons and then split into both winter and summer. The number of SMDD events is outlined in Appendix
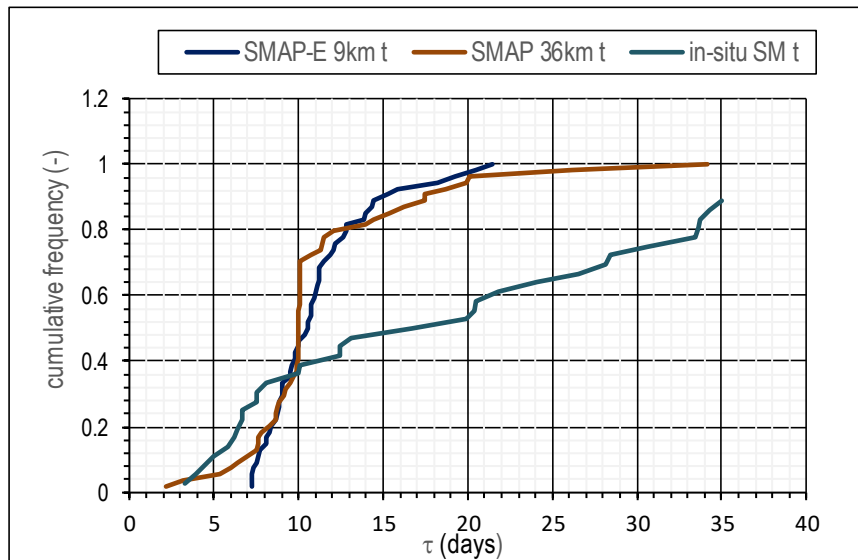
Figure 6.3: A comparison of τ based on cumulative frequencies for SMAP 36 km, SMAP-E 9 km and *in-situ* SM at Twente network both at *5 cm* depth.
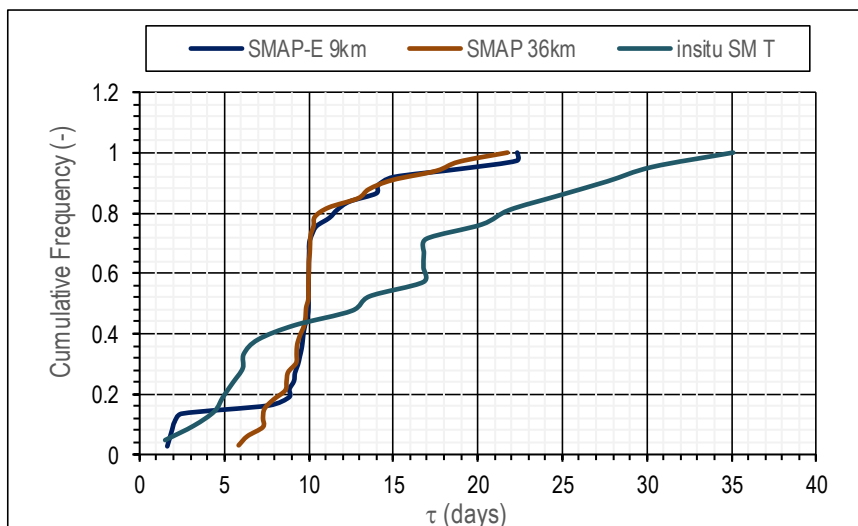
Figure 6.4: A comparison of τ based on cumulative frequencies for SMAP 36 km, SMAP-E 9 km and *in-situ* SM at Raam network both at 5 cm depth.

Exponential drying timescale (τ) is variant from as low as ≈2 days to more than 20 days across the three soil moisture products at Twente network. A similar observation can be made at Raam network (see Table 6.1 and Table 6.2). The characteristic dry-down length for the SMAP products is ≈10 days at both Twente and Raam network (Figure 6.3 and Figure 6.4). SMAP 36 km shows a sharp and rapid dry-down way before attaining 80% mark (median of 10.01 days for Twente and 9.98 days for Raam). It is followed closely by SMAP-E 9 km whose drying rapidity is slightly less than that of SMAP 36 km. It gradually peaks as from 10 days but a little later (median of 10.53 days for Twente and 9.99 days for Raam). At Raam network, τ for both SMAP 36 km and SMAP-E 9 km matches very closely with that of Twente network.

They both have a consistent trend achieving the characteristic dry down length at almost the same time. The *in-situ* SM τ is the slowest having no specific dry down characteristic length with a median of 19.93 days at the Twente and a median of 13.60 days at the Raam SM networks (see Table 6.1).The difference in the sensing depths between the SMAP SM estimates and the *in-situ* measurements could explain the difference observed in the soil moisture drying process as Shellito et al. (2016) found out. It is also worth noting that L-band radiometers detect moisture content at the limits not exceeding of 5 cm depth (Njoku and Kong, 1977) while *in-situ* probes detect soil moisture at the point where the probes are installed and therefore, there is a likelihood that the topmost soil moisture is not captured by the *in-situ* probes. Owe and Van De Griend (1998) noted that increased soil moisture causes a shallower penetration depth, which helps explains the possible reason why the drying process displayed by SMAP products is faster than that of the *in-situ*. SM recorded at Twente network is wetter than that observed at the Raam network.

The τ obtained in this study (and summarised in as shown in Table 6.1 and Table 6.2 are in agreement with the finding of Kurc and Small (2007) and Teuling et al. (2006) who reported τ to vary significantly from several days to ≈ 20 days both at individual sites and at model scales. The minimum and maximum τ were 3.13 and 34.16 days for SMAP 36 km, 7.25 and 21.45 days for SMAP-E, 3.93 and 47.63 days for the *in-situ* SM measurements, respectively, for the Twente network. Similarly, for Raam, the minimum and maximum for SMAP 36 km were 5.85 and 21.76 days, for SMAP-E 1.63 and 22.33 days while for the *in-situ* measurements 1.51 and 35.11 days respectively. This shows that τ is within similar ranges for the SMAP and the *in-situ* measurements.

The rate of drying is faster at the beginning but reduces with time. The τ values for SMAP 36 km are almost like those of SMAP-E 9 km with a small difference but for the *in-situ* SM, τ values are larger. The median τ and the mean τ for SMAP 36 km and SMAP-E is closely related (Table 6.1 and Table 6.2). These τ results are in agreement with findings of McColl et al, (2017) where dry-down events extent is a minimum of 9 days, and the median dry down length in various areas ought to be either longer or within the same range. The τ (mean and median) for Twente network, when compared to that at Raam network, shows a slight difference for both the SMAP and *in-situ*. SM dry-downs. At Raam, it is higher than that at the Twente network.

Table 6.1: Exponential time-scales across all seasons, winter and summer seasons at Twente SM network

	All seasons (days)			Winter (days)			Summer (days)		
	SMAP 36 km	SMAP-E 9 km	*in-situ* SM	SMAP 36 km	SMAP-E 9 km	*in-situ* SM	SMAP 36 km	SMAP-E 9 km	*in-situ* SM
Median	10.01	10.53	19.93	10.03	11.20	22.29	10.00	9.00	18.33
Mean	11.33	11.15	20.22	12.29	12.04	21.31	10.56	9.23	19.86
Minimum	3.13	7.25	3.93	5.36	7.38	3.93	6.39	7.25	6.67
Maximum	34.16	21.45	47.63	34.16	21.45	47.63	26.19	15.31	46.10
N	42	52	34	26	37	18	16	15	16

Table 6.2: Exponential time scales across all seasons, winter and summer seasons at Raam network

	All seasons			Winter			Summer		
	SMAP 36 km	SMAP-E 9 km	in-situ SM	SMAP 36 km	SMAP-E 9 km	in-situ SM	SMAP 36 km	SMAP-E 9 km	*in-situ* SM
Median	9.98	9.99	13.60	9.99	9.42	9.20	9.81	10.00	15.20

Mean	10.50	10.10	14.36	10.94	8.22	12.97	10.18	11.89	15.88
Minimum	5.85	1.63	1.51	7.29	1.63	1.51	5.85	7.63	4.93
Maximum	21.76	22.33	35.11	17.55	15.02	30.33	21.76	22.33	35.11
N	33	37	21	14	18	11	19	19	10

The drying process was also investigated based on seasons, i.e., summer and winter seasons. The summer season was taken from the months of June to September while the winter season was taken from the months of October to May. This comparison was used to test for soil moisture dry-down seasonality as shown in Figure 6.5 and Figure 6.6. As seen in Table 6.1, the median τ for SMAP 36 km is 10.02 and 9.9 days, SMAP-E 9 km has 11.17 and 8.94 days while *in-situ* has 20.49 and 16.74 days for winter and summer respectively. Soil moisture drying is slower during the winter seasons as compared to the summer seasons at the Twente and Raam networks. Again, the speed of soil moisture drying between SMAP-E 9 km and SMAP 36 km are almost similar with a negligible difference per season but for the *in-situ*, a slower rate persists. In summer, the, the graph steeps earlier than it does in winter. The τ parameter varies both temporally and spatially and therefore the drying process depends on both season and location.
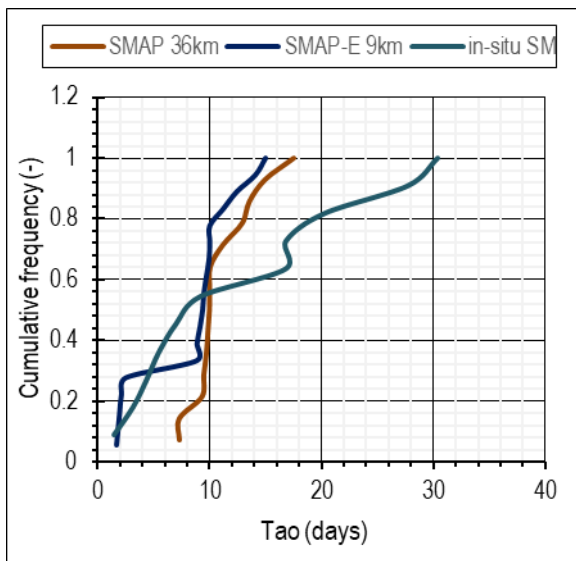
Winter season   Summer season
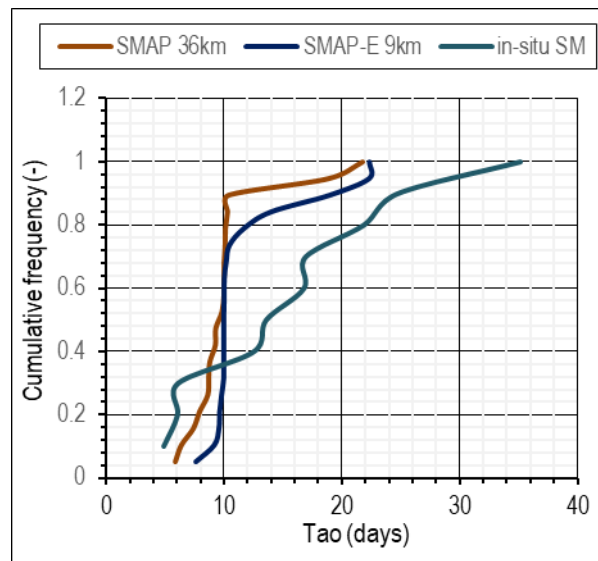
Figure 6.5: A comparison of τ based on cumulative frequencies for SMAP 36 km, SMAP-E 9 km and *in-situ* SM at Twente network for both winter and summer periods both at 5 cm depth.
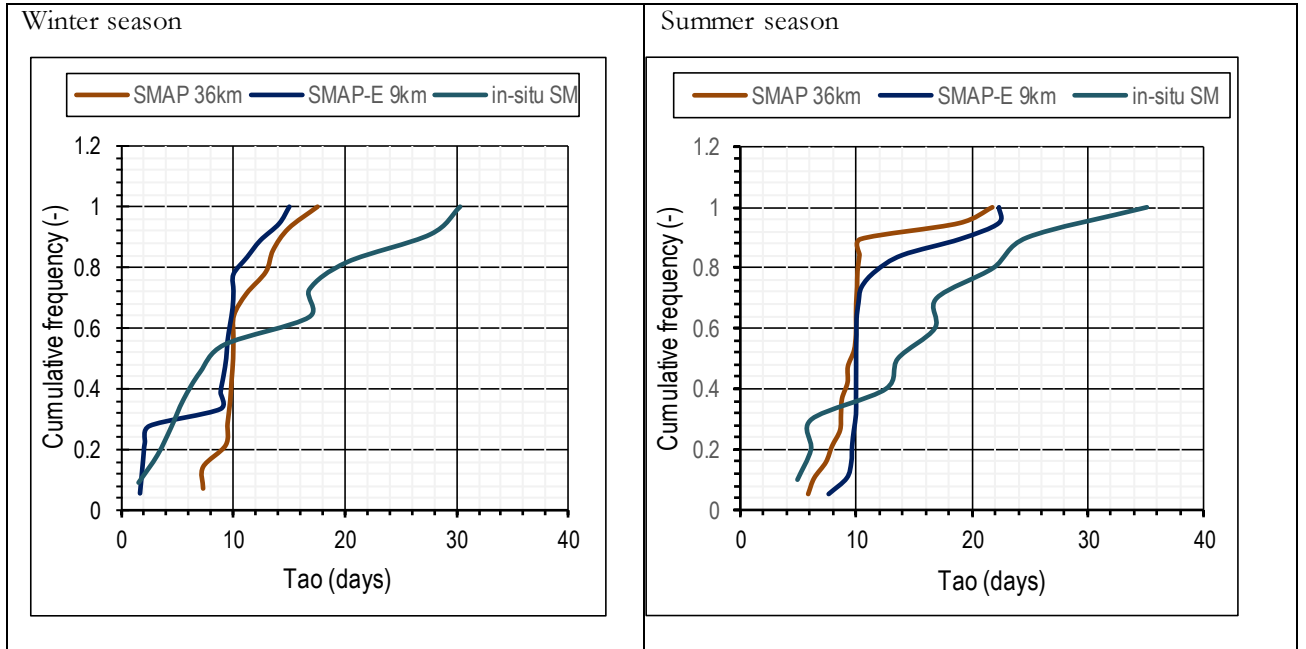
Figure 6.6: A comparison of τ based on cumulative frequencies for SMAP 36 km, SMAP-E 9 km and *in-situ* SM at Raam network for both winter and summer periods both at 5 cm depth.

Based on individual years, the model parameters were compared as in Figure 6.7 for 2016 to 2018 (Twente network) and 2016 to 2017 (Raam network). The winter season drying time scale is considerably slower than that experienced in summer. In-situ SM dry-downs are in winter are slower than in summer time.
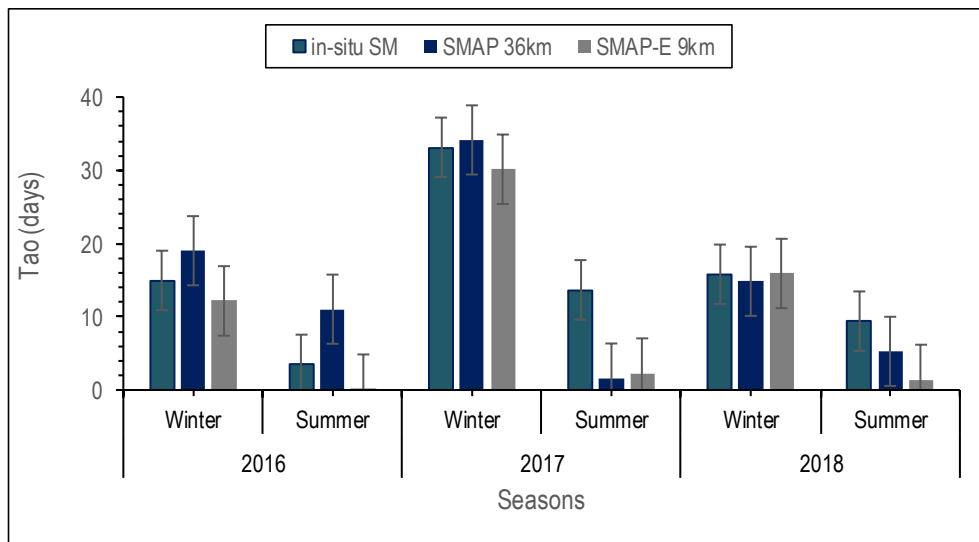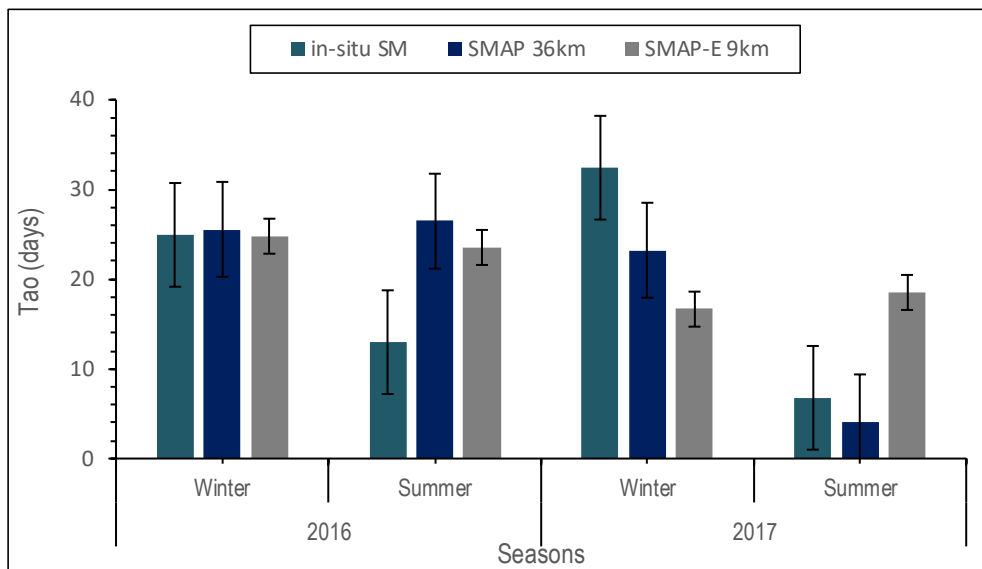
Figure 6.7: τ differences between summer and winter seasons for the period between 2016 and 2017 at Twente (top) and Raam (bottom) network.

6.2.2. The magnitude of soil moisture drying process (A)

The A parameter is used to refer to a positive rise of soil moisture content following a dry-down episode. Its values are considerably low at the start of the dry-down event but grow gradually (see Figure 6.8). SMAP-E 9 km exhibits a greater magnitude of drying at Twente network as compared to SMAP 36 km. However, there is a variation at Raam network where a greater magnitude is observed with the SMAP 36 km. For the *in-situ* A parameter, the degree of the drying process is consistently slower than that depicted with the SMAP products. It is worth noting that the A parameter at Twente network among the three SM products is considerably unvarying as compared to that at Raam network. It is possible for a surface soil layer with a faster drying rate also to dampen faster in presence of a rainfall event. This may result in a wet bias that blocks a lengthy dry bias and hence a small magnitude of the dry-down process is encountered as highlighted in Rondinelli et al. (2015). SMAP-E 9 km shows a higher magnitude of drying at Twente network while SMAP 36 km shows a larger magnitude of drying at the Raam network as seen from their median and mean values in Table 6.3.
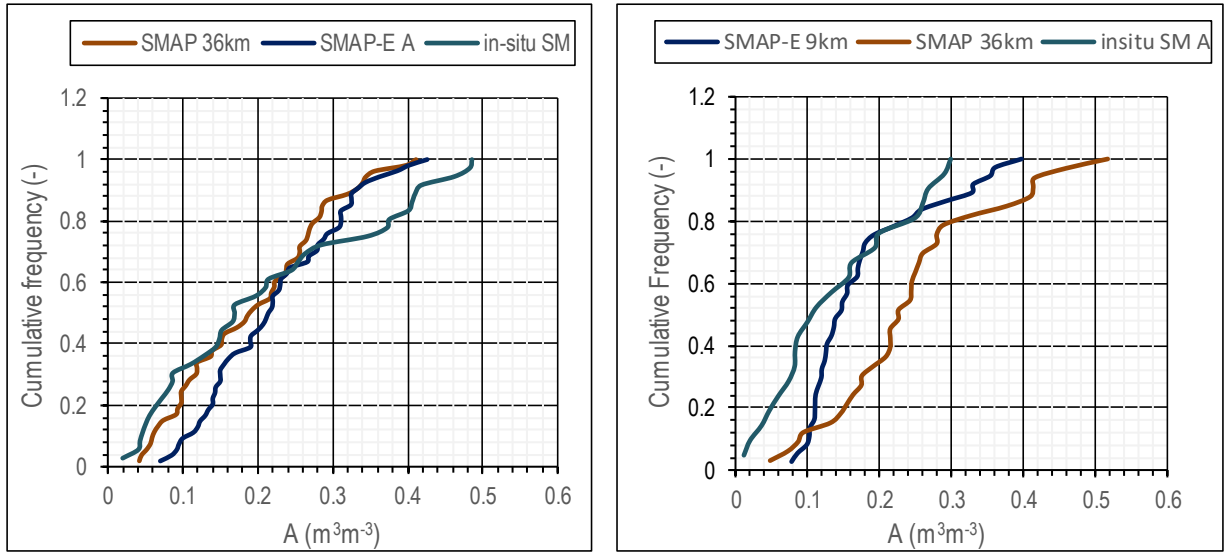
Figure 6.8: Cumulative frequency graph for A parameter at Twente and Raam network both at *5 cm* depth.

Table 6.3: Descriptive statistical scores for the A parameter at both Twente and Raam network.

Statistics	Twente[m³m⁻³]			Raam[m³m⁻³]		
	SMAP 36 km	SMAP-E 9 km	*in-situ* SM	SMAP 36 km	SMAP-E 9 km	*in-situ* SM
Median	0.197	0.219	0.169	0.234	0.148	0.123
Mean	0.196	0.224	0.218	0.249	0.179	0.146
Minimum	0.045	0.085	0.041	0.073	0.086	0.020
Maximum	0.411	0.426	0.486	0.517	0.397	0.299
Count	52	53	35	32	36	20

6.2.3. The final soil moisture content (θf)

The median value for θ_f is considerably 0.02 m³m⁻³ (see Figure 6.9 and Table 6.4) at both Twente and Raam networks in most of the products. Contrally to the figures showing τ, with θ_f plots, SMAP 36 km has the least value slightly less than SMAP-E 9km. From Table 6.4, SMAP-E 9 km has an exemptional trend in its wilting point value of 0.043 m³m⁻³ and 0.17 m³m⁻³ at Twente and Raam respectively. According to Chan et al. (2018), both SMAP 36 km and SMAP-E generally have a similar track along spatial patterns in an unbiased way but in some instances, SMAP-E shows some enhanced visual details due to some additional spatial information. This could explain some of the differences observed between the two products' drying process.
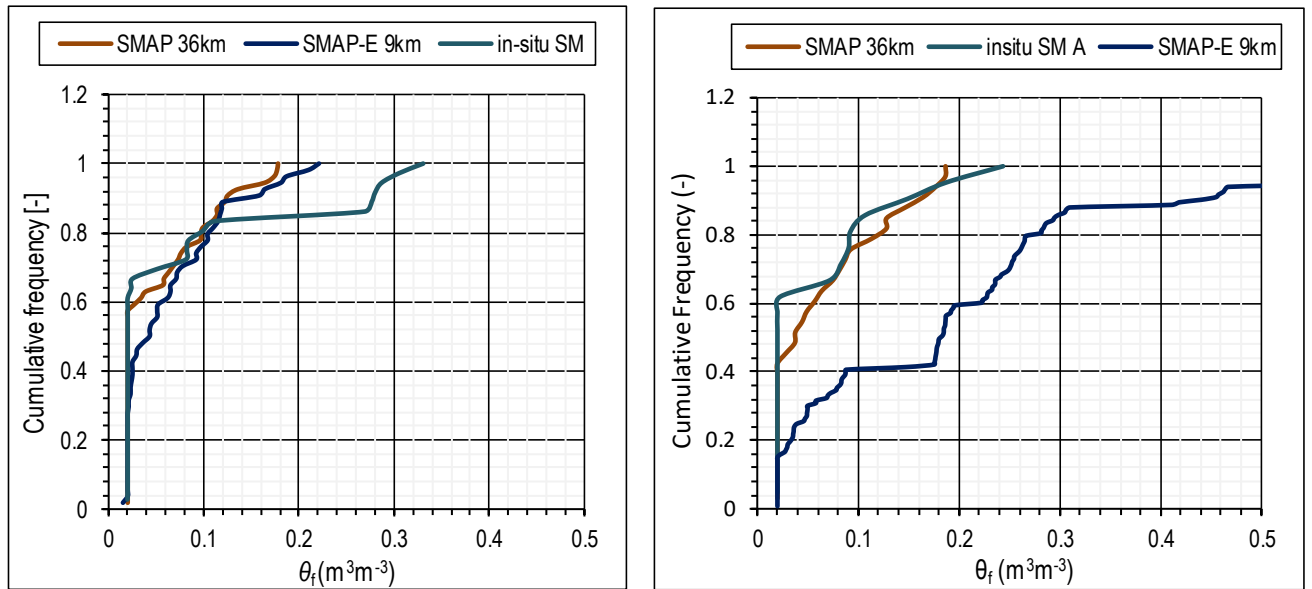
Figure 6.9: Cumulative frequency graph for theta-f parameter at Twente and Raam networks respectively both at 5 cm depth.

Table 6.4: Descriptive statistical scores for the θ_f parameter at both Twente and Raam network

Statistics	Twente			Raam		
	SMAP 36 km	SMAP-E 9 km	*in-situ* SM	SMAP 36 km	SMAP-E 9 km	*in-situ* SM
Median	0.020	0.043	0.020	0.041	0.170	0.020
Mean	0.054	0.065	0.078	0.067	0.161	0.063
Minimum	0.020	0.020	0.020	0.020	0.036	0.020
Maximum	0.178	0.221	0.331	0.187	0.253	0.244
Count	53	53	35	32	36	20

6.3.   Mapping soil moisture dry-downs

Coarse resolution SMAP images were mapped to derive the dry down timescale for the Netherlands. Median τ, A and θ_f maps are created and displayed in Appendix . Modeling soil moisture dry downs consisted of three parameters: τ, A and θ_f. The main aim was to characterize the hydrological system for the Netherlands to understand the soil moisture drying process for purposes of efficient water resources management. In Figure 6.10, Figure 6.11, and Figure 6.12 maps showing τ, A and θ_f have been displayed. The white regions represent areas that were exempted from analysis due to poor curve fit results. This means that the R^2 for these grids was below the threshold of 0.7. This could be as a result of frozen soils, water bodies present in these locations, dense vegetation cover or failure to achieve 4 or more than 4 time-steps. High values of τ define areas with a slow drying process while low values of τ define areas with a faster drying process. τ map is highly heterogeneous in both SMAP 36 km and SMAP-E 9 km but they share some common spots and the time-scale is within a similar range.

Arable lands and areas with permanent crops (see land-cover map in Figure 2.9) show a relatively higher drying time-scale as compared to the wetlands, pastures and mosaics and forested areas. The magnitude of soil drying, based on the A parameter maps for the Netherlands (Figure 6.11) are very variant but with a similar trend in the Eastern side where the values are consistently low and in the Western part where the

values are consistently higher. This magnitude depends on the time elapsed after a rainfall occurrence as argued in Shellito et al. (2018) in addition to the prevailing wetness in that particular area. How long soil moisture drying takes place is relative to the interactions between hydrologic processes, atmospheric conditions, and land cover influences. θ_{fc} maps (Figure 6.12) for both SMAP 36 km and SMAP-E 9 km shows a good correlation with the wetland areas showing considerably high soil moisture residuals. High values of θ_{fc} represent areas with a slower drying process while lower values represent a faster drying process.

Salvia et al. (2018) reported higher spatial resolution products to show spatial features more clearly than the other products due to its extensive number of grid points. The same case applies to SMAP-E 9 km which has a better resolution than SMAP 36 km. The SM dry-downs characteristics are more evident with the SMAP-E than the SMAP 36 km.
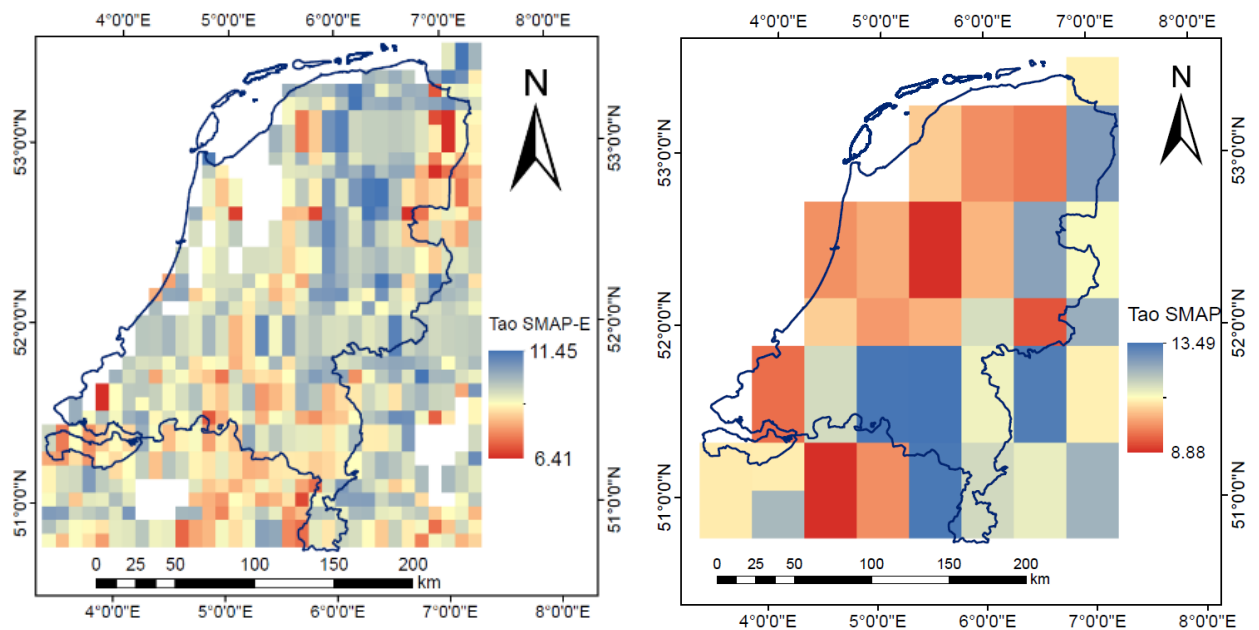
Figure 6.10: Mean estimated τ parameter derived from SMAP-E 9 km and SMAP 36 km for the Netherlands

.
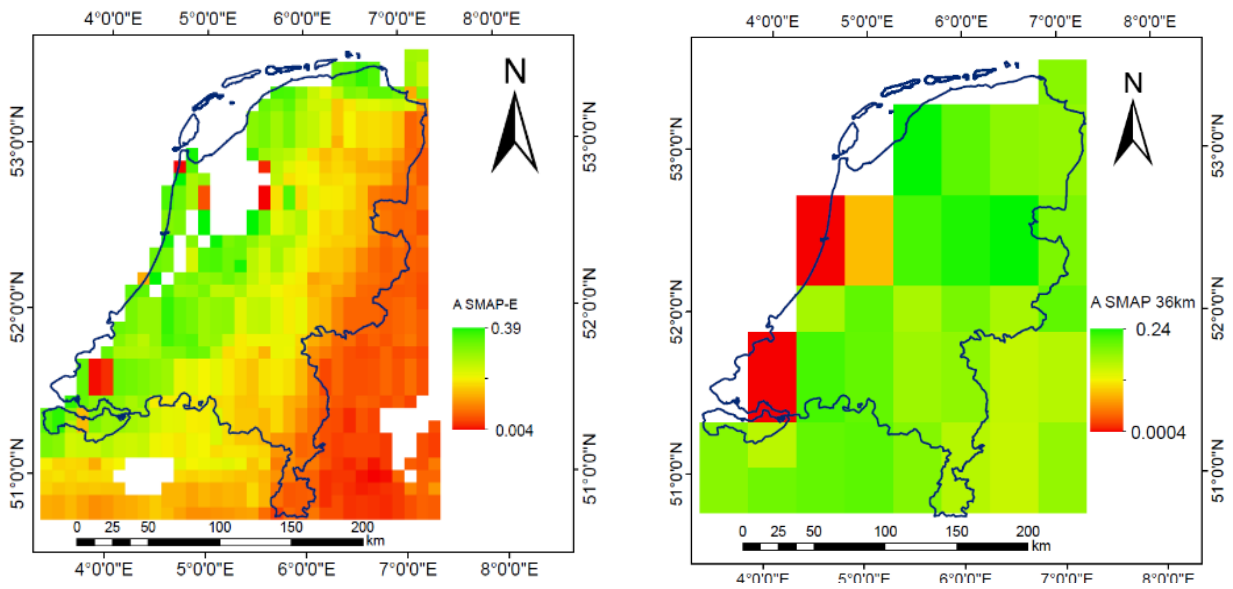
Figure 6.11: Mean estimated A parameter derived from SMAP-E 9 km and SMAP 36 km for the Netherlands
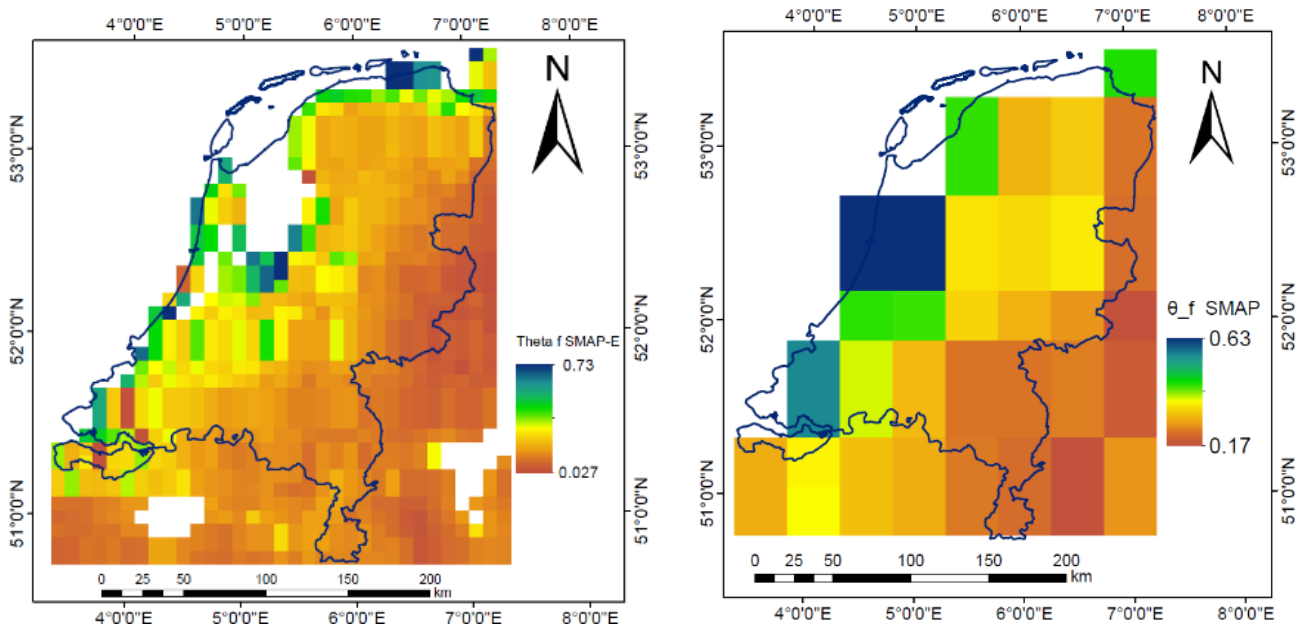
Figure 6.12: Mean estimated θ_f parameter derived from SMAP-E 9 km and SMAP 36 km for the Netherlands

7.   ANALYSIS

To understand how diverse landcover and soil texture influences the sensitivity of the backscatter signal, two performance metrics (bias and UbRMSD) for the three soil moisture networks were analyzed. The land cover and soil texture for each network are described in section 2.2. The metrics discussed in this section are drawn from section 5.3 and the calculated performance metrics are displayed in Appendix A and B. The microwave radiation is not only sensitive to the soil moisture but also on other land surface characteristics. This modifies and attenuates the microwave signal prompting low accuracies. Sources of such characteristics could be soil texture, landcover, and surface roughness.In this section, soil texture and landcover effects are discussed in sections 7.1and 7.2. A brief overview follows

7.1.   Effects of soil texture heterogeneity on soil moisture retrievals

Heterogeneity is used to refer to diversified soil texture or landcover characteristics within satellite grids. At both Twente and Raam network, sandy and loamy sandy soils are the most dominant while at Flevoland, clayey soils dominate. Using these three categories of soil texture, the performance metrics for each soil type were compared. For each network, bias and UbRMSD per individual product were plotted against each other. The bias on sites covered with sand is lower than for the sites with loamy sand generally. This is the case for the Twente with all the satellite products. But this is not true for the Raam network because the SMAP products show a larger bias with both sandy and loamy sandy soils. Also, with sandy soils, the UbRMSD is better than with the loamy sandy soils. But there is a slight difference for sentinel-1 at Raam network which shows better performance with loamy sandy soils.

For the Twente network, there is either under- or over-estimation of the SM estimates with most of the products. For the Raam network, the satellite products overestimated the SM measurements apart from Sentinel -1 at one incidence over loamy sandy soils where an underestimation was noted. For Flevoland, clayey soils dominate the entire area. The bias for the three products is good probably because of land surface homogeneity. Over clayey soil texture, as seen at Flevoland, σ^o sensitivity to SM is higher and hence better retrievals with Sentinel 1. Sentinel-1 SM records under-estimated SM estimates with respect to the *in-situ* measurements in all the networks. The UbRMSD at Flevoland for the three products seems almost similar differing with a small margin. According to Benninga et al. (2018), most of the stations at Raam have very high sand contents apart from Rm6 and Rm7 whose volume is highly composed of silt and clay. The representation of loamy sandy soils for the Raam network is a computation of performance metrics from one site (Rm07). This could have exaggerated the results. Sandy soils show a sooner saturation point because of its limited water holding capacity alluded to its larger pores. In this context, the overestimation would result from the difference in the dynamic ranges between *in-situ* theta probes and the SMAP sensors.

Figure 7.1: A comparison of the UbRMSD and the Bias between the satellite estimates and the *in-situ* measurements based on soil texture for Twente, Raam, and Flevoland SM network

7.2.   Effects of landcover on soil moisture retrievals

Based on landcover, a comparison of the bias and the UbRMSD was based upon four vegetation types that include grassland, sugar beets, onions, and corn. At the Twente, the focus was only on grassland and corn, at Flevoland only grass type of landcover while at Raam SM network four types of crops were considered i.e. grass, corn, sugar beets, and onions. Soil moisture retrievals on corn dominated sites seem to be better compared with other crops at both Twente and Raam. The retrieval of satellite estimates under the corn is good as compared to grass, sugar beets and onions. There is a high response on bare land as compared to cropped land. With corn, the retrievals are better when it is cleared from the field and this contributes to its overall better performance. SM retrievals are good on grasslands at Twente and Flevoland but at Raam network, the performance is quite low like the onions and sugar beets dominated fields. From Colliander et al., (2017), SMAP products perform well on areas that are crop free. This is because the SMAP retrieval algorithm lacks the capacity to capture the land surfaces which that are highly heterogenous over the seasons. This could explain why corn dominated fields perform well when the fields are cleared. Presence of vegetated land surfaces alters and attenuates the microwave radiation and hence complicates SM retrieval on these surfaces. This becomes a major cause of low accuracy in satellite derived soil moisture.
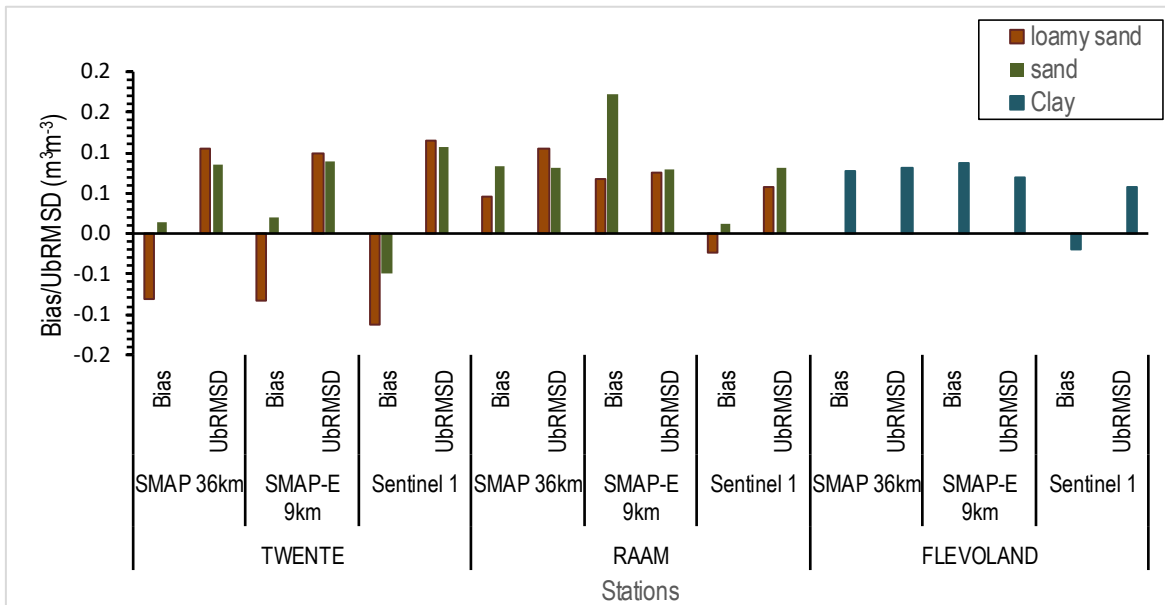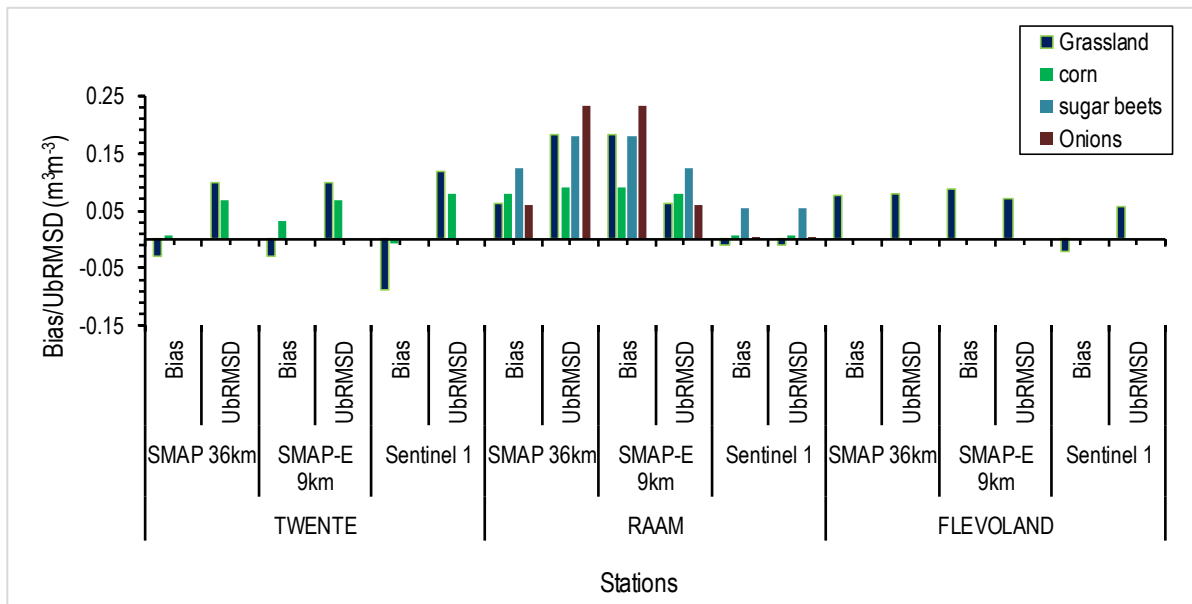
Figure 7.2: A comparison of the UbRMSD and the mean difference between the satellite estimates and the in-situ measurements based on landcover for Twente, Raam and Flevoland SM network

7.3. Discussion

Based on landcover the three products performance in the two land cover types at the three networks is within the same brackets (0.06 and 0.07m^3m^{-3}). The spatial variability of SM at Twente, Raam and Flevoland SM networks is steered by the high landcover inconsistency and soil texture and probably the prevailing meteorological conditions, bound within their localities. Based on Panciera et al. (2008) findings, different spatial patterns of soil texture and landcover within satellite footprints greatly advance soil moisture variability. In their work, they observed that soils with more sand content consistently show drier soil moisture conditions than soils with lower amounts of sand. Also, heterogeneity in the soil influences the distribution of soil moisture through varying texture, organic matter content, porosity and structure (Crow et al., 2012). According to Kim and Stricker (1996), SM retrievals on loamy soils are greatly influenced by soil heterogeneity due to their relatively high retaining capacity while sandy soils exhibit water budget discrepancies in response to antecedent rainfall variations. This causes widespread differences in soil moisture over short distances and this also alludes to variations in soil particle and pore size distributions and hence a tangible effect on soil moisture retrievals.

Other sources of biases could be an inappropriate characterization of the land surface in the retrieval algorithm or uneven sensitivity of the satellite sensor to the dynamics of the soil moisture as argued in van der Velde et al. (2012). The satellite footprint scale is incomparable to the relatively small number of samples from *in-situ* measurements which are usually less than 10 (N<10) for any area corresponding to the satellite grid (Loew and Schlenz, 2011). These ground-based networks represent very small volumes in the order of 10^{-4} m^3 and therefore they are entirely locally based. Large SM spatial variability in the satellite grid contribute to the large uncertainties in the validation of the satellite products with the *in-situ* measurements and therefore appropriate upscaling schemes should be adopted during validation exercise as previously suggested in Loew and Schlenz (2011).

The number of stations required to obtain a specific accuracy varies depending on the area heterogeneity and the soil moisture dynamics at the specific area. Using statistical approaches, Tayfur et al. (2014) concluded that 15 to 35 SM stations within a satellite grid are needed to obtain an accuracy of 0.02m^3 m^{-3}

at an area of 10000 m² while Loew & Schlenz, (2011) argued that more than 20 SM stations are required to estimate soil moisture at an accuracy better than 0.04 m³ m⁻³ at an area of 2500 km² with a lesser number within very wet and dry conditions. For the current study, the number of SM stations within the validation grid was limited and not meeting highlighted thresholds, which can explain the poor performance exhibited in the SM products.

The quality of the SMAP and Sentinel-1 soil moisture products varies both spatially and temporally, and thus, their usage requires expert knowledge for purposes of choosing the correct field of application (Alexakis et al., 2017). There is a relatively clear difference between sensors that operate at varying wavelengths according to Entekhabi et al. (2010). In their work, they explained the difference in the sensing depth between L-band and C-band, whereby L band retrievals can meet the accuracy requirements, but the C band only represents measurements at the top 1 cm or fewer as compared to L-band sensing depth of *5 cm*. Again, any high vegetation water content, (> ≈3kgm⁻²) causes signal attenuation leading to high SM insensitivity. This could contribute to the observed difference between the SMAP retrievals and Sentinel-1 SAR estimates. Radiometers measure the integrated response of the satellite grid and therefore the central region dominates the amount of soil moisture that is estimated compared to the rest of the satellite grid. This mainly has an effect on more heterogeneous surfaces (Chan et al., 2016).

During SM drying conditions, bias is anticipated between satellites and *in-situ* SM measurements due to differences in sensing depths. *In-situ* SM probes are fixed at *5 cm* depth and therefore can detect moisture ≈1-9cm while the L-band satellites signals operate at depths of ≈0-*5 cm* for average soils under average conditions. Based on the findings of Escorihuela et al. (2010), the sensing depth for L-band can be as low as ≈1 cm in very wet areas. A similar result has been observed both at Twente and Raam SM network. Such a scenario also occurred for two sites at Australia as reported by Shellito et al. (2016), regardless of them using vertically reversed probes. Therefore, the surface soil moisture may be drier than the measurements presented by *in-situ* probes dependent on the underlying climatic conditions.

SMAP data from the analysis show that a faster drying of the soils occurs immediately after a rainfall event. This drying is continuous for SMAP data and approaches ≈0 soil moisture after ≈ 10 days. This applies to both SMAP 36 km and SMAP-E 9 km. With the *in-situ* SM, it experiences a slower drying process that continues for a longer time than the SMAP estimates and rarely approaches zero. It exhibits a linear drying process. During summer periods, the evapotranspiration rate is very high as shown in Figure 2.6. During such periods, the soils are a bit dry and therefore the atmospheric demand (ET) is limited by inadequate moisture content. At this time due to issues related to the sensing depth, it seems that SMAP products detect a land surface that is presumably dry. *In-situ* SM measurements during such periods show more drying but linearly. This could explain why *in-situ* SM exhibit more frequent drying towards and during summer (Figure 6.1).

Different land cover and soil texture around each pixel could also contribute to the different τ values. For example, τ decreases as the sand fraction on the soil surface increases because sand has a low water retention capacity as reported by (McColl et al., 2017). For Raam network, where sandy soils dominate shows a smaller τ as compared to the Twente network where both sandy and loamy sandy soils at almost same frequencies dominate. Soil moisture drying is determined by the availability of soil moisture and ET rates. Evaporation is limited in the presence of vegetation cover. They are inversely related and therefore it means in the presence of landcover, a slow drying process occurs.

8.   CONCLUSION AND RECOMMENDATIONS

8.1.   Conclusion

The objective of this study was to assess the performance of three satellite-based SM estimates (SMAP, SMAP-E and Sentinel-1) against *in-situ* SM measurements from three SM monitoring networks, analyse the dry-down cycles to characterize the hydrological system in the Netherlands and relate the accuracy and the dry-down events to land-cover and soil texture in the respective study areas. SM estimates from the SMAP products were retrieved from the NSIDC site while SM estimates from sentinel-1 SAR was derived using change detection algorithm from the Google Earth Engine. The products provide soil moisture estimates for the soil surface layer of approximately $0 - 5$ cm depth, which is comparable to the *in-situ* measurements at 5 cm depth.

Validation based on pixel matchups was carried out for the SMAP 36 km and SMAP-E 9km only. For the SM network and station matchup, all the three SM satellite products were validated. Finally, a comparison based on seasons was done. The upscaling technique applied was arithmetic averaging of the *in-situ* SM measurements with (a) complete *in-situ* SM data and (b) with stations missing just a few data points. The validation period was from April 2016 to April 2018. For the dry-down cycles analysis, two SM networks (Twente and Raam) were used. Flevoland was exempted due to many data gaps. Matchups between SMAP 36km, SMAP-E 9 km, and *in-situ* SM dry-downs were compared for Raam and Twente. For the Netherlands, SMAP 36 km and SMAP-E 9 km was used. Based on our analysis, the following conclusions are made in sub-section 8.1.1 (validation) and 8.1.2 (soil moisture dry-down characterization) and the recommendations follow in section 8.2.

8.1.1.   Validation

The differences in the validation metrics for the SMAP 36 km and the SMAP-E 9 km products are negligible, and therefore the two products can be used inter-changeably in various fields of applications. This could be related to their retrieval algorithms. Thus, the difference in the resolutions does not have a big impact in terms of their accuracy.

Based on the three satellite products, the SMAP 36 km outperformed the rest at Twente SM network, SMAP-E at Raam SM network and Sentinel-1 at Flevoland. This could be because the Raam network is denser (more stations per square kilometer) than the Twente and Flevoland networks. SMAP-E 9 km also overestimates SM, and this could be caused by its smaller dynamic range compared to the other satellite products. Sentinel-1 performs better at Flevoland network, probably because the area is dominated by clay soils where the dielectric constant is minimally influenced and so the retrieval of soil moisture is better.

A good agreement was found in SMAP and Sentinel-1 SM estimates when compared with *in-situ* measurements in all the networks apart from SMAP-E 9 km at Raam network which was largely overestimating the SM estimates. This could be attributed to the smaller dynamic range that it possesses in comparison to SMAP 36 km.

Though the SM products do not meet the SMAP accuracy requirements of $0.04 m^3 m^{-3}$, their accuracies were within the accuracy requirement of high-resolution soil moisture products of $0.06 m^3 m^{-3}$ defined for radar sensors by the SMAP mission. The accuracy of the products seems to be affected by data collected during the winter seasons, probably because complete flagging of the frozen soils was not done. Another limitation to the validation procedure is a scale mismatch between the SM satellite products and the point

measurements. The upscaling technique adopted was spatial averaging which is usually limited. This is because the method works well with dense and well spread *in-situ* SM measurements for a better performance as mentioned (Colliander et al., 2017).

A robust analysis of the satellite products requires many sites representing diverse conditions to derive a fair comparison. With three sites having slightly different soil texture and landcover types, it can be concluded that retrieval of satellite estimates over sandy soils is better than that of loamy sandy soils. Over clayey soil texture, as seen at Flevoland, σ^o sensitivity to SM is higher and hence better retrievals also. The retrieval of satellite estimates under the corn is good as compared to grass, sugar beets and onions. Under heavy biomass, the σ^o response would be rather poor, but the good retrieval could be attributed to scattering along the soil vegetation pathways

Finally, the three satellite products show a good agreement with the prevailing meteorological conditions in all the seasons. There are clear highs during rainfall events and clear lows during periods of no rain.

8.1.2. Soil moisture dry-down characterization

The findings of this study confirm that the exponential decay of surface soil moisture is a very useful model. The exponential decay function provides a good fit of the SMAP and the *in-situ* measurements dry-down episodes.

The representation of soil drying subsequent to rainfall events by the SMAP SM estimates and *in-situ* SM measurements differs. SMAP products show faster dry-down episodes than *in-situ* soil moisture measurements. Besides, the magnitude of drying is also greater than that of the *in-situ* measurements. The matchup results when *in-situ* measurements were concurrent with the SMAP product timing and frequency yielded similar result as when the individual products were compared at their own frequency and timing. This, therefore, means that the difference could be related to their different sensing depth.

The SMAP SM product's L-band radiometer has a higher response to soil moisture at the depths of 5cm or less and the evaporation process is principally dominant from these topsoil columns which are the L-band's sensing depths. Evaporation process and soil moisture drying being linearly related to VSM explain this scenario.

SMAP 36 km and SMAP-E 9 km have almost similar drying trends with SMAP 36 km showing slightly faster drying in most instances. Both the SMAP products can be used to map dry-down episodes to characterize areas that dry faster than others, but SMAP-E 9 km shows the dry-down characteristic better visually.

The drying process for the SMAP products is faster at the beginning of a dry-down but slows with time attaining a characteristic dry-down length of $\approx$10 days. For the *in-situ* measurements, the dry-down length is variant but its more than 10 days. With time, a plateau level is reached indicative of probably water limited situation levels with SMAP products almost attaining zero values.

There are slight seasonal differences in the drying process. The drying process in winter is considerably slower than that in summer which could be as a result of the high evaporative demand in summer as compared to the winter seasons. In terms of temporal and spatial correlation of the soil moisture dry-downs, seems that there is a slight difference in both space and time. Raam network is dominated by sandy soils majorly. It shows lesser values of τ in relation to Twente network which is composed of both sandy and sandy loamy soils. This means it experiences a faster drying than the Twente network, but the

range is still within the characteristic depth. Therefore, the difference is sparingly related to soil texture. Though extensive analysis based on land cover were not carried out, it is worth noting that SM drying is determined by the availability of soil moisture and ET rates. Evaporation is limited in the presence of vegetation cover and therefore it means in the presence of landcover, slow drying occurs.

Comparing the SMAP SM estimates with *in-situ* SM measurements during the dry-down episode yields better accuracy results which are comparable with the SMAP accuracy requirements and this contributes up-to-date information in the use of SMAP SM estimates.

Previous research has employed different approaches in the selection of dry-down events ranging from different rainfall measurements to not using any rainfall measurements. Defining the onset and cessation of a dry-down based on the rainfall measurements is a challenge in fitting the exponential model to the dry down. Truncation of the dry-down events due to the abrupt increase of soil moisture as a result of rainfall that is not captured in the data set being used. This poses a methodological difficulty.

8.2.   Recommendations

Based on findings of this study, SMAP 36 km and SMAP-E 9km can be both employed in mapping dry-down episodes to establish wetting and drying processes at both local and regional scales, but SMAP-E 9 km has a better representation of SMDD characteristics. A probable limitation would, however, be SMAP's shorter recording length (3 days). The τ map is comparable with other drought index maps for the Netherlands. Therefore, a SMAP drought-related index can also be established to help in identifying anonymously wet and dry regions. The use of the G.E.E platform in the estimation of soil moisture using sentinel-1 is a good emerging approach. However, it requires stand-alone research where all the concentration will be directed to it. Many processing steps are possible with it, but the challenge in this research was that it was broad with many different things to handle at the same time and therefore less was achieved. The same case applies to dry-down characterization. Being a major topic, it would require a study on its own to get an in-depth understanding of the drying process and the underlying controls on the drying rates. To further build on this research, it would be of much interest to explore the following:

- Studying *in-situ* SM dry-downs in this research show that they present more frequent dry-downs than the SM satellite products. Therefore, exploring soil moisture dry-downs based on *in-situ* SM measurements at the 5 cm 10 cm, 20 cm, 40 cm or even 80 cm depth would be interesting. In a nutshell, soil moisture dry-downs at varying timescales and soil depths are key for diversified processes.
- Exploring the effects of non-uniform rainfall representation on the soil drying process, since different satellite products uniquely represent rainfall amounts dependent on several factors including retrieval algorithm, surface characteristics, among others.
- Extending on seasonal and spatial analysis of soil moisture dry-downs (τ) which has not received wide attention in the previous works,
- Exploring upscaling techniques of point-based SM measurements for validating soil moisture satellite products at various scales,
- Soil moisture drying rates in relation to evapotranspiration, NDVI and soil texture which act as the driving forces on the drying process would be interesting to study.

LIST OF REFERENCES

Akbar, R., Short Gianotti, D. J., McColl, K. A., Haghighi, E., Salvucci, G. D., & Entekhabi, D. (2018). Estimation of Landscape Soil Water Losses from Satellite Observations of Soil Moisture. *Journal of Hydrometeorology*, *19*(5), 871–889. https://doi.org/10.1175/JHM-D-17-0200.1

Al-Yaari, A., Wigneron, J.-P., Ducharne, A., Kerr, Y., de Rosnay, P., de Jeu, R., … Mialon, A. (2014). Global-scale evaluation of two satellite-based passive microwave soil moisture datasets (SMOS and AMSR-E) with respect to Land Data Assimilation System estimates. *Remote Sensing of Environment*, *149*, 181–195. https://doi.org/10.1016/J.RSE.2014.04.006

Alexakis, D. D., Mexis, F. D. K., Vozinaki, A. E. K., Daliakopoulos, I. N., & Tsanis, I. K. (2017). Soil moisture content estimation based on Sentinel-1 and auxiliary earth observation products. A hydrological approach. *Sensors (Switzerland)*, *17*(6), 1–16. https://doi.org/10.3390/s17061455

Benninga, H. F., Carranza, C. D. U., Pezij, M., van Santen, P., van der Ploeg, M. J., Augustijn, D. C. M., & van der Velde, R. (2018). The Raam regional soil moisture monitoring network in the Netherlands. *Earth System Science Data*, *10*(1), 61–79. https://doi.org/10.5194/essd-10-61-2018

Bindlish, R., Colliander, A., Chen, F., Dunbar, S., Piepmeier, J., Cosh, M., … D-, J. (2016). *Soil Moisture Active Passive (SMAP) Project: Calibration and Validation for the L2/3_SM_P Version 4 and L2/3_SM_P_E Version 1 Data Products Citation*. Retrieved from https://pdms.jpl.nasa.gov/

Brocca, L., Ciabatta, L., Massari, C., Camici, S., & Tarpanelli, A. (2017). Soil Moisture for Hydrological Applications: Open Questions and New Opportunities. *Water*, *9*(2), 140. https://doi.org/10.3390/w9020140

Carranza, C. D. U., van der Ploeg, M. J., & Torfs, P. J. J. F. (2018). Using lagged dependence to identify (de)coupled surface and subsurface soil moisture values. *Hydrology and Earth System Sciences*, *22*(4), 2255–2267. https://doi.org/10.5194/hess-22-2255-2018

Chan, S. K., Bindlish, R., O'Neill, P. E., Njoku, E., Jackson, T., Colliander, A., … Kerr, Y. (2016). Assessment of the SMAP Passive Soil Moisture Product. *IEEE Transactions on Geoscience and Remote Sensing*, *54*(8), 4994–5007. https://doi.org/10.1109/TGRS.2016.2561938

Chan, S. K., Bindlish, R., O'Neill, P., Jackson, T., Njoku, E., Dunbar, S., … Kerr, Y. (2018). Development and assessment of the SMAP enhanced passive soil moisture product. *Remote Sensing of Environment*, *204*, 931–941. https://doi.org/10.1016/J.RSE.2017.08.025

Chen, X., Pang, J., Zhang, Z., & Li, H. (2014). Sustainability Assessment of Solid Waste Management in China: A Decoupling and Decomposition Analysis. *Sustainability*, *6*(12), 9268–9281. https://doi.org/10.3390/su6129268

Colliander, A., Jackson, T. J., Bindlish, R., Chan, S., Das, N., Kim, S. B., … Yueh, S. (2017). Validation of SMAP surface soil moisture products with core validation sites. *Remote Sensing of Environment*, *191*, 215–231. https://doi.org/10.1016/j.rse.2017.01.021

Colliander, A., Jackson, T. J., Bindlish, R., Chan, S., Das, N., Kim, S. B., … Yueh, S. H. (2017). Validation of SMAP surface soil moisture products with core validation sites. Retrieved from https://www.semanticscholar.org/paper/Validation-of-SMAP-surface-soil-moisture-products-Colliander-Jackson/b18630cd8970daf82eb73c57682ea9aa81809003

Colliander, A., Jackson, T. J., Chan, S. K., O'Neill, P., Bindlish, R., Cosh, M. H., … Yueh, S. H. (2018). An assessment of the differences between spatial resolution and grid size for the SMAP enhanced soil moisture product over homogeneous sites. *Remote Sensing of Environment*, *207*, 65–70. https://doi.org/10.1016/J.RSE.2018.02.006

Corradini, C. (2014). Soil moisture in the development of hydrological processes and its determination at different spatial scales. *Journal of Hydrology*, *516*, 1–5. https://doi.org/10.1016/j.jhydrol.2014.02.051

Crow, W. T., Berg, A. A., Cosh, M. H., Loew, A., Mohanty, B. P., Panciera, R., … Walker, J. P. (2012). Upscaling sparse ground-based soil moisture observations for the validation of coarse-resolution satellite soil moisture products. *Reviews of Geophysics*, *50*(2). https://doi.org/10.1029/2011RG000372

Cui, C., Xu, J., Zeng, J., Chen, K. S., Bai, X., Lu, H., … Zhao, T. (2018). Soil moisture mapping from satellites: An intercomparison of SMAP, SMOS, FY3B, AMSR2, and ESA CCI over two dense network regions at different spatial scales. *Remote Sensing*, *10*(1). https://doi.org/10.3390/rs10010033

Das, N., & Dunbar, R. S. (2017). Soil Moisture Active Passive (SMAP) Mission Level 2 SMAP/Sentinel Active/Passive Soil Moisture Product Specification Document Initial Release.

Das, N. N., Entekhabi, D., Dunbar, S., Kim, S., Yueh, S., Colliander, A., … Lopez-Baeza, E. (2017). *Soil Moisture Active Passive (SMAP) Project Assessment Report for the L2SMSP Beta-Release Data Products*. Retrieved from https://pdms.jpl.nasa.gov/

Das, N. N., Entekhabi, D., Kim, S., Yueh, S., & O'Neill, P. (2016). Combining SMAP and Sentinel data for high-resolution Soil Moisture product. In *2016 IEEE International Geoscience and Remote Sensing Symposium (IGARSS)* (pp. 129–131). IEEE. https://doi.org/10.1109/IGARSS.2016.7729024

Dean, T. J., Bell, J. P., & Baty, A. J. B. (1987). Soil moisture measurement by an improved capacitance technique, Part I. Sensor design and performance. *Journal of Hydrology*, *93*(1–2), 67–78. https://doi.org/10.1016/0022-1694(87)90194-6

Dente, L., Su, Z., & Wen, J. (2012). Validation of SMOS soil moisture products over the Maqu and Twente Regions. *Sensors (Switzerland)*, *12*(8), 9965–9986. https://doi.org/10.3390/s120809965

Dente, L., Vekerdy, Z., Su, Z., Ucer, M., & Dente, L. (2011). *Twente soil moisture and soil temperature monitoring network*. Retrieved from https://webapps.itc.utwente.nl/librarywww/papers_2011/scie/dente_twe.pdf

Dirmeyer, P. A., Schlosser, C. A., Brubaker, K. L., Dirmeyer, P. A., Schlosser, C. A., & Brubaker, K. L. (2009). Precipitation, Recycling, and Land Memory: An Integrated Analysis. *Journal of Hydrometeorology*, *10*(1), 278–288. https://doi.org/10.1175/2008JHM1016.1

Ebrahimi, M., Alavipanah, S. K., Hamzeh, S., Amiraslani, F., Neysani Samany, N., & Wigneron, J. P. (2018). Exploiting the synergy between SMAP and SMOS to improve brightness temperature simulations and soil moisture retrievals in arid regions. *Journal of Hydrology*, *557*, 740–752. https://doi.org/10.1016/j.jhydrol.2017.12.051

Entekhabi, D., Yueh, Si., O'Neil, P. E., Kellogg, K. H., Allen, A., Bindlish, R., & Administration, N. A. and S. (2014). SMAP Handbook. *Mapping Soil Moisture and Freeze/Thaw from Space*, 192.

Entekhabi, D., Njoku, E. G., O'Neill, P. E., Kellogg, K. H., Crow, W. T., Edelstein, W. N., … Van Zyl, J. (2010). The Soil Moisture Active Passive (SMAP) Mission. *Proceedings of the IEEE*, *98*(5), 704–716. https://doi.org/10.1109/JPROC.2010.2043918

Entekhabi, D., Reichle, R. H., Koster, R. D., Crow, W. T., Entekhabi, D., Reichle, R. H., … Crow, W. T. (2010). Performance Metrics for Soil Moisture Retrievals and Application Requirements. *Journal of Hydrometeorology*, *11*(3), 832–840. https://doi.org/10.1175/2010JHM1223.1

Esa. (2012). *SENTINEL-1 ESA's radar observatory mission for GMES operational services. ESA Special Publication*. https://doi.org/10.1016/j.rse.2011.11.026

Escorihuela, M. J., Chanzy, A., Wigneron, J. P., & Kerr, Y. H. (2010). Effective soil moisture sampling depth of L-band radiometry: A case study. *Remote Sensing of Environment*, *114*(5), 995–1001. https://doi.org/10.1016/j.rse.2009.12.011

Ford, T. W., McRoberts, D. B., Quiring, S. M., & Hall, R. E. (2015). On the utility of in situ soil moisture observations for flash drought early warning in Oklahoma, USA. *Geophysical Research Letters*, *42*(22), 9790–9798. https://doi.org/10.1002/2015GL066600

Gorelick, N., Hancher, M., Dixon, M., Ilyushchenko, S., Thau, D., & Moore, R. (2017). Google Earth Engine: Planetary-scale geospatial analysis for everyone. *Remote Sensing of Environment*, *202*, 18–27. https://doi.org/10.1016/j.rse.2017.06.031

Gupta, D., Rajendra, P., Narayan, M., Ajeet, V., & Kumar, S. (2015). Support Vector Regression for Retrieval of Soil Moisture Using Bistatic Scatterometer Data at X-Band. *International Scholarly and Scientific Research & Innovation*.

Hallikainen, M., & Ulaby, F. (1985). Microwave dielectric behavior of wet soil-part 1: empirical models and experimental observations. *… and Remote Sensing …*, (1), 25–34. https://doi.org/10.1109/TGRS.1985.289497

Hayes, M., Svoboda, M., Wall, N., & Widhalm, M. (2011). The Lincoln Declaration on Drought Indices: Universal Meteorological Drought Index Recommended. *Bulletin of the American Meteorological Society*, *92*(4), 485–488. https://doi.org/10.1175/2010BAMS3103.1

Hornacek, M., Wagner, W., Sabel, D., Truong, H.-L., Snoeij, P., Hahmann, T., … Doubkova, M. (2012). Potential for High Resolution Systematic Global Surface Soil Moisture Retrieval via Change Detection Using Sentinel-1. *IEEE Journal of Selected Topics in Applied Earth Observations and Remote Sensing*. https://doi.org/10.1109/JSTARS.2012.2190136

Kennedy, R. E., Yang, Z., Gorelick, N., Braaten, J., Cavalcante, L., Cohen, W. B., & Healey, S. (2018). remote sensing Implementation of the LandTrendr Algorithm on Google Earth Engine. https://doi.org/10.3390/rs10050691

Kim, C. P., & Stricker, J. N. M. (1996). Influence of spatially variable soil hydraulic properties and rainfall intensity on the water budget. *Water Resources Research*, *32*(6), 1699–1712. https://doi.org/10.1029/96WR00603

Kim, S.-B., Huang, H., Liao, T.-H., & Colliander, A. (2018). Estimating Vegetation Water Content and Soil Surface Roughness Using Physical Models of L-Band Radar Scattering for Soil Moisture Retrieval. *Remote Sensing*, *10*(4), 556. https://doi.org/10.3390/rs10040556

Kim, Y., & Van Zyl, J. J. (2009). A time-series approach to estimate soil moisture using polarimetric radar data. *IEEE Transactions on Geoscience and Remote Sensing*. https://doi.org/10.1109/TGRS.2009.2014944

Kolassa, J., Reichle, R. H., Liu, Q., Alemohammad, S. H., Gentine, P., Aida, K., … Walker, J. P. (2018). Estimating surface soil moisture from SMAP observations using a Neural Network technique. *Remote Sensing of Environment*, *204*(October 2017), 43–59. https://doi.org/10.1016/j.rse.2017.10.045

Kornelsen, K. C., & Coulibaly, P. (2013). Advances in soil moisture retrieval from synthetic aperture radar and hydrological applications. *Journal of Hydrology*, *476*, 460–489. https://doi.org/10.1016/J.JHYDROL.2012.10.044

Kurc, S. A., & Small, E. E. (2007). Soil moisture variations and ecosystem-scale fluxes of water and carbon in semiarid grassland and shrubland. *Water Resources Research*, *43*(6), 1–13. https://doi.org/10.1029/2006WR005011

Laio, F., Porporato, A., Ridolfi, L., & Rodriguez-Iturbe, I. (2001). Plants in water-controlled ecosystems: Active role in hydrologie processes and responce to water stress II. Probabilistic soil moisture dynamics. *Advances in Water Resources*, *24*(7), 707–723. https://doi.org/10.1016/S0309-1708(01)00005-7

Li, C., Lu, H., Yang, K., Han, M., Wright, J. S., Chen, Y., … Gong, W. (2018). The evaluation of SMAP enhanced soil moisture products using high-resolution model simulations and in-situ observations on the Tibetan Plateau. *Remote Sensing*, *10*(4), 1–16. https://doi.org/10.3390/rs10040535

Lievens, H., Reichle, R. H., Liu, Q., De Lannoy, G. J. M., Dunbar, R. S., Kim, S. B., … Wagner, W. (2017). Joint Sentinel-1 and SMAP data assimilation to improve soil moisture estimates. *Geophysical Research Letters*, *44*(12), 6145–6153. https://doi.org/10.1002/2017GL073904

Lievens, H., & Verhoest, N. E. C. (2012). Spatial and temporal soil moisture estimation from RADARSAT-2 imagery over Flevoland, The Netherlands. *Journal of Hydrology*, *456–457*, 44–56.

https://doi.org/10.1016/j.jhydrol.2012.06.013

Link, C., Piles, M., Member, S., Entekhabi, D., & Member, S. (2018). A Change Detection Algorithm for Retrieving High-Resolution Soil Moisture From SMAP Radar and Radiometer Observations.

Loew, A., Bell, W., Brocca, L., Bulgin, C. E., Burdanowitz, J., Calbet, X., … Verhoelst, T. (2017). Validation practices for satellite based earth observation data across communities. *Reviews of Geophysics*. https://doi.org/10.1002/2017RG000562

Loew, A., & Schlenz, F. (2011). Sciences A dynamic approach for evaluating coarse scale satellite soil moisture products, (2010), 75–90. https://doi.org/10.5194/hess-15-75-2011

Martinis, S., Plank, S., & Ćwik, K. (2018). The Use of Sentinel-1 Time-Series Data to Improve Flood Monitoring in Arid Areas. *Remote Sensing*, *10*(4), 583. https://doi.org/10.3390/rs10040583

McColl, K. A., Wang, W., Peng, B., Akbar, R., Short Gianotti, D. J., Lu, H., … Entekhabi, D. (2017). Global characterization of surface soil moisture drydowns. *Geophysical Research Letters*, *44*(8), 3682–3690. https://doi.org/10.1002/2017GL072819

Mckee, T. B., Doesken, N. J., & Kleist, J. (1993). The relationship of drought frequency and duration to time scales. *AMS 8th Conference on Applied Climatology*. https://doi.org/citeulike-article-id:10490403

Menzel, W. P. (2001). Surface Temperature. *Applications With Meteorological Satellites*, (051).

Mladenova, I. E., Jackson, T. J., Bindlish, R., & Hensley, S. (2013). Incidence Angle Normalization of Radar Backscatter Data. *IEEE Transactions on Geoscience and Remote Sensing*, *51*(3), 1791–1804. https://doi.org/10.1109/TGRS.2012.2205264

Moghaddam, M., … D. E.-I. J. of, & 2010, undefined. (n.d.). A wireless soil moisture smart sensor web using physics-based optimal control: Concept and initial demonstrations. *Ieeexplore.Ieee.Org*. Retrieved from https://ieeexplore.ieee.org/abstract/document/5658194/

Musial, J., Dabrowska-zielinska, K., Kiryla, W., Oleszczuk, R., Gnatowski, T., & Jaszczynski, J. (2016). Derivation and validation of the high resolution satellite soil moisture products : a case study of the Biebrza Sentinel-1 validation sites, *8*(1), 37–53.

Njoku, E. G., & Entekhabi, D. (1996). Passive microwave remote sensing of soil moisture. *Journal of Hydrology*, *184*(1–2), 101–129. https://doi.org/10.1016/0022-1694(95)02970-2

Njoku, E. G., & Kong, J.-A. (1977). Theory for passive microwave remote sensing of near-surface soil moisture. *Journal of Geophysical Research*, *82*(20), 3108–3118. https://doi.org/10.1029/JB082i020p03108

O'neill, P., Chan, S., Njoku, E., Jackson, T., & Bindlish, R. (2016). *Soil Moisture Active Passive (SMAP) Algorithm Theoretical Basis Document Level 2 & 3 Soil Moisture (Passive) Data Products*. Retrieved from https://nsidc.org/sites/nsidc.org/files/technical-references/L2_SM_P_ATBD_revision_C_Dec2016_v2.pdf

Owe, M., & Van De Griend, A. A. (1998). *Comparison of soil moisture penetration depths for several bare soils at two microwave frequencies and implications for remote sensing. WATER RESOURCES RESEARCH* (Vol. 34). Retrieved from https://research.vu.nl/ws/portalfiles/portal/860717/117052.pdf

Paloscia, S., Pettinato, S., Santi, E., Notarnicola, C., Pasolli, L., & Reppucci, A. (2013). Soil moisture mapping using Sentinel-1 images: Algorithm and preliminary validation. *Remote Sensing of Environment*, *134*, 234–248. https://doi.org/10.1016/j.rse.2013.02.027

Panciera, R., Walker, J. P., Kalma, J. D., Kim, E. J., Hacker, J. M., Merlin, O., … Skou, N. (2008). The NAFE'05/CoSMOS Data Set: Toward SMOS Soil Moisture Retrieval, Downscaling, and Assimilation. *IEEE Transactions on Geoscience and Remote Sensing*, *46*(3), 736–745. https://doi.org/10.1109/TGRS.2007.915403

Petropoulos, G. P., Ireland, G., & Barrett, B. (2015). Surface soil moisture retrievals from remote sensing: Current

status, products & future trends. https://doi.org/10.1016/j.pce.2015.02.009

Rodriguez-Fernandez, N. J., Aires, F., Richaume, P., Kerr, Y. H., Prigent, C., Kolassa, J., … Drusch, M. (2015). Soil Moisture Retrieval Using Neural Networks: Application to SMOS. *IEEE Transactions on Geoscience and Remote Sensing*, *53*(11), 5991–6007. https://doi.org/10.1109/TGRS.2015.2430845

Rondinelli, W. J., Hornbuckle, B. K., Patton, J. C., Cosh, M. H., Walker, V. A., Carr, B. D., & Logsdon, S. D. (2014). Different Rates of Soil Drying after Rainfall Are Observed by the SMOS Satellite and the South Fork in situ Soil Moisture Network. https://doi.org/10.1175/JHM-D-14-0137.1

Rondinelli, W. J., Hornbuckle, B. K., Patton, J. C., Cosh, M. H., Walker, V. A., Carr, B. D., … Logsdon, S. D. (2015). Different Rates of Soil Drying after Rainfall Are Observed by the SMOS Satellite and the South Fork in situ Soil Moisture Network. *Journal of Hydrometeorology*, *16*(2), 889–903. https://doi.org/10.1175/JHM-D-14-0137.1

Salvia, M., Ruscica, R., Sorensson, A., Polcher, J., Piles, M., & Karszenbaum, H. (2018). Seasonal Analysis of Surface Soil Moisture Dry-Downs in a Land-Atmosphere Hotspot as Seen by LSM and Satellite Products. In *IGARSS 2018 - 2018 IEEE International Geoscience and Remote Sensing Symposium* (pp. 5521–5524). IEEE. https://doi.org/10.1109/IGARSS.2018.8518548

Shellito, P. J., Small, E. E., Colliander, A., Bindlish, R., Cosh, M. H., Berg, A. A., … Walker, J. P. (2016). SMAP soil moisture drying more rapid than observed in situ following rainfall events. *Geophysical Research Letters*, *43*(15), 8068–8075. https://doi.org/10.1002/2016GL069946

Shellito, P. J., Small, E. E., & Livneh, B. (2018). Controls on surface soil drying rates observed by SMAP and simulated by the Noah land surface model. *Hydrology and Earth System Sciences*, *22*(3), 1649–1663. https://doi.org/10.5194/hess-22-1649-2018

Sun, Y., Fu, R., Dickinson, R., Joiner, J., Frankenberg, C., Gu, L., … Fernando, N. (2015). Drought onset mechanisms revealed by satellite solar-induced chlorophyll fluorescence: Insights from two contrasting extreme events. *Journal of Geophysical Research: Biogeosciences*, *120*(11), 2427–2440. https://doi.org/10.1002/2015JG003150

Tayfur, G., Zucco, G., Brocca, L., & Moramarco, T. (2014). Coupling soil moisture and precipitation observations for predicting hourly runoff at small catchment scale. *Journal of Hydrology*, *510*, 363–371. https://doi.org/10.1016/j.jhydrol.2013.12.045

Teuling, A. J., Seneviratne, S. I., Williams, C., & Troch, P. A. (2006). Observed timescales of evapotranspiration response to soil moisture. *Geophysical Research Letters*, *33*(23), L23403. https://doi.org/10.1029/2006GL028178

van der Velde, R., Su, Z., van Oevelen, P., Wen, J., Ma, Y., & Salama, M. S. (2012). Soil moisture mapping over the central part of the Tibetan Plateau using a series of ASAR WS images. *Remote Sensing of Environment*, *120*, 175–187. https://doi.org/10.1016/j.rse.2011.05.029

Vereecken, H., Weynants, M., Javaux, M., Pachepsky, Y., Schaap, M. G., & Genuchten, M. T. van. (2010). Using Pedotransfer Functions to Estimate the van Genuchten–Mualem Soil Hydraulic Properties: A Review. *Vadose Zone Journal*, *9*(4), 795. https://doi.org/10.2136/vzj2010.0045

Wien, T. U., & Zürich, N. (2018). *ESA Climate Change Initiative Phase II-Soil Moisture Algorithm Theoretical Baseline Document (ATBD) D2.1 Version 04.2 Active Soil Moisture Retrievals Earth Observation Data Centre for Water Resources Monitoring (EODC) GmbH in cooperation with*. Retrieved from http://www.esa-cci.org/.

Wösten, J. H. M., & De, F. (2016). *BOFEK2012 versie 2; Status A*. Retrieved from http://library.wur.nl/WebQuery/wurpubs/fulltext/404573

Wösten, J. H. M., Veerman, G. ., DeGroot, W. J. ., & Stolte, J. (2001). Waterretentie- en doorlatendheidskarakteristieken van boven- en ondergronden in Nederland: de Staringreeks. *Alterra Rapport*, *153*, 86. https://doi.org/153

APPENDICES

Appendix A: Appendix A

Pixel matchup between the SMAP estimates and *in-situ* measurements for pixel 1,0 and pixel 1,1.
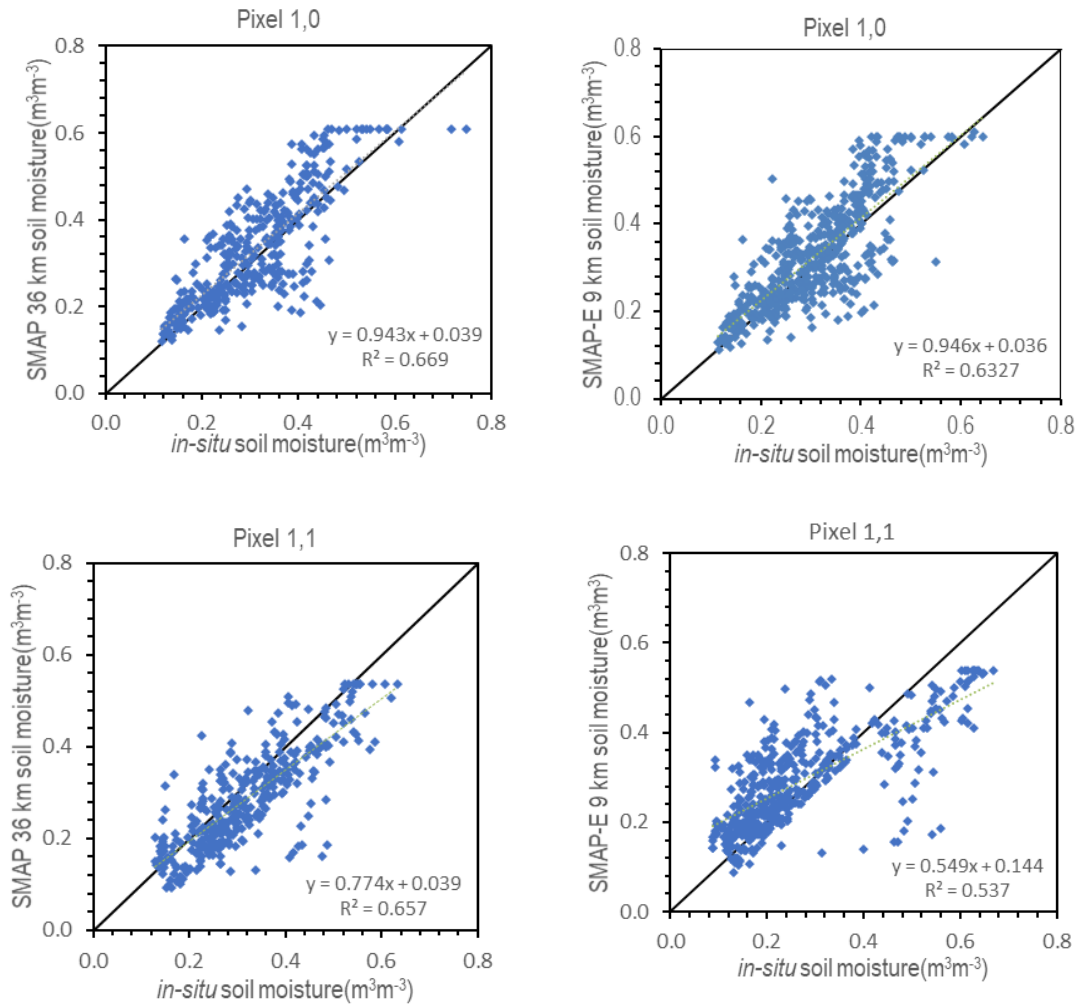
Appendix B: Appendix B

Bias, UbRMSD and R² at Twente, Raam and Flevoland per individual year,2016,2017 and 2018.

product	year	Bias [m³m⁻³]			UbRMSD[m³m⁻³]			R²[-]		
		Twente	Rm	FP	Twente	Rm	FP	Twente	Rm	FP
SMAP	2016	-0.002	0.085	0.043	0.051	0.052	0.060	0.498	0.639	0.304
	2017	-0.034	0.073	0.064	**0.033**	0.047	0.054	0.895	0.744	0.541
	2018	0.007	0.084	0.031	0.065	0.079	0.035	0.580	0.509	0.838
SMAP-E	2016	-0.003	0.093	0.076	0.058	0.046	0.047	0.439	0.713	0.237
	2017	-0.027	0.093	0.114	**0.034**	0.043	0.063	0.889	0.761	0.221
	2018	0.009	0.078	0.068	0.071	0.090	0.034	0.481	0.739	0.701
Sentinel-1	2016	-0.020	0.029	-0.043	0.062	0.059	0.043	0.248	0.185	0.608
	2017	-0.057	0.026	-0.015	0.086	0.057	0.055	0.422	0.229	0.435
	2018	-0.035	-0.06	-0.038	0.089	0.037	0.046	0.234	0.530	0.617

Appendix C: Appendix C

Performance metrics (Bias, UbRMSD and R²) for SMAP 36km, SMAP-E 9 km and Sentinel -1 based on the landcover dominating each SM network

| | Landcover | SMAP 36 km | | SMAP-E 9 km [m³m⁻³] | | Sentinel 1[m³m⁻³] | |
		Bias [m³m⁻³]	UbRMSD [m³m⁻³]	Bias [m³m⁻³]	UbRMSD [m³m⁻³]	Bias [m³m⁻³]	UbRMSD [m³m⁻³]
Twente	Grassland	-0.028	0.099	-0.030	0.098	-0.088	0.117
	Corn	0.008	0.068	0.033	0.067	-0.008	0.081
Raam	Grass	0.063	0.184	0.184	0.063	-0.011	-0.011
	Sugar beets	0.124	0.180	0.180	0.124	0.054	0.054
	Onions	0.061	0.232	0.232	0.061	0.001	0.001
	Corn	0.078	0.090	0.090	0.078	0.007	0.007
Flevoland	Grass	0.077	0.081	0.087	0.070	-0.020	0.057

Appendix D: Appendix D

Performance metrics (Bias, UbRMSD and R2) for SMAP 36km, SMAP-E 9 km and Sentinel -1 based on the soil texture dominating each SM network

| | | SMAP 36 km | | SMAP-E 9 km | | Sentinel 1 | |
		Bias [m³m⁻³]	UbRMSD [m³m⁻³]	Bias [m³m⁻³]	UbRMSD [m³m⁻³]	Bias [m³m⁻³]	UbRMSD [m³m⁻³]
Twente	loamy sand	-0.081	0.104	-0.082	0.099	-0.113	0.115
	sand	0.014	0.086	0.020	0.089	-0.050	0.108
Raam	loamy sand	0.045	0.104	0.067	0.075	-0.024	0.057
	sand	0.083	0.082	0.173	0.078	0.012	0.080
Flevoland	clayey	0.077	0.081	0.087	0.070	-0.020	0.057

Appendix E: Appendix E

SMDD events per network

| | Twente SMDD events | | | Raam SMDD events | | |
	SMAP 36 km	SMAP-E 9 km	In-situ SM	SMAP 36 km	SMAP-E 9 km	In-situ SM
2016	2	5	9	6	4	6
2017	4	4	7	3	3	7
2018	8	6	8	2	2	2
Total	14	15	24	11	9	15

Appendix F: Appendix F

Sentinel 1 images for the Raam soil moisture monitoring

network
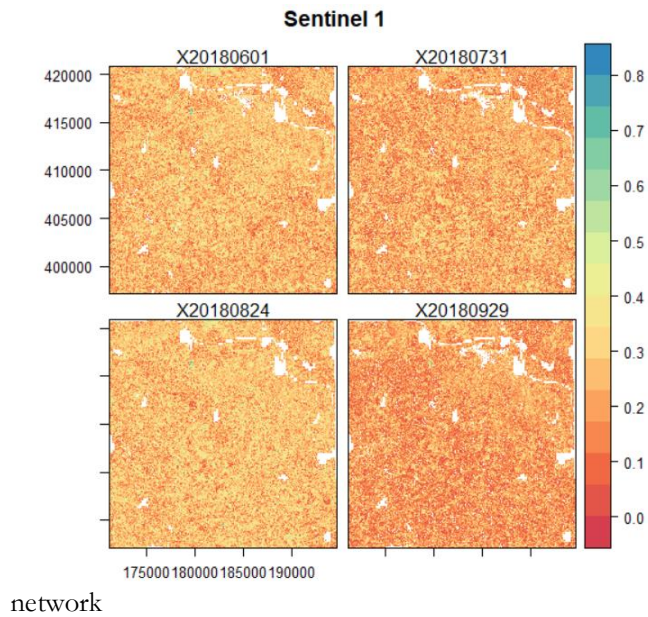
Appendix G: Appendix G

(i) Soil moisture dry-down time-scale (ii) Magnitude of soil moisture drying process and (iii) Final soil moisture content maps respectively for SMAP-E and SMAP 36km